

Classification Accuracy Enhancement of fNIR based Imagery Movement by Modified Common Spatial Pattern

By

Md. Faisal Kabir

Roll: 1615551

A thesis submitted in partial fulfillment of the requirement for the degree of
Master of Science in Biomedical Engineering



Khulna University of Engineering & Technology (KUET)

Khulna 9203, Bangladesh

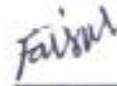
January 2019

Declaration

This is to certify that the project work entitled “**Classification Accuracy Enhancement of FNIR Based Imagery Movement by Modified Common Spatial Pattern**” has been carried out by **Md. Faisal Kabir** in the Department of Biomedical Engineering, Khulna University of Engineering & Technology (KUET), Khulna, Bangladesh. The above project work or any part of this work has not been submitted anywhere for the award of any degree or diploma.



Signature of Supervisor


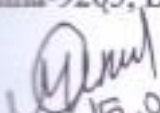
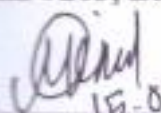

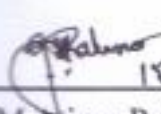


Signature of Candidate

Approval

This is to certify that the thesis work submitted by Md. Faisal Kabir entitled "Classification Accuracy Enhancement of fNIR Based Imagery Movement by Modified Common Spatial Pattern" has been approved by the board of examiners for the partial fulfillment of the requirements for the degree of M. Sc. Engineering (M. Sc. Eng.) in the Department of Biomedical Engineering, Khulna University of Engineering & Technology (KUET), Khulna, Bangladesh in January 2019.

BOARD OF EXAMINERS

1. 
15/01/2019
Dr. Sheikh Md. Rabiul Islam
Professor
Dept. of Electronics and Communication Engineering (ECE)
Khulna University of Engineering & Technology (KUET)
Khulna-9203, Bangladesh
Chairman
(Supervisor)
2. 
15.01.2019
Head of the Department
Dept. of Biomedical Engineering (BME)
Khulna University of Engineering & Technology (KUET)
Khulna-9203, Bangladesh
Member
3. 
15.01.2019
Dr. Muhammad Muinul Islam
Assistant Professor
Dept. of Biomedical Engineering (BME)
Khulna University of Engineering & Technology (KUET)
Khulna-9203, Bangladesh
Member
4. 
15/01/2019
Dr. Mohiuddin Ahmad
Professor
Dept. of EEE
Khulna University of Engineering & Technology (KUET)
Khulna-9203, Bangladesh
Member
5. 
15.01.19
Dr. G M Atiqur Rahaman
Professor
Computer Science and Engineering Discipline
Khulna University, Khulna
Member
(External)

Dedicated to-
My Beloved Parents

Acknowledgement

In the ending of my thesis work for M.Sc. Eng. degree, first of all, I am mostly thankful to the Almighty Allah for giving me the strength and confidence to complete it successfully.

In this stage, I would like to thank my graduation committee. It is pleasure to express my deepest sense of gratitude and respect to my honorable thesis advisor, **Prof. Dr. Sheikh Md. Rabiul Islam**, Department of Electronics and Communication Engineering (ECE), KUET, who was my inspiration during my thesis work. His invaluable suggestions, proper guidance, and encouragement helped to finish my work. His activeness, friendly behavior, and motivation were really memorable. I think my expression and gratitude on my supervisor cannot be summarized with a few words of thank.

In addition, I wish to express my sincere gratitude to **Dr. Muhammad Muinul islam**, Head, Department of Biomedical Engineering for giving me many good pieces of advice. I am also too much grateful to **Prof. Dr. Mohiuddin Ahmad**, Dean, Faculty of Electrical and Electronic Engineering for his loving guidance and advices to prepare my thesis paper more correctly. It is my pleasure to acknowledge the roles of **Engr. Md. Asadur Rahman**, PhD Candidate, Department of BME who was with me from the beginning of my thesis work, helped me, and supported me.

Besides, I am very much grateful to my parents and by brothers and sisters who sacrificed a lot to provide me the freedom to engage with this thesis work and believing in me that I could be able to accomplish this journey. I am grateful to all the BME faculty members, staffs, and postgraduate students who helped me directly or indirectly.

Author

January 2019

Abstract

Motor imagery event classification from functional near-infrared spectroscopy (fNIRS) is one of the most interesting problems of current brain-computer interfaces (BCIs) challenges because it needs no additional data guiding visual or listening protocol. A vital step of the fNIRS signal classification by machine learning approach is feature extraction. The feature extraction from multiple channel fNIRS signal is always challenging due to its high dimensionality. There exist several conventional feature extraction procedures like principal component analysis, nonlinear principal component analysis, independent component analysis, norm analysis, spectral norm analysis, etc. This research work studies such existing feature extraction method to classify the hand movement events of fNIRS signals. The accuracies of these methods have been found less than the expectation. Therefore, some more accurate method is needed. In this regard, usually common spatial pattern (CSP) is used to reduce the dimensional reduction and improving the classification accuracy. The conventional CSP method can be proven also ineffective for the motor imagery fNIRS signal due to its high level of trial to trial variations. The present research work proposes an algorithm named by standardized common spatial pattern (SCSP) based feature extraction method for fNIRS based motor imagery classification which can perform well in the context of the trial to trial significant variation. The classification results corresponding to the proposed feature extraction method reveal that the proposed SCSP algorithm outperformed the conventional CSP method and channel-wise method for classifying the two motor imagery event classifications. For classification accuracy measurement, four well-known classifiers: artificial neural network (ANN), k-nearest neighbor (kNN), support vector machine (SVM), and linear discriminant analysis (LDA) have been used. We have utilized both the fNIRS data of oxidized hemoglobin (HbO) and deoxidized hemoglobin (HbR) for classifying the motor imagery fNIRS data with the conventional and proposed methods. From the comparisons, we have found that in both cases, the proposed method outperforms the conventional methods in the context of the classification accuracies. To validate the classification accuracies, the sensitivities and specificities of the classifier are also calculated in this work. We believe that the proposed SCSP method will contribute in the field of feature extraction method for other types of fNIRS based BCI system, effectively. In addition, this method may be applied for the feature extraction to the other multidimensional signals so far.

List of Publications

- [1] **Md. Faisal Kabir**, Sheikh Md. Rabiul Islam, and X. Huang, “Towards the Appropriate Feature Extraction and Event Classification Methods for NIRS Data,” *International Conference on Computer, Communication, Chemical, Material and Electronic Engineering (IC4ME2)*, Rajshahi, 2018, pp. 1-4.
- [2] **Md. Faisal Kabir**, Sheikh Md. Rabiul Islam, and Md. Asadur Rahman, “Accuracy Improvement of fNIRS based Motor Imagery Movement Classification by Standardized Common Spatial Pattern,” 4th *International Conference on Electrical Engineering and Information & Communication Technology (ICEEICT)*, 13-15 September, 2018, Military Institute of Science and Technology, Dhaka, Bangladesh, pp. 1-06.

Contents

	Page No
Title Page	<i>i</i>
Declaration	<i>ii</i>
Approval	<i>iii</i>
Acknowledgement	<i>v</i>
Abstract	<i>vi</i>
List of Publications	<i>vii</i>
Contents	<i>viii</i>
List of Tables	<i>xi</i>
List of Figures	<i>xii</i>
List of Abbreviations	<i>xv</i>
CHAPTER I Introduction	1-9
1.1 General Scope	2
1.2 Motivation	3
1.3 Problem Statements and Scopes	4
1.4 Objectives	5
1.5 Thesis Outlines	5
<i>Reference</i>	<i>7</i>
CHAPTER II Theoretical Background	10-23
2.1 Introduction	11
2.2 Background of fNIRS	11
2.2.1 Near Infrared Spectroscopy	11
2.2.2 History of fNIRS	13
2.2.3 Oximetry and Hemodynamic Response	15
2.2.4 Mathematical Modeling of Oximetry	17
2.3 Types of fNIRS Technique	19
2.4 Main characteristics of fNIRS Techniques	20
2.5 Main Fields of fNIRS Application	21
2.6 Chapter Summary	21

	<i>Reference</i>	22
CHAPTER III	Proposed Methodology	24-52
3.1	Introduction	26
3.2	Data Collection	25
	3.2.1 Imagery Hand Movement with Pain Data	25
	3.2.2 Imagery Hand Movement without Pain Data	25
3.3	Data Acquisition	26
	3.3.1 1 Experimental Setup for Imagery Hand Movement with Pain	26
	3.3.2 Experimental Setup for Imagery Hand Movement without Pain	28
3.3	Proposed Research Work	30
3.4	Filtering and Baseline Correction	32
3.5	Feature Extraction Using Conventional Method	32
	3.5.1 Mean	32
	3.5.2 Median	33
	3.5.3 Slope	33
	3.5.4 Variance	34
	3.5.5 L_1 -Norm	35
	3.5.6 L_2 -Norm	35
	3.5.7 L_∞ -Norm	36
	3.5.8 Principle Component Analysis (PCA)	36
	3.5.9 Nonlinear PCA (NLPCA)	37
	3.5.11 Independent Component Analysis (ICA)	38
3.6	Proposed Feature Extraction Method	39
	3.6.1 Modified Common Spatial Pattern	39
3.7	Classification Methodology	43
	3.7.1 Artificial Neural Network (ANN)	44
	3.7.2 k-Nearest Neighbor Algorithm (kNN)	45
	3.7.3 Support Vector Machine (SVM)	46
	3.7.4 Linear Discriminant Analysis	47
3.8	Performance Measurement Criteria	49
3.9	Chapter Summary	49

	<i>Reference</i>	50
CHAPTER IV	Experimental Results and Discussions	52-84
4.1	Introduction	53
4.2	Experimental results for Conventional Method	53
4.3	Experimental results of Imagery Hand Movement	61
4.4	Result Analysis	70
	4.4.1 Results of Statistical Analysis	70
	4.4.2 Results of Classification	71
4.6	Comparison Between Result of Proposed Work and Recent Years Work	82
4.7	Chapter Summary	83
	<i>Reference</i>	84
CHAPTER V	Conclusions	85-87
5.1	Introduction	86
5.2	Future Perspective	87

List of Tables

Table No.	Description	Page No
2.1	Overall chronology of the major events leading up to human functional cortical imaging by fNIRS	13
2.2	Main characteristics and Measurable Parameter of fNIRS Techniques	20
2.3	Fields of fNIRS application	21
4.1	Classification Performance of patients 1-7	57
4.2	Accuracy of the Training and Testing of the Classification LH and RH Imagery Movement fNIR Data	68
4.3	Sensitivity and Specificity With Respect to the Accuracy of the SCSP Algorithm.	69
4.4	Significance level of the features due to the performed tasks	71
4.5	Comparison of different parameter of classification of different feature of oxygenated hemoglobin (HbO) for the participants	72
4.6	Comparison of different parameter of classification of different features of deoxygenated hemoglobin (HbR) for the participants	75
4.7	Comparison of Different Parameter of Classification of Different Feature of oxygenated hemoglobin (HbO) for the Participants	77
4.8	Comparison of Different Parameter of Classification of Different Feature of deoxygenated hemoglobin (HbR) for the Participants	80
4.9	Comparison between result of proposed work and some recent years work	82

List of Figures

Figure No	Description	Page No
2.1	Absorption coefficient of HbR, HbO, and H ₂ O with respect to the light wavelength	12
2.2	A 16 Channel fNIR signal Acquisition device (Biopac 1200 Model)	1
2.3	Relation between hemodynamic response and oxygen concentration	16
2.4	Position of fNIRS source and detector on human scalp	17
2.5	16 Channel fNIR compact band of source and detector	18
3.1	Patient with acupuncture needle in Hegu point	27
3.2	Tasks and time description in the data, one channel only	28
3.3	Total hardware connection including sensor pad, imager, data multiplexer, and computer	29
3.4	Scheduling of the performed tasks. This pattern has followed 20 times by each participant which gave 20 trials of every imagery tasks	30
3.5	Block diagram of proposed methodology	31
3.6	(a) Standard PCA applied to a simple two-dimensional data set & (b) Nonlinear PCA (auto encoder neural network) applied to a 3/4 circle with noise	38
3.7	Flow diagram of spatial filtering weight matrix estimation technique for modified common spatial pattern	41
3.8	Pattern of extracted features to be loaded in a classifier for training and testing.	43
3.9	fNIR signal classification by the proposed method	44
3.10	Architecture of artificial neural network	45
3.11	Example of kNN classification	46
3.12	A model of hyperplane that differs the feature space	47
3.13	Illustration of LDA classification method	48
4.1	HbO data for all 24 channel for participant 1 right arm	54
4.2	HbO data from left and right hand of same participant (ch19-ch24)	54
4.3	Confusion matrix for NLPCA (of HbO data for participant 2 right arm)	56

4.4	Comparison of average accuracy of ANN,kNN, SVM for different features for right arm movement of 7 pateints	58
4.5	Comparison of average accuracy of ANN, kNN, SVM for different features for left arm movement of 7 pateints	59
4.6	Comparison of average sensitivity of ANN, kNN, SVM for different features for right arm movement of 7 pateints	59
4.7	Comparison of average sensitivity of ANN, kNN, SVM for different features for left arm movement of 7 pateints	60
4.8	Comparison of average specificity of ANN, kNN, SVM for different features for right arm movement of 7 pateints	60
4.9	Comparison of average specificity of ANN, kNN, SVM for different features for left arm movement of 7 patients	61
4.10	Raw and filtered fNIRS data of HbO and HbR of participant 1. This data is representing the information of only one channel among sixteen	6
4.11	Functional images of different taks with respect to the activation level of HbO. The black color gives the highest activation while the yellow gives the lowesactivaton and the red represent the neutral activation as rest	63
4.12	Functional images of different taks with respect to the activation level of HbR.	64
4.13	Functional images of different taks with respect to the activation level of HbO	66
4.14	Training state of participant#1 with LDA classifier considering the 10 set of features (mean, slope, and variance) of iLH and iRH	67
4.15	The confusion matrix of the classification results regarding the testing features of the participant 1	67
4.16	Comparison of the proposed SCSP algorithm with the others considering the accuracy% \pm standard deviation in training and testing	69
4.17	Comparison of average accuracy of different classifier for different features of HbO data (imagery hand movement with pain task) for the participants	73
4.18	Comparison of average sensitivity of different classifier for different features of HbO data (imagery hand movement with pain task) for the participants	73
4.19	Comparison of average specificity of different classifier for different	74

	features of HbO data (imagery hand movement with pain task) for the participants.	
4.20	Comparison of average accuracy of different classifier for different features of HbR data (imagery hand movement with pain task) for the participants.	75
4.21	Comparison of average sensitivity of different classifier for different features of HbR data (imagery hand movement with pain task) for the participants	76
4.22	Comparison of average specificity of different classifier for different features of HbR data (imagery hand movement with pain task) for the participants	76
4.23	Comparison of average accuracy of different classifier for different features of HbO data (imagery hand movement without pain task) for the participants	78
4.24	Comparison of average sensitivity of different classifier for different features of HbO data (imagery hand movement without pain task) for the participants	78
4.25	Comparison of average specificity of different classifier for different features of HbO data (imagery hand movement without pain task) for the participants	79
4.26	Comparison of average accuracy of different classifier for different features of HbR data (imagery hand movement without pain task) for the participants	80
4.27	Comparison of average sensitivity of different classifier for different features of HbR data (imagery hand movement without pain task) for the participants	81
4.28	Comparison of average specificity of different classifier for different features of HbR data (imagery hand movement without pain task) for the participants	81

List of Abbreviations

Abbreviated Form	Elaboration
ANN	Artificial Neural Network
BCI	Brain Computer Interface
CC	Covariance Coefficient
CSP	Common Spatial Pattern
EEG	Electroencephalography
FIR	Finite Impulse Response
fMRI	Functional Magnetic Resonance Imaging
FN	False Negative
fNIRS	Functional Near Infrared Spectroscopy
FP	False positive
GSC	Global Spatial Covariance
HbO	Oxygenated Hemoglobin
HbR	Deoxygenated Hemoglobin
Hbt	Total Hemoglobin
ICA	Independent Component Analysis
iLH	Imagery Left Hand
iRH	Imagery Right Hand
kNN	k Nearest Neighbor
LDA	Linear Discriminant Analysis
NLPCA	Nonlinear Principle Component Analysis
NSC	Normalized Spatial Covariance
OSC	Overall Spatial Covariance
PCA	Principle Component Analysis
SCSP	Standardized Common Spatial Pattern
SVM	Support Vector Machine
TN	True Negative
TP	True Positive

CHAPTER I: Introduction

Chapter Outlines

1.1 General Scopes

1.2 Motivation

1.3 Problem Statements and Scopes

1.4 Objectives

1.5 Thesis Outlines

References

CHAPTER I

Introduction

1.1 General Scopes

Brain-computer interface (BCI) is one of the important topics of the modern neuro-computing research area. BCI system offers a direct communication pathway between the brain and real world [1.1]. It has potential application in neuro-rehabilitation basically for the paralyzed or motor impaired patients. BCI system needs two important factors-scanning neuro-activities and decoding them that can control computer or devices. Though promising methods of scanning the neuro activities are Electroencephalography (EEG), Functional Magnetic Resonance Imaging (fMRI), and Functional Near-Infrared Spectroscopy (fNIRS), fNIRS is getting more attentions over the last decades due to its high spatial resolution, moderate temporal resolution, and less noise sensitivity [1.2]. Another important issue is to decode the recorded neuronal signals.

fNIRS is an optical and non-invasive method of brain activity measurement, with high spatial resolution and reliability. So, it becomes one of the best choices for brain computer interface (BCI) [1.3]. The fNIRS method depends on changes of blood flow and it measures the concentration of oxygenated and deoxygenated hemoglobin (HbO and HbR) from the super-facial layers of the human cortex. It actually measures the change in oxygen saturation and hemoglobin concentration in brain tissue. fNIRS can offer simultaneous measurements from dynamic changes of HbO and HbR in the brain cortex with a reasonable temporal resolution (< 1 sec) and spatial resolution (~ 3 cm) [1.4]. fNIRS employs low-energy optical radiation (mostly in 2-3 different wavelengths between 700-900 nm) to assess the change in absorption by the chromophores (HbO & HbR) in the underlying brain tissue [1.5]. In fact, this absorption changes reflect the changes in local HbO and HbR concentration, which in turn are related to and triggered by the alternation in neuronal activities. Therefore, fNIRS is an imaging tool which utilizes endogenous chromophores to assess brain's functional activities, non-invasively. By this functional

brain imaging modality, it is possible to detect HbO and HbR of imagery movements, cognitive task, mental math task, n -back memory test, emotion recognitions, etc. [1.6].

The NIRS data is analyzed using different feature extraction method and classification method. Common spatial pattern (CSP) based feature extraction method is used to improve the classifying accuracy [1.7]. Principal component analysis (PCA) is used to identify the principal components of the data. The weights of the independent component analysis (ICA) and non-linear principal component analysis (NLPCA) are also used as the features of the NIRS data. On the other hand, for fNIRS data classification, the artificial neural network (ANN), k-nearest neighbor (k-NN) algorithm, support vector machine (SVM) and linear discriminant analysis (LDA) are extensively used [1.8].

1.2 Motivation

A number of research works have been demonstrated regarding BCI applications through fNIRS where motor imagery based BCI system is one of the most examined BCI paradigms [1.9]. In addition, there are also some research works [1.10-1.12] those have conducted the BCI based on the voluntary movement-related tasks. In this contrast, the real execution of hand movements recognition or classification is easier than that of imagery movements. Motor execution by left hand and right hand corresponding fNIRS data can be classified by very high accuracy (about 90%) [1.13-1.14]. On the other hand, achieving the accuracy up to 70% for imagery movement is crucial. Therefore, it is a challenging task to discriminate the neuro-activations due to motor imagery based stimuli because it is reported in [1.15] that the activation due to imagine movements is only 30% of voluntary movements. Therefore, the system definitely needs highly intelligent computational algorithm that can differentiate even the little variation occurred for the different imagery movements. In order to classify the fNIRS data of motor imagery, different classifiers like LDA, SVM, ANN etc. are often used. These classification techniques require suitable features or attributes to differentiate the classes. As a result, efficient feature extraction is also very important obligation before task classification.

In the field of BCI, the researchers proposed a number of methods regarding fNIRS signal filtering, preprocessing, feature extraction, and classification [1.13-1.17]. For either voluntary or imagery movement classification [1.13-1.18] from fNIRS signal different types of statistical features have been proposed like mean, standard deviation, variances,

slope, median, skewness, and kurtosis. We found that these research works used different features and classifiers to classify the activities from the signal.

Again, there are a number of research works those reported that the CSP based feature extraction method can improve the quality of classifiers and increase the classification accuracy [1.19-1.22]. Unfortunately, all of these articles are EEG based BCI. Concerning fNIRS based BCI system, only a handful research work used CSP method to extract feature for the training of the predictive network. So far the knowledge of the authors CSP method has been applied in [1.23] where the fNIRS data were of voluntary movements. The motor imagery movement classification with the help of CSP method has been accomplished in [1.8] for the first time where they reported this method can improve the classification accuracy more than 9% in average and reached up to 72% to 75% but this accuracy for two class classification is not enough for achieving highly accurate BCI system.

1.3 Problem Statements and Scopes

From the aforementioned research works two major issues have been found that create scope for further study:

- i)* Regarding these classifiers and used feature types, there arise questions that which type of features will be fruitful for the classifier and which classifier will show the best accuracy for NIRS data.
- ii)* For motor imagery events, for significant classification accuracy CSP can be applied because CSP is better method than that of the conventional multiple channel averaging method. Nonetheless, the existing CSP method has some limitations that creates obstacle to achieve the high accuracy. The limitation can be presented by the following points:
 - Existing CSP method consider the signals of all the trials as same weight.
 - Final spatial filtering weight matrix is produced by simple averaging.
 - Covariance coefficient calculating procedure of the existing common spatial pattern does not cover the global spatial pattern.

Therefore there are two major thesis questions that should be answered. At, first a wide investigation is necessary to find the best features and corresponding classifier to achieve

the best classification accuracy for the development of an efficient BCI system. Secondly, to achieve very high classification accuracy especially, for motor imagery event classification, the limitations of the existing CSP has to overcome.

1.4 Objectives

Concerning the previous issues this thesis work scope to perform several steps of study with some specific objectives. The significant objectives of the proposed thesis work can be listed as:

- To find the effective features for fNIRS signal for significant classification accuracies.
- To reveal the appropriate classifier for fNIRS data classification.
- To modify the conventional CSP method based on the consideration of global spatial covariance.
- To measure the classification accuracies of both CSP and modified CSP methods by extracting features from motor imagery fNIRS signal by the conventional CSP and modified CSP method.
- Enhancing the classification accuracy by the modified CSP method with compared to the conventional CSP method by conditioning its proper standardization.

1.5 Thesis Outlines

- **Chapter One:** The general scopes and the significance of this type of thesis work have been reported in this chapter. In addition the relevant research work has been discussed with their limitations. We also discussed the possible scopes to overcome the limitations of the existing work. The significant objectives of the proposed thesis work have been reported here.
- **Chapter Two:** The theoretical knowledge about the fNIRS system, mathematical modeling, and different significant features of the fNIRS signals are discussed in this Chapter. In addition, the main characteristics and field of application of fNIRS has also been explained here.

- **Chapter Three:** The technical details of the proposed methodologies of this work are given in this Chapter. The mathematical backgrounds of the different filtering criteria, feature extraction methodologies, classification techniques, etc. are broadly explained here.
- **Chapter Four:** The main outcomes of the proposed work have been reported in this Chapter. The results have been presented in tabular and graphical form with neat and detail discussions.
- **Chapter Five:** The total thesis work has been concluded in this chapter. Here, the future perspectives have also been a concerning issue that will be helpful for the future researchers to work more efficiently in this arena.

REFERENCES

- [1.1] S. Gao, Y. Wang, X. Gao, B. Hong, Visual and auditory brain-computer interfaces, *IEEE Transactions on Biomedical Engineering*, vol. 61, no. 5, pp. 1436-1447, 2014.
- [1.2] M. Ferrari, V. Quaresima, A brief review on the history of human functional near-infrared spectroscopy (fNIRS) development and fields of application, *NeuroImage*, vol. 63, pp. 921-935, 2012.
- [1.3] Y. Liu, H. Ayaz, A. Curtin, B. Onaral, and P. A. Shewokis, "Towards a hybrid p300-based BCI using simultaneous fNIR and EEG," *Lecture Notes in Computer Science*, vol. 8027. pp. 335-344, Springer, Berlin, 2013.
- [1.4] Ariely and G. S. Berns, "Neuromarketing: the hope and hype of neuroimaging in business," *Nature Reviews Neuroscience*, vol. 11, pp. 284–292, April 2010.
- [1.5] M. Ferrari and V. Quaresima, "A brief review on the history of human functional near-infrared spectroscopy (fNIRS) development and fields of application", *NeuroImage*, vol. 63, no. 2, pp. 921-935, March 2012.
- [1.6] M. Strait and M. Scheutz, "What we can and cannot (yet) do with functional near infrared spectroscopy," *Frontiers in Neuroscience*, vol. 8, no. 117, pp. 1-12, May 2014.
- [1.7] S. Zhanga, Y. Zheng, D. Wang, L. Wang, J. Maa, J. Zhanga, W. Xua, D. Lia, D. Zhangd, "Application of a common spatial pattern-based algorithm for an fNIRS-based motor imagery brain-computer interface," *Neuroscience Letters*, 2018.
- [1.8] K. Hong, M. J. Khan, and M. J. Hong, "Feature extraction and classification methods for hybrid fNIRS-EEG brain-computer interfaces," *Frontiers in Human Neuroscience*, vol. 12, no. 246, 2018.
- [1.9] N. Naseer and K. S. Hong, "fNIRS-based brain-computer interfaces: a review," *Frontiers in Human Neuroscience*, vol. 9, no. 3, pp. 1-15, 2015.
- [1.10] M. Roth, J. Decety, M. Raybaudi, R. Massarelli, C. Delon-Martin, C. Segebarth, S. Morand, A. Gemignani, M. Decorps, and M. Jeannerod, "Possible involvement of

- primary motor cortex in mentally simulated movement: A functional magnetic resonance imaging study,” *NeuroReport*, vol. 7, pp. 1280-1284, 1996.
- [1.11] D. Wu, J. T. King, C. H. Chuang, C. T. Lin and T. P. Jung, “spatial filtering for EEG-based regression problems in brain–computer interface (BCI),” *IEEE Transactions on Fuzzy Systems*, vol. 26, no. 2, pp. 771-781, April 2018.
- [1.12] M. Spuler, A. Walter, W. Rosenstiel, and M. Bogdan, “Spatial filtering based on canonical correlation analysis for classification of evoked or event-related potentials in EEG data,” *IEEE Transactions on Neural Systems and Rehabilitation Engineering*, vol. 22, no. 6, pp. 1097–1103, Nov. 2014.
- [1.13] N. Naseer and K. S. Hong, “Classification of functional near infrared spectroscopy signals corresponding to the right- and left wrist motor imagery for development of a brain-computer interface,” *Neuroscience Letter*, vol. 553, no: pp.84–89, October 2013.
- [1.14] K. S. Hong, N. Naseer, and Y. H. Kim, “Classification of prefrontal and motor cortex signals for three-class fNIRS–BCI,” *Neuroscience Letter*, vol. 587, pp. 87–92, February 2015.
- [1.15] N. T. Hai, N. Q. Cuong, T. Q. Dang Khoa, and V. V. Toi, “Temporal hemodynamic classification of two hands tapping using functional nearinfrared spectroscopy,” *Frontiers in Human NeuroScience*, vol. 7, no. 516, pp. 1-12, September 2013.
- [1.16] M. A. Rahman and M. Ahmad, “Movement Related Events Classification from Functional Near Infrared Spectroscopic Signal,” 19th International Conference on Computer and Information Technology, December 18-20, 2016, North South University, Dhaka, Bangladesh.
- [1.17] A. M. Batula, Y. E. Kim, and H. Ayaz, “Virtual and Actual Humanoid Robot Control with Four-Class Motor-Imagery-Based Optical Brain-Computer Interface,” *Computational Intelligence and Neuroscience*, volume 2017, Article ID 1463512, pp. 1-13, July 2017.
- [1.18] M. A. Rahman, M. M. Haque, A. Anjum, M. N. Mollah, and M. Ahmad, “Classification of motor imagery events from prefrontal hemodynamics for BCI application,” *International Joint Conference on Computational Intelligence (IJCCI)*, 2018.

- [1.19] D. Wu, J. T. King, C. H. Chuang, C. T. Lin and T. P. Jung, “spatial filtering for EEG-based regression problems in brain–computer interface (BCI),” *IEEE Transactions on Fuzzy Systems*, vol. 26, no. 2, pp. 771-781, April 2018.
- [1.20] M. Spuler, A. Walter, W. Rosenstiel, and M. Bogdan, “Spatial filtering based on canonical correlation analysis for classification of evoked or event-related potentials in EEG data,” *IEEE Transactions on Neural Systems and Rehabilitation Engineering*, vol. 22, no. 6, pp. 1097–1103, Nov. 2014.
- [1.21] R. N. Roy, S. Bonnet, S. Charbonnier, P. Jallon, and A. Campagne, “A comparison of ERP spatial filtering methods for optimal mental workload estimation,” *37th Annual Int. Conf. of the IEEE Engineering in Medicine and Biology Society (EMBC)*, 2015, pp. 7254– 7257.
- [1.22] Y. Kim, J. Ryu, K. K. Kim, C. C. Took, D. P. Mandic, and C. Park, “Motor imagery classification using mu and beta rhythms of EEG with strong uncorrelating transform based complex common spatial patterns,” *Computational Intelligence and Neuroscience*, vol. 2016, Article ID 1489692, 2016.
- [1.23] S. H. Jin, S. H. Lee, G. Jang, Y. J. Lee, H. K. Shik and J. An, “An application of common spatial pattern algorithm for accuracy improvement in classification of cortical activation pattern according to finger movement,” *54th Annual Conference of the Society of Instrument and Control Engineers of Japan (SICE)*, Hangzhou, 2015, pp. 1260-1264.

CHAPTER II: Theoretical Background

Chapter Outlines

2.1 Introduction

2.2 Background of fNIRS

2.3 Types of fNIRS Technique

2.4 Main characteristics of fNIRS Techniques

2.5 Main Fields of fNIRS Application

References

CHAPTER II

Theoretical Background

2.1 Introduction

In this chapter, the theoretical knowledge about the fNIRS system, mathematical modeling, and different significant features of the fNIRS signals are discussed. In addition, the main characteristics and fields of application of fNIRS have also been explained in this chapter. The aim of this chapter is to present a clear conception of the fNIRS modality and the perspective of its applicability.

2.2 Background of fNIRS

2.2.1 Near Infrared Spectroscopy

Most biological tissues are comparatively transparent to light in the near-infrared range between 700 to 900 nm because the absorbance of the main constituents in the human tissue like H₂O, HbO, and HbR is small in this range [2.1]. The absorbance coefficient of H₂O, HbO, and HbR as well as the optical window of fNIRS are shown in Figure 2.1.

At a high temporal resolution fNIRS can measure to capture additional frequency band and participant does not need to lay down at a supine position. fNIRS is a portable device that can be used in more normal setting like setting at a small table and even with moveable subject walking outdoors [2.3]. fNIRS is free from most of the art effects like eye blink, muscle activities and offer a unique transaction between spatial and temporal resolution. It also used in other measurement system such as neurostimulation, EEG, physiological signal [2.4]. A 16 channel fNIRS device are shown in Figure 2.2.

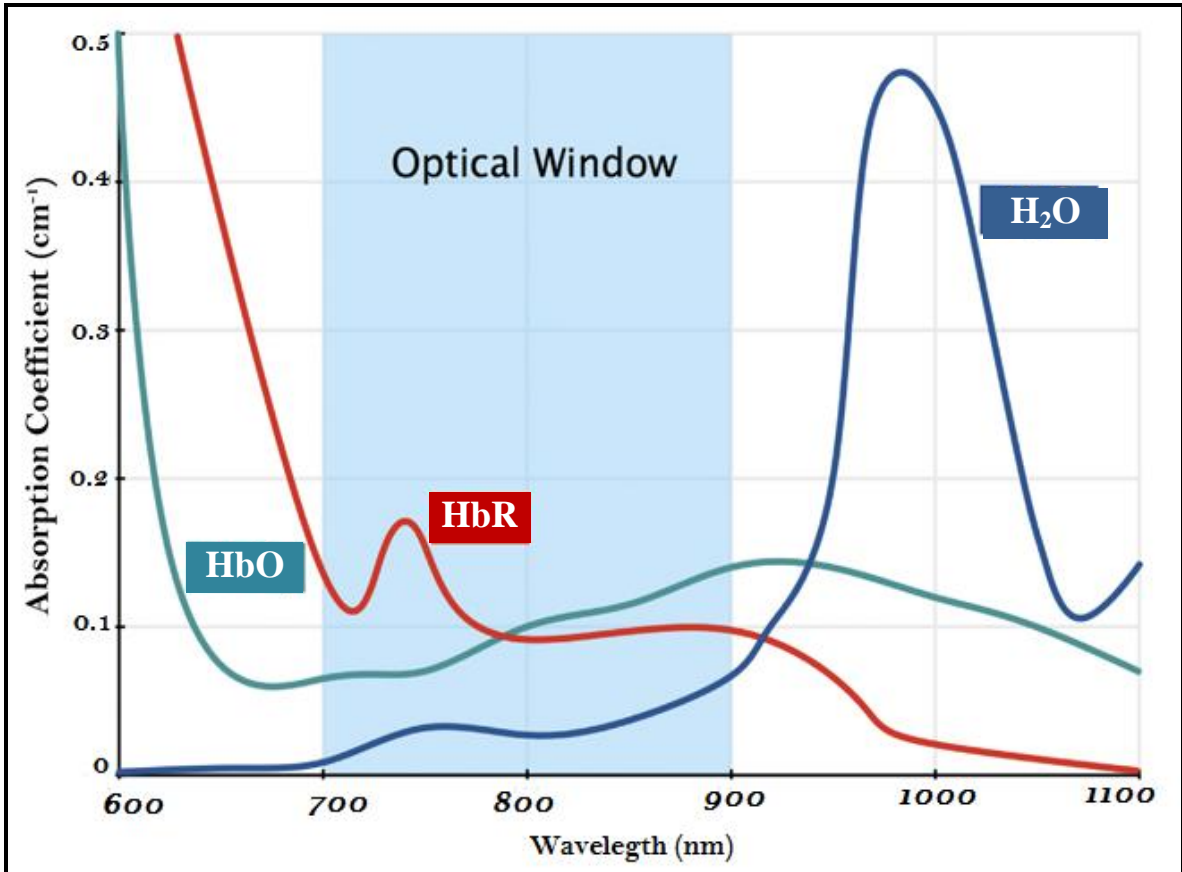


Figure 2.1: Absorption coefficient of HbR, HbO, and H₂O with respect to the light wavelength [2.2].



Figure 2.2: A 16 Channel fNIR signal Acquisition device. (Biopac 1200 Model)

In general configuration light source and detectors of the fNIRS probe are placed on the brain scalp and two different wavelengths approximately 700 and 900 of lights are transmitted through the upper layer of cerebral cortex. Injected photons follow various paths inside the head at the time of light in NIR range being shone through the human scalp. Few numbers of these photons are absorbed by skull, skin and brain. After following the so-called “banana” pattern rest of the photons exit the head due to scattering effect of the tissue [2.5]. The main absorbers in the NIR range are blood chromophores of HbO and HbR whereas water and lipid are relatively transparent to NIR light. Therefore, changes in the amplitude of backscattered light can be represented as changes in blood chromophore concentrations. fNIRS means the estimating technique of HbR and HbO concentrations by means of near infrared light.

2.2.2 History of fNIRS

The discovery of near-infrared energy is ascribed to William Herschel in the 19th century, but the first industrial application began in the 1950s. In the first applications, NIRS was used only as an add-on unit to other optical devices that used other wavelengths such as ultraviolet (UV), visible (Vis), or mid-infrared (MIR) spectrometers. The chronology of the major events leading up to human functional cortical imaging by fNIRS is reported in **Table 2.1**.

Table 2.1: Overall chronology of the major events leading up to human functional cortical imaging by fNIRS [2.6]

Year	Major events
1977	Jöbsis determines the possibility to detect changes of adult cortical oxygenation during hyperventilation by near-infrared spectroscopy
1985	First NIRS clinical studies on newborns and adult cerebrovascular patients (Brazy; Ferrari)
1989	First commercial single-channel CW clinical instrument: NIRO-1000 by Hamamatsu Photonics, Japan
1991-	First fNIRS studies carried out independently by Chance, Kato, Hoshi, and Villringer

1992	by using single-channel instruments
1993	Publication of the first 6 fNIRS studies Simultaneous monitoring of different cortical areas by 5 single-channel instruments (Hoshi)
1994	First application of fNIRS on subjects affected by psychiatric disorders by using a single-channel system (Okada); Hitachi company (Japan) introduces a 10-channel CW system (Maki); First simultaneous recording of positron emission tomography and fNIRS data (Hoshi)
1995	First evidence of a fast-optical signal related to neuronal activity (Gratton); First two-dimensional image of the adult occipital cortex activation by a frequency domain spectrometer (Gratton)
1996	First simultaneous recording of fMRI and CW fNIRS data (Kleinschmidt); First simultaneous recording of fMRI and TRS fNIRS data (Obrig)
1998	First application of fNIRS on newborns using a commercial single-channel CW system (Meek) First images of the premature infant cortex upon motor stimulation by using a CW-fNIRS prototype (Chance); First application of the Hitachi 10-channel system in clinics (Watanabe)
1999	First introduction of a 64-channel TRS system for adult optical tomography (Eda); First introduction of a 32-channel TRS system for infant optical tomography (Hebden); First optical tomography TRS images of the neonatal head (Benaron); Introduction of the first compact 8-channel TRS system (Cubeddu); TechEn company (USA) starts to release its first fNIRS commercial system
2000	Hitachi company starts to release its first commercial system: (ETG-100, 24 channels)
2001	First fNIRS study using a single-channel CW portable instrument and telemetry (Hoshi); Shimadzu company (Japan) starts to release its first commercial system: (OMM-2001, 42 channels); ISS Inc. (USA) starts to release the frequency domain system: Imagent (up to 128 channels); First three-dimensional CW tomographic imaging of the brain (DYNOT, NIRx Medical Technologies, US) (Bluestone)

2002	Hitachi company starts to release the ETG-7000 (68 channels)
2003	Hitachi company starts to release the ETG-4000 (52 channels) Artinis company (The Netherlands) starts to release the Oxymon MkIII (up to 96 channels)
2004	Shimadzu company (Japan) starts to release the NIRStation (64 channels) First simultaneous recording of DC-magneto encephalography and CW fNIRS data (Mackert)
2005	Hitachi company starts to release the ETG-7100 (72 channels)
2007	Shimadzu company starts to release the FOIRE-3000 (52 channels)
2009	fNIR Devices company (USA) starts to release a wearable 16-channel system for adult PFC measurements Hitachi company starts to release a battery operated wearable/wireless 22-channel system for adult prefrontal cortex measurements
2011	NIRx Medical Technologies company (USA) starts to release a battery operated wearable/wireless 256-channel system for adult frontal cortex measurements.

2.2.3 Oximetry and Hemodynamic Response

The variation in the concentrations of HbO and HbR in the brain tissue occurs according to the change in cognitive activity. Cerebral hemodynamic changes are related to functional brain activity through a mechanism called neurovascular coupling [2.7]. The Figure 2.3 and the following steps can be stated that the relation between oximetry and hemodynamic activation.

- Neurons consume energy (glucose) at the time of becoming activated.
- To metabolize the glucose Oxygen is required.
- Clusters of neurons being activated, there is an increased need for oxygen in that area.
- To neural tissue via HbO in the Blood Oxygen is transported.
- In the capillary beds, the oxygen exchange is occurred

- HbO giving up oxygen to the neural tissue is transformed into deoxygenated HbR [2.8].

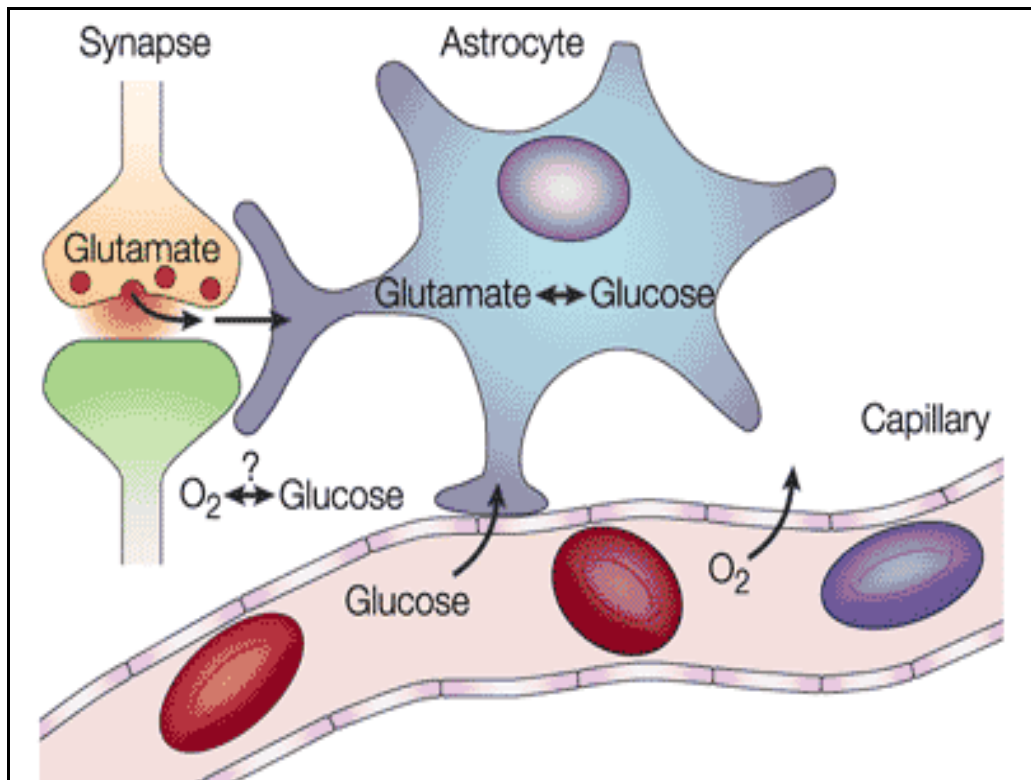


Figure 2.3: Relation between hemodynamic response and oxygen concentration [2.9]

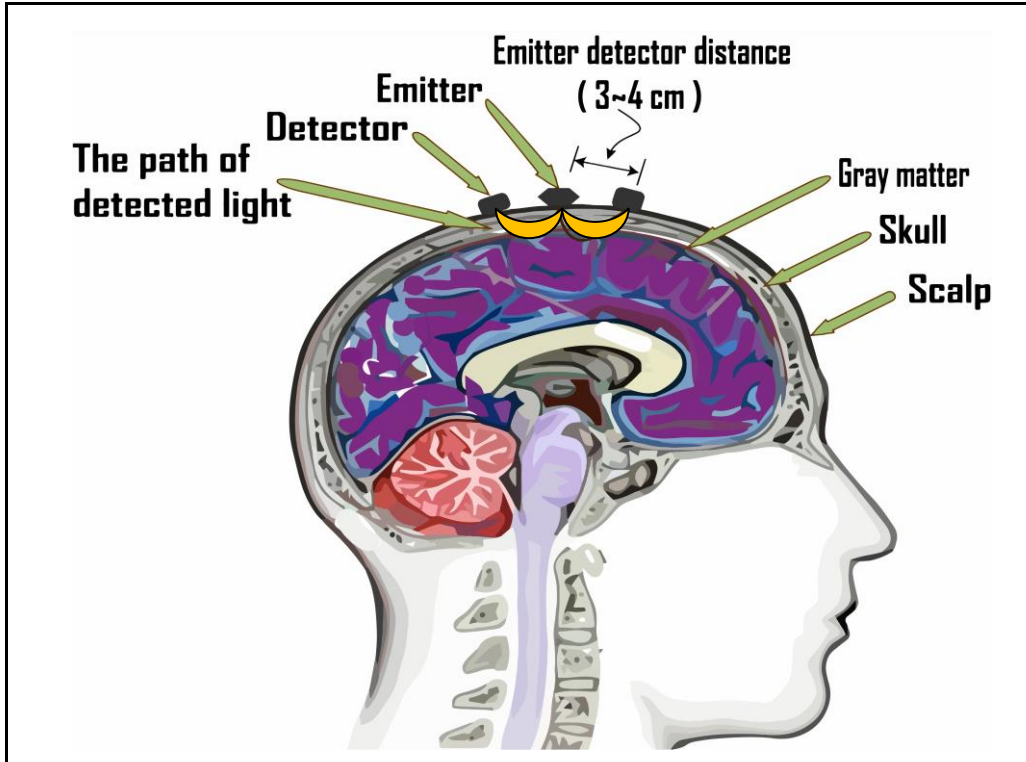


Figure 2.4: Position of fNIRS source and detector on human scalp

2.2.4 Mathematical Modeling of Oximetry

In training the detector and the IR emitter diode are placed 3-4 cm separately as Figure 2.4. It traces a banana-shaped path from emitter to detector like Figure 2.4 as NIR light enters the cerebrum. An array of sources and detectors, secured in a headband such as 16 channel FNIRS as in Figure 2.5, allows the hemoglobin concentrations measurement at various places in the cerebrum. Using the modified Beer-Lambert law, the attenuation of light between the source and detector can be formulated as [2.10],

$$I = I_{in}10^{-OD_{\lambda}} \quad (2.1)$$

Where OD_{λ} is the optical density at the wavelength λ . The optical density can be found as,

$$OD_{\lambda} = -\log \frac{I_{out}}{I_{in}} = Attenuation = A_{\lambda} + S_{\lambda} \quad (2.2)$$

Here A_λ and s_λ are the absorbing and scattering factors, respectively. In this case, main absorbers of light are blood chromophores HbO and HbR in the NIR spectra. Therefore, absorption of light can be formulated as,

$$A_\lambda = \sum_{i=Hb,HbO_2} \varepsilon_{i,\lambda} C_i L_\lambda \quad (2.3)$$

In (2.3), $\varepsilon_{i,\lambda}$, is the specific extinction coefficient of blood chromophore for wavelength λ and C_i is the concentration of blood chromophores and L_λ is the path-length of light at λ . Path-length is a very important parameter which can be expressed in terms of source detector separation as,

$$A_\lambda = d.DPF_\lambda \quad (2.4)$$

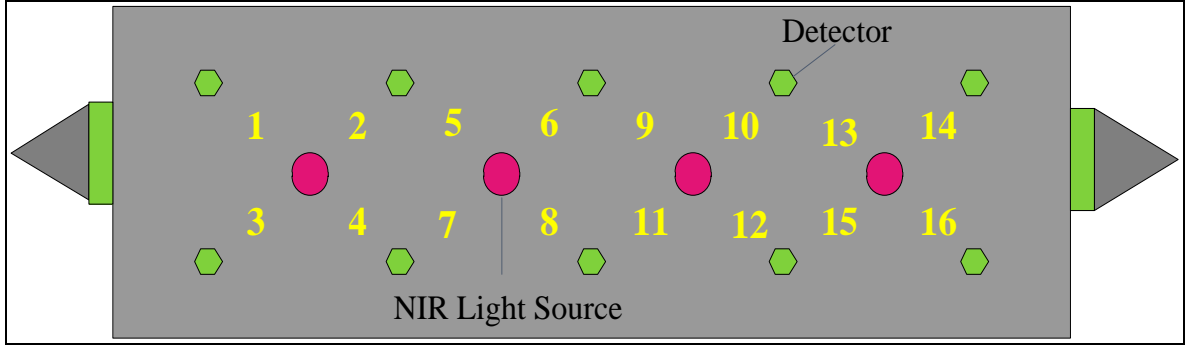


Figure 2.5: 16 Channel fNIRS compact band of source and detector

In (2.4), d is the linear difference between the light emitter and detector and the DPF stands for differential path factor. Differential path-length factor is the actual factor to correct the proper length of the light travels. DPF can apparently calculated as,

$$DPF_\lambda = \frac{1}{2} \left(\frac{3\mu'_{s,\lambda}}{\mu_{a,\lambda}} \right) \quad (2.5)$$

Where μ_a is the absorption coefficient, and $\mu'_{s,\lambda}$ is the reduced scattering coefficient at wavelength λ .

To remove the effect of scattering two successive measurements, yield the differential value of optical density and the procedure can be described as,

$$OD_\lambda = OD_{\lambda,final} - OD_{\lambda,initial}$$

$$= \sum_{i=Hb, HbO_2} \varepsilon_{i,\lambda} \cdot \Delta C_i \cdot d \cdot DPF_{\lambda} \quad (2.6)$$

Now the effect of scattering is cancelled. Since each chromophore has a specific extinction coefficient and differential pathlength factor, measurement with two wavelengths leads to:

$$\overline{\Delta OD} = \overline{M} \times \overline{\Delta C} \quad (2.7)$$

Where the values of OD, C, and M are given below.

$$\overline{\Delta OD} = \begin{bmatrix} OD_{\lambda_1} \\ OD_{\lambda_2} \end{bmatrix} \quad (2.8)$$

$$\overline{\Delta OC} = \begin{bmatrix} OC_{HbO_1} \\ OC_{Hb_2} \end{bmatrix} \quad (2.9)$$

$$M = \left(\begin{bmatrix} \varepsilon_{HbO_2, \lambda_1} & \varepsilon_{HbO_2, \lambda_2} \\ \varepsilon_{Hb, \lambda_1} & \varepsilon_{Hb, \lambda_2} \end{bmatrix} \times \begin{bmatrix} DFL_{\lambda_1} & 0 \\ 0 & DFL_{\lambda_2} \end{bmatrix} \right)^T \quad (2.10)$$

From (2.9) we get a transformation from light output change to change in blood chromophore concentrations. By using blood chromophore concentrations, we can define two parameters, namely, oxygenated blood concentration (*OXY*) and blood volume (*BV*) which are determined as [2.11]-[2.14],

$$OXY = \Delta C_{HbO_2} - \Delta C_{Hb} \quad (2.11)$$

$$BV = \Delta C_{HbO_2} + \Delta C_{Hb} \quad (2.12)$$

2.3 Types of fNIRS Technique

There are three different fNIRS techniques are used which are based on a specific type of illumination:

- (i) **The continuous wave (CW) modality-** which based on constant tissue illumination, simply measures light attenuation through the head.
- (ii) **The frequency-domain (FD) method-** which illuminating the head with intensity-modulated light, measure both attenuation and phase delay of emerging light.

(iii) **The time-domain (TD) technique-** which illuminating the head with short pulses of light, detects the shape of the pulse after propagation through tissues [2.15].

2.4 Main Characteristics of fNIRS Techniques

Different fNIRS instruments with related key features, advantages and disadvantages, and parameters measurable by using different fNIRS techniques is given in **Table 2.2**.

Table 2.2: Main characteristics and Measurable Parameter of fNIRS Techniques [2.6].

Main characteristics	fNIRS techniques-based instrumentation		
	Continuous wave	Frequency-domain	Time-domain
Sampling rate (Hz)	≤ 100	≤ 50	≤ 10
Spatial resolution (cm)	≤ 1	≤ 1	≤ 1
Penetration depth with a 4 cm source-detector distance	Low	Deep	Deep
Discrimination between cerebral and extra-cerebral tissue (scalp, skull, CSF)	N. A.	Feasible	Feasible
Possibility to measure deep brain structures	Feasible on newborns	Feasible on newborns	Feasible on newborns
Instrument size	Some bulky, some small	Bulky	Bulky
Instrument stabilization	N. R.	N. R	Required
Transportability	Some easy, some feasible	Feasible	Feasible
Instrument cost	Some low, some high	Very high	Very high
Telemetry	Available	Difficult	Not easy
Measurable parameter [O ₂ Hb], [HHb], [tHb]	Yes, changes	Yes, absolute value	Yes, absolute value

CSF= Cerebrospinal fluid, **HHb**= Deoxyhemoglobin, **N. A.** = not available, **N. R.** = not required, **O₂Hb**= Oxyhemoglobin, **tHb**= O₂Hb+HHb.

2.5 Main Fields of fNIRS Application

In recent year fNIRS develops rapidly, because of its advantages. The main application field of fNIRS like as brain structure and function research, brain computer interface, adaptive interface, monitoring of newborn, mental fatigue, medical rehabilitation etc is shown in bellow-[2.16].

Table 2.3: Fields of fNIRS application-

Field's	Application
Neurology	Alzheimer's Disease, Dementia, Depression, Epilepsy, Parkinson's Disease, Post-Neuro Surgery Dysfunction, Rehabilitation, Etc.
Psychiatry	Anxiety Disorders, Childhood Disorder's, Eating Disorders, Mood Disorder's, Personality Disorder's, Substances Related Disorder's, Schizophrenic Disorders, Etc.
Psychology/ education	Attention, Body Representation, Comprehension, Developmental Disorder's, Developmental Psychology, Emotion, Functional Connectivity, Gender Differences, Language, Memory, Social Brain, Etc.
Basic research	Brain Computer Interface, Fusion Neuroergonomics, Pain Research, Sleep Research, Sports Science Research

2.6 Chapter Summery

In this chapter various terms related with the study have been discussed. The basic concepts regarding these terminologies must be clear to understand this study, completely. Main characteristics and fields of fNIRS application are also discussed here.

REFERENCES

- [2.1] F. F. Jöbsis, “Noninvasive infrared monitoring of cerebral and myocardial oxygen sufficiency and circulatory parameters,” *Science*, vol. 198, no. 4323, pp. 1264–1267, December 1977.
- [2.2] T. G. Phan, and A. Bullen, “Practical intravital two-photon microscopy for immunological research: faster, brighter, deeper,” *Immunology and Cell Biology*, vol. 88, pp. 438-444, January 2010.
- [2.3] R. Mckendrick, R. Perasuraman, R. Murtza et al., “Into the wild: neuroergonomic differentiation of hard-held and augmented reality wearable display during outdoor navigation with functional near infrared spectroscopy,” *Frontiers in Human Neuroscience*, vol. 10, article 216, 2016.
- [2.4] R. Zimmermann, L. Marchal-Craspo, J. Edelmann et al., “Detection of motor excution using a hybrid fNIRS-BiosignalBCI: a feasibility study,” *Journal of NeuroEngineering andRehabilitation*, vol. 10, no 1. Article 4, 2013.
- [2.5] M. Amouroux, W. Uhring, T. Pebayle, P. Poulet, and L. Marlier, “A safe, low-cost and portable instrumentation for bedside time-resolved picosecond near infrared spectroscopy,” *Novel Optical Instrumentation for Biomedical Applications IV*, vol. 1, pp.7371-7377, July 2009.
- [2.6] M. Ferrari, V. Quaresima., “A brief review on the history of human functional near-infrared spectroscopy (fNIRS) development and fields of application,” *NeuroImage*, vol. 63, pp. 921-935, March 2012,
- [2.7] Y. Hoshi, “Towards the next generation of near infrared spectroscopy,” *Philosophical transactions of the royal society A*, vol. 369, pp. 4425-4439, November 2011.
- [2.8] J. S. Damoiseaux, S. A. R. B. Rombouts, F. Barkhof, P. scheltens, C. J. Stam, S. M. Smith, and C. F. Beckmenn, “Consistent resting state networks across healthy subjects,” *Proceeding of the national academy of sciences of the United States of America*, vol. 103, no. 37, pp. 13848-13853, February 2006.
- [2.9] D. J. Heeger & D. Ress, “What does fMRI tell us about neural activity?,” *Nature Reviews Neuroscience*, vol. 3, pp. 142-151, February 2002.

- [2.10] D. A. Gusnard, E. Akbudak, G. L. Shulman, and M. E. Raichle, "Medial prefrontal cortex and self-referential mental activity: Relation to a default mode of brain function," *Proceedings of the National Academy of Sciences of the United States of America*, vol. 98, no. 7, pp. 4259-4264, March 2001.
- [2.11] M. Izzetoglu, S.C. Bunce, K.Izzetoglu, B. Onaral, and K. Pourrezaei, "Functional brain imaging using near infrared technology," *IEEE Engineering in Medicine and Biology Magazine*, vol. 26, no. 4, July/August 2007.
- [2.12] Villringer and B. Chance, "Non-invasive optical spectroscopy and imaging of human brain function," *Trends in Neurosciences*, vol. 20, no. 10, pp. 435-442, October 1997.
- [2.13] H. Obrig and A. Villringer, "Beyond the visible- imaging the human brain with light," *Journal of Cerebral Blood Flow & Metabolism*, vol.23, no. 1, pp. 1-18, January 2003.
- [2.14] Y. Liu, H. Ayaz, A. Curtin, B. Onaral, and P. A. Shewokis, "Towards a hybrid p300-based BCI using simultaneous fNIR and EEG," *Springer-Verlag Berlin Heidelberg*, pp. 335-344, 2013.
- [2.15] G. Strangman, D. A. Boas, J. P. Sutton, "Non-invasive neuroimaging using near infrared light." *Society of Biol. Psychiatry*, vol.52, pp. 679-693, 2002.
- [2.16] J. J. Pan, X. J. Jiao, "New application, Development and aerospace prospect of fNIR," *Engineering*, vol. 5, pp. 47-52, May 2013.

CHAPTER III: Proposed Methodology

Chapter Outlines

3.1 Introduction

3.2 Data collection

3.3 Data Acquisition

3.4 Proposed Thesis Work

3.5 Filtering and Baseline Correction

3.6 Feature Extraction Using Conventional Method

3.7 Proposed Feature Extraction Method

3.8 Classification Methodology

3.9 Performance Measurement Criteria

References

CHAPTER III

Proposed Methodology

3.1 Introduction

In this section, proposed methodology has been widely discussed. This chapter covers the clarification about the data collections, modality specifications, preprocessing the fNIR signals, feature extracting methods, and classifications. In addition, the proposed method is also described with compared to the existing methodologies mentioning the novel contribution of this work.

3.2 Data Collection

The fNIRS data were collected by using two different tasks from two different laboratories. The left- and right-hand movements with and without pain data were taken for conventional methods and for the proposed method.

3.2.1: Imagery Hand Movement with Pain Data: The imagery hand movement with pain data have been collected from the School of Oral Medicine of Taipei Medical University (TMU) in collaboration with the University of Canberra (UC), Australia.. The data consists of left hand and right-hand imagery movement with pain of seven participants. The data consists of both HbO and HbR concentration data.

3.2.2 Imagery Hand Movement without Pain Data: The Imagery hand movement without pain fNIRS data has been collected from the Neuroimaging Laboratory of the Department of Biomedical Engineering, Khulna University of Engineering & Technology (KUET). The data contain 16 channel fNIRS data of HbO and HbR of four participants (age=22±1.5). Each participant performed 20 trials of each task (imagery left hand, iLH) and (imagery right hand, iRH).

3.3 Data Acquisition

Hemodynamic measurement was performed using an optical topography system. The topography system uses functional near-infrared spectroscopy (fNIRS) to investigate cerebral hemodynamics. Optical topography makes use of the different absorption spectra of oxygenated and deoxygenated hemoglobin in the near infrared region. The fNIRS system produces two different wavelengths of fNIRS signals through frequency-modulated laser diodes. These fNIRS signals are transmitted to the brain using optical fiber emitters. Near-infrared light penetrates head tissue and bone, generally it reaches 2 to 3 cm into the cerebral cortex. Once fNIRS light reaches the cerebral cortex, it is absorbed by hemoglobin, while the non-absorbed fNIRS signals are reflected to the source, where it is sampled by a high-sensitivity photodiode. NIR light between emitters and detectors is sampled at a given time point named channels. Since Oxy-hemoglobin (HbO) and Deoxy-hemoglobin (HbR) absorb NIR light differently, two wavelengths of light are used. In this way, it is possible to read these two types of hemoglobin simultaneously. Data has been collected from two different laboratories by using two different procedures. The total experimental procedure for the collection of data has been described elaborately below.

3.3.1 Experimental Setup for Imagery Hand Movement with Pain

The experiment was designed by the School of Oral Medicine of Taipei Medical University (TMU) in collaboration with the University of Canberra (UC), Australia. In the present study, seven healthy individuals (3 females, 4 males) participated in the experiment, aged 25 to 35 years old. All participants provided written consent and the experiment was approved by the Ethics Committee of TMU. The experiment was carried out in the Brain Research Laboratory at TMU in a quiet, temperature (22-24°C) and humidity (40-50%) controlled room. The experiments were done in the morning (10:00am-12:00pm) and each experiment lasted around 30 minutes. Quantitative data was collected using the ETG-4000 with the patients sat down in an ergonomic chair near the topography system. The sampling period was 0.1 sec. and the sampling frequency was 10Hz. The wavelength range of each data was between 695-830nm. The experiment was designed to recognize left and right arm imagery movement with pain stimulation and pain release in patients through hemodynamic responses. In order to identify the imagery hand movement with pain through fNIRS, acupuncture was used to induce pain stimulation in a safe manner. Brand new acupuncture needles were used for each experiment, and using

traditional Chinese acupuncture techniques that were performed by an acupuncturist of TMU Hospital. The puncture point used for stimulation was the “Hegu Point”, located on top of the hand, between the thumb and forefinger. This acupuncture point (acupoint) is known by its property to relieve pain, especially headaches and toothaches. This acupoint is also used to reduce fever, eliminate congestion in the nose, stop spasms, and decrease toothache. A western name for this acupoint is “the dentist’s point” because it can stop tooth pain while moist the throat and tongue. This point was used because it is an area of easy access and the hand can be set aside while the patient is relaxed on the chair. Each patient was punctured on both hands which has shown in Figure 3.1, one hand on a day and the opposite hand on another day; each hand was treated as a separated experiment. The data base was organized of 12 data sets of changes in Hemoglobin files, two sets (right and left hands) per each subject.



Figure 3.1: Patient with acupuncture needle in Hegu point.

Three types of pain stimulations (acupuncture techniques) were applied for the imagery hand movement in the experiment, needle insertion (Task 1, T1), needle twirl (Task 2, T2), and needle removal (Task 3, T3). The first type of stimulation (T1) was carried out 30

seconds after the start of experiment and it lasted for 6 seconds. The second type of stimulation (T2) was applied for 30 seconds (rest time) after T1 and it lasted for 10 seconds, this stimulation was repeated three times after 30 second resting time. The last stimulation (T3), was carried out after the third application of task 2, and it lasted for 5 seconds with a 30 seconds recovery time and 15 seconds post-time to finish the experiment. The patients were explained about the acupuncture procedure and experiment. In addition, patients were given a brief explanation of side effects of acupuncture in case they had any symptoms during the experiment; no side effects were reported during and after experiment. After the briefing, the patient was told to sit down on the chair, told to relax and close the eyes to reduce visual evoked stimulation. The optical topography system was set to record after all conditions were met and patient was relaxed. Tasks and time description in the data for one channel has shown in figure 3.2.

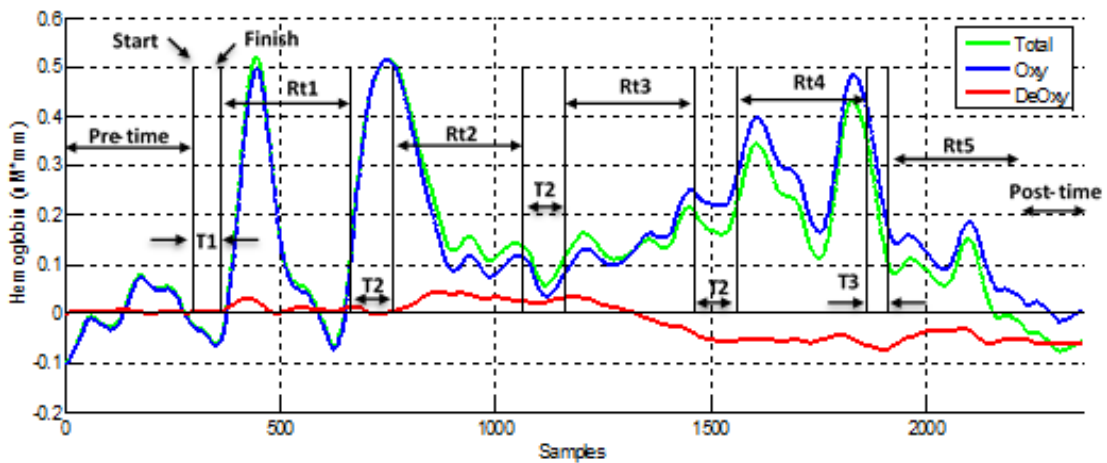


Figure 3.2. Tasks and time description in the data, one channel only.

3.3.2 Experimental Setup for Imagery Hand Movement without Pain

In this study, a continuous-wave functional brain imaging system (Biopac 1200 fNIR imager) was used to acquire the brain signal from the dorsolateral prefrontal cortex (DLPFC) and the data acquisition sampling rate was 2 Hz. The sensor pad of this device contains 16 channels with 4 NIR light and 10 detectors.

Four healthy subjects among them 3 male (mean age) and 1 female (mean age 24.5 ± 2.5 years) participated in the experiment. All subjects are right handed based on the recommendation of Edinburg Handedness Inventory. All subjects had no history of psychiatric, neurological or visual disorder, no pain in both hands, and they are all

informed verbally about the experimental protocol. The data acquisition procedures regarding motor imagery hand movement data without pain have been completed in the NeuroImaging Laboratory of the department of Biomedical Engineering of Khulna University of Engineering & Technology (KUET).

Furthermore this side of the head band is kept on the skin of DLPFC or forehead. The head band is placed on forehead in such way that the bottom row of detectors will be located just above the eyebrows [3.1]. Thus, the detectors can detect the total activation of the prefrontal cortex of the brain. A subject wearing the fNIRS head band while data acquisition was going on, is shown in Figure 3.3. This figure illustrates the procedure to place the head band on DLPFC.

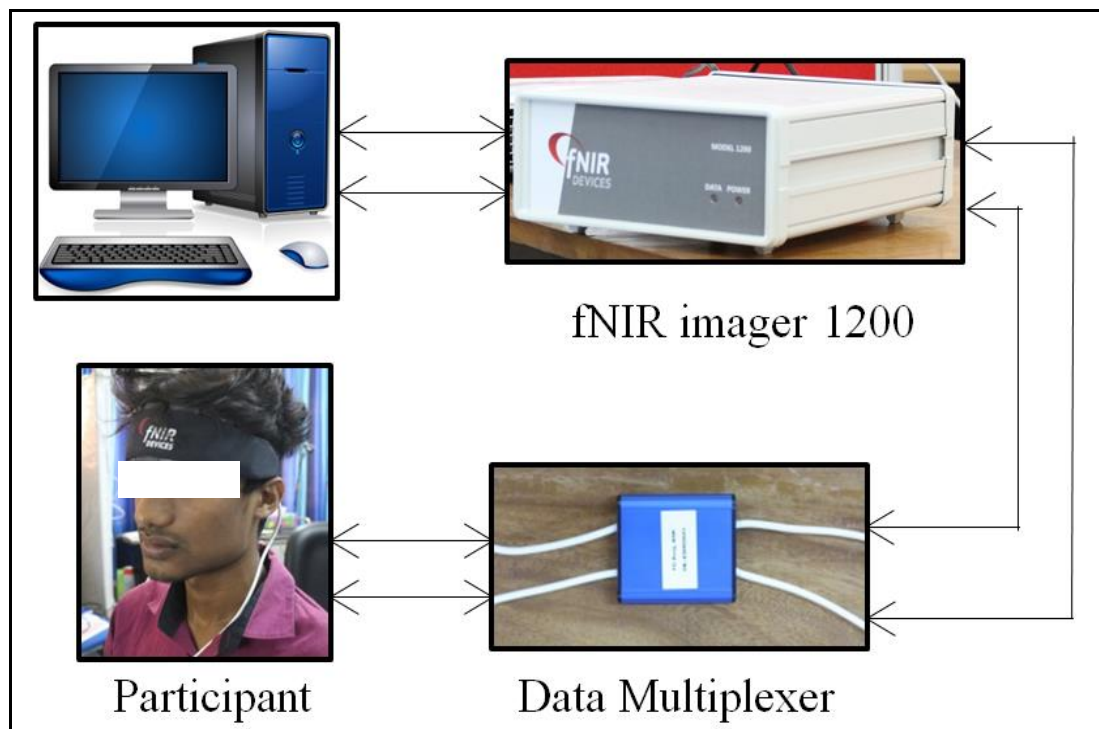


Figure 3.3: Total hardware connection including sensor pad, imager, data multiplexer, and computer.

All the data of a participant of left hand (LH) and right hand (RH) imagery movements were within one file as distributed as 5 sec task with 15 sec rest. The data acquisition paradigm with necessary steps is given in Figure 3.4.

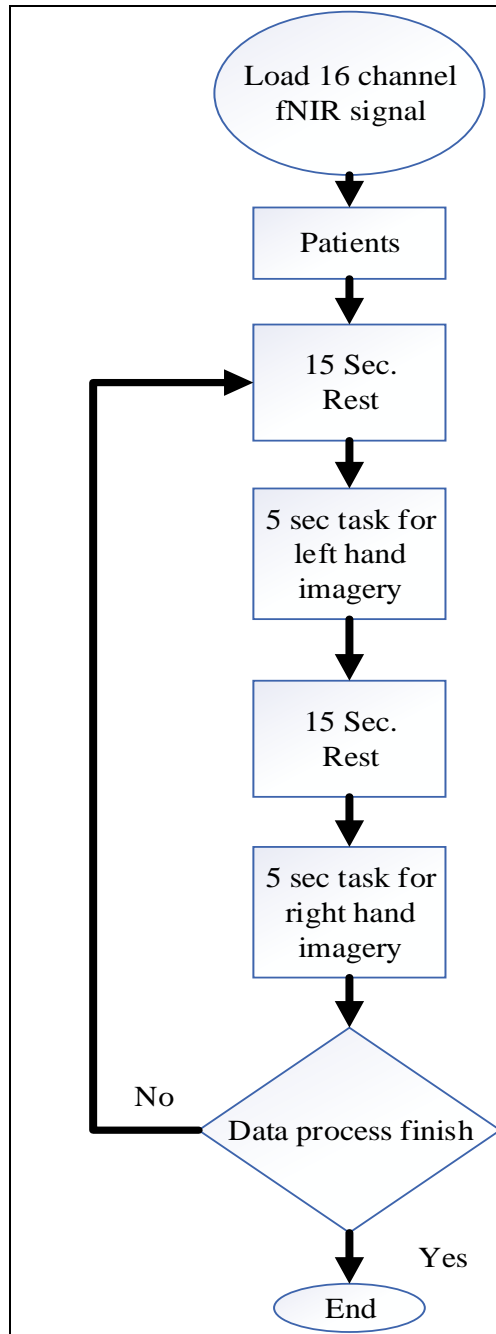


Figure 3.4: Scheduling of the performed tasks. This pattern has followed 20 times by each participant which gave 20 trials of every imagery tasks.

3.4 Proposed Thesis Work

MATLAB simulation software is used to analyze the fNIRS data. HbO and (HbR data were analyzed differently. For same person right arm's data and left arm's data were analyzed differently. Raw fNIRS signal is filtered by lowpass FIR filter by hamming

window considering the cutoff frequency as 0.1Hz. For the raw data processing, fNIRS soft (v4.4) [3.2] has been used in this thesis work. This software was used to convert the optical data to hemoglobin concentration data. The other analytical results like filtering, data segmentation, CSP and SCSP transformation, feature extraction, and classifications were performed by MATLAB 2017a. The block diagram of proposed methodology is given in Figure 3.5.

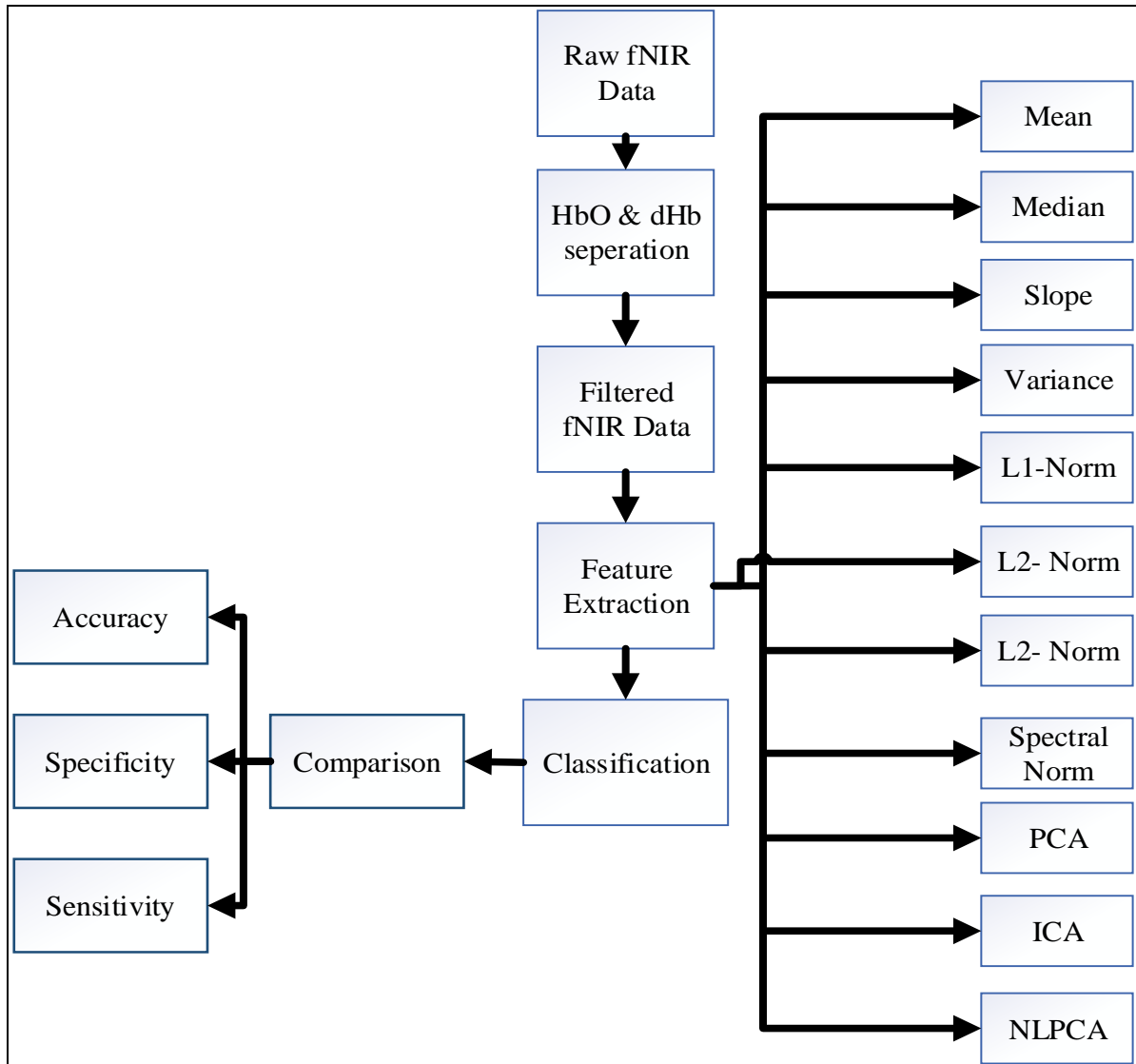


Figure 3.5: Block diagram of proposed methodology

The data of two simple features-mean and median have been extracted from all dataset. For special features extraction, PCA, NLPCA, and ICA are used. For feature extraction, the raw data's are loaded and then using some methods or algorithms to extract the features. Some very common feature of any signal like mean, median, slope, variance, L₁-

norm, L_2 -norm, L_∞ -norm, spectral norm [3.3] are extracted here. The extracted features are then classified by using different classifier such as ANN, KNN, SVM, and LDA. The classification methods are evaluated by their specification like accuracy, sensitivity and specificity.

3.5 Filtering and Baseline Correction

Since the raw fNIRS data is high degree of noisy drift, to filter the noisy fNIRS signal generally a low pass filter based on FIR hamming window method is applied. The sampling period was 0.1 sec. and the sampling frequency was 10Hz and the wavelength range of each data was between 695-830nm for conventional method. The order of FIR filter should be considered as 20 for 2Hz fNIRS signal for proposed method. The cut-off frequency should be taken 0.1 Hz because meaningful information remains usually inside the band [3.4]. For each trial of the fNIRS data had been corrected by subtracting baseline from the original signal. Baseline was calculated from the average of the first five seconds of the task. This consideration helps to represent the activation in such a way that the starting of the task, the hemodynamic activation remains at the baseline.

3.6 Feature Extraction Using Conventional Method

For feature extraction, the raw data are loaded and then using some methods or algorithms to extract the features. Some very common feature like mean, median, slope, variance, L_1 -norm, L_2 -norm, L_∞ -norm, spectral norm are extracted here. Two important feature of fNIRS data, PCA and ICA are used to find the principal components and the independent components. For the non-linearity of the signal, non-linear principal components are also extracted.

3.6.1 Mean

For a data set, the terms arithmetic mean, mathematical expectation, and sometimes average is used synonymously to refer to a central value of a discrete set of numbers: specifically, the some of the values divided by the number of values [3.5]. The arithmetic means of a set of numbers x_1, x_2, \dots, x_n is typically denoted by, pronounced “x bar”. If the data set were based on a series of observations obtained by sampling from a statistical population, the arithmetic mean is termed the sample mean. For matrix, S is a row vector containing the mean value of each column if S is the mean.

3.6.2 Median

The median is the value separating the higher half of a data sample, a population, or a probability distribution, from the lower half. In simple terms, it may be thought of as the "middle" value of a data set [3.6]. For example, in the data set {1, 3, 3, 6, 7, 8, 9}, the median is 6, the fourth number in the sample. The median is a commonly used measure of the properties of a data set in statistics and probability theory. The median normalized angular frequency of the power spectrum of the time domain signal in vector form can be used as a feature. It has units of radians/second. If x is a matrix, median normalized angular frequency computes the median frequency of each column in X independently. It uses a rectangular window when computing the spectrum. The median frequency is defined as the frequency at which the power spectrum is divided into two equal areas via rectangular integral approximation.

3.6.3 Slope

Suppose, there are n data points $\{(x_1, y_1), (x_2, y_2), \dots, (x_n, y_n), i = 1, 2, 3, \dots, n\}$. The function that can describes all x and y can be represented as,

$$y_i = \alpha + \beta x_i + e_i \quad (3.1)$$

Here, e_i is the error in linear estimation for the data point (x_i, y_i) . Suppose we consider a line as (3.4) through our data set. It is true that all points do not touch the line. Therefore, a measure of the discrepancy can be determined by sum of the squared errors (SSE). The equation of SSE is as (3.5).

$$y = \alpha + \beta x \quad (3.2)$$

$$SSE = s = \sum_{i=1}^n e_i^2 = \sum_{i=1}^n (y_i - \alpha - \beta x_i)^2 \quad (3.3)$$

To achieve the best fit we have to minimize the error. Therefore differentiating (3.5) with respect to α and β we get (3.6) and (3.7)

$$\frac{\partial s}{\partial \alpha} = -2 \sum_{i=1}^n (y_i - \alpha - \beta x_i) \quad (3.4)$$

$$\frac{\partial s}{\partial \beta} = -2 \sum_{i=1}^n x_i (y_i - \alpha - \beta x_i) \quad (3.5)$$

If, we want to reach the best linear fit or for minimum error, (3.6) and (3.7) will be zero. This gives us,

$$\alpha + \beta\bar{x} = \bar{y} \quad (3.6)$$

$$\alpha\bar{x} + \beta\bar{x}^2 = \bar{x}\bar{y} \quad (3.7)$$

Eventually, from (3.8) and (3.9), it can be shown that,

$$\begin{aligned} \hat{\beta} &= \frac{\sum_{i=1}^n (x_i - \bar{x})(y_i - \bar{y})}{\sum_{i=1}^n (x_i - \bar{x})^2} \\ &= \frac{1/n(x_i y_i) - \bar{y} \sum_{i=1}^n x_i - \bar{x} \sum_{i=1}^n y_i + n \bar{x} \bar{y}}{\sum_{i=1}^n x_i^2 - 2\bar{x} \sum_{i=1}^n x_i + n\bar{x}^2} \\ &= \frac{\bar{x}\bar{y} - \bar{x} \bar{y}}{\bar{x}^2 - \bar{x}^2} = \frac{\text{cov}[x, y]}{\text{var}[x]} \end{aligned} \quad (3.8)$$

Consequently, $\hat{\alpha} = \bar{y} - \hat{\beta}\bar{x}$ and the required slope is $\hat{\beta}$ of the best linear fit of data points [3.7].

3.6.4 Variance

The variance is a numerical value used to indicate how widely individuals in a group vary. If individual observations vary greatly from the group mean, the variance is big and vice versa. It is important to distinguish between the variance of a population and the variance of a sample. The variance of a population is denoted by σ^2 and the variance of a sample by s^2 .

The variance of a population is defined by the following formula:

$$\sigma^2 = \sum (x_i - \bar{x})^2 / N \quad (3.9)$$

Where σ^2 is the population variance, \bar{x} is the population mean, x_i is the i th element from the population, and N is the number of elements in the population [3.8].

The variance of a sample is defined by the slightly different formula:

$$s^2 = \sum (x_i - \bar{x})^2 / (n-1) \quad (3.10)$$

Where s^2 is the sample variance, \bar{x} is the sample mean, x_i is the element from the sample, and n is the number of elements in the sample. Using this formula, the variance of the

sample is an unbiased estimate of the variance of the population. So the variance is equal to the square of the standard deviation.

3.6.5 L₁-Norm

L₁ norm also known as mean norm or latest absolute deviation (LAD). It is calculate from the sum of the absolute values of the dataset [3.9].

$$L_1 - norm = \sum_{k=1}^n |x_k| \quad (3.11)$$

L₁ is the sum of the magnitudes of the vectors in a space. It is the most natural way of measure distance between vectors that is sum of the absolute difference of the components of the vectors. In this norm all the components of the vector are weighted equally.

3.6.6 L₂-Norm

L₂ norm is the mean square norm or latest square norm and illustrate as the square root of the sum of the absolute values of the dataset [3.10].

$$L_2 - norm = \sqrt{\sum_{k=i}^n |x_k|^2} \quad (3.12)$$

Where $|x_k|$ on the right denotes the complex module. The L₂ norm is the vector norm that is commonly encountered in vector algebra and vector operations, where it is commonly denoted $|x|$. However if desired a more explicit notion $|x|_2$ can be used to emphasize the distinction between the vector norm $|x|$ and complex modulus $|z|$ together with the fact that the L₂ norm is just one of several possible types of norms.

For real vectors, the absolute value sign indicating that a complex modulus is being taken on the right of equation (3.13) may be dropped. So, for example, the L₂ norm of the vector $x = (x_1, x_2, x_3)$ is given by

$$|x| = \sqrt{x_1^2 + x_2^2 + x_3^2} \quad (3.13)$$

L₂ is the shortest distance to go from one point to another.

3.6.7 L_∞ Norm

L_∞ norm also known as max norm or uniform norm and describe as the maximum of the absolute values of the dataset [3.11].

$$L_\infty - norm = \max|x_i| \quad (3.14)$$

L_∞ norm gives the largest magnitude among each elements of a vector.

3.6.8 Principle Component Analysis (PCA)

PCA is a linear transformation technique that uses the orthogonal transformation method to convert a set of related variables to a set of linearly uncorrelated variables. The first principal component belongs the largest possible variance and other succeeding components have the highest possible variance obeying orthogonal to each other components. The derivations of principal components are based on the consideration that the signal is Gaussian distributed. Therefore, a random process with zero-mean can be characterized by $R_x = E[xx^T]$. The principal components of the signal $x(t)$ are linearly mixed by uncorrelated sources as $\zeta(t) = [\zeta_1, \zeta_2, \dots, \zeta_N]$. Therefore, we can present it as [3.12],

$$w = \zeta^T x, \quad (3.15)$$

Where $w = [w_1, w_2, \dots, w_N]^T$ is the mixing matrix those are mutually uncorrelated. We can obtain the first principal component by performing a scalar product, $w_1 = \zeta_1^T x$, where the ζ_1 is chosen according to the relation given below.

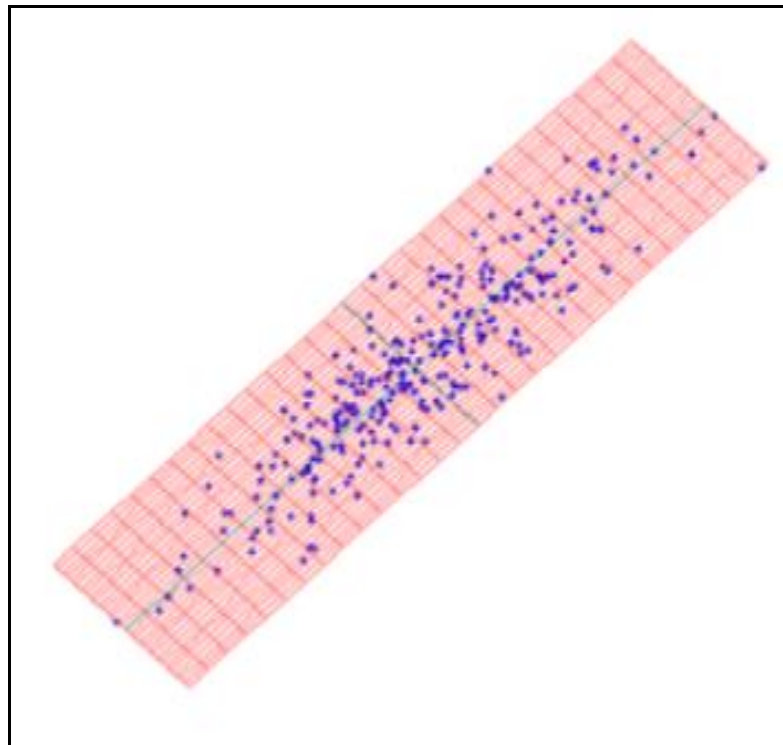
$$\begin{aligned} E[w_1^2] &= E[\zeta_1^T x x^T \zeta_1] \\ &= \zeta_1^T R_x \zeta_1, \end{aligned} \quad (3.16)$$

$E[w_1^2]$ is generally maximized considering the constraint $\zeta_1^T \zeta_1 = 1$. The maximal variance can be achievable if ζ_1 is taken into account as the normalized eigenvector regarding to the largest eigenvalue of R_x that can be denoted by λ_1 . Therefore, the resulting variance is following:

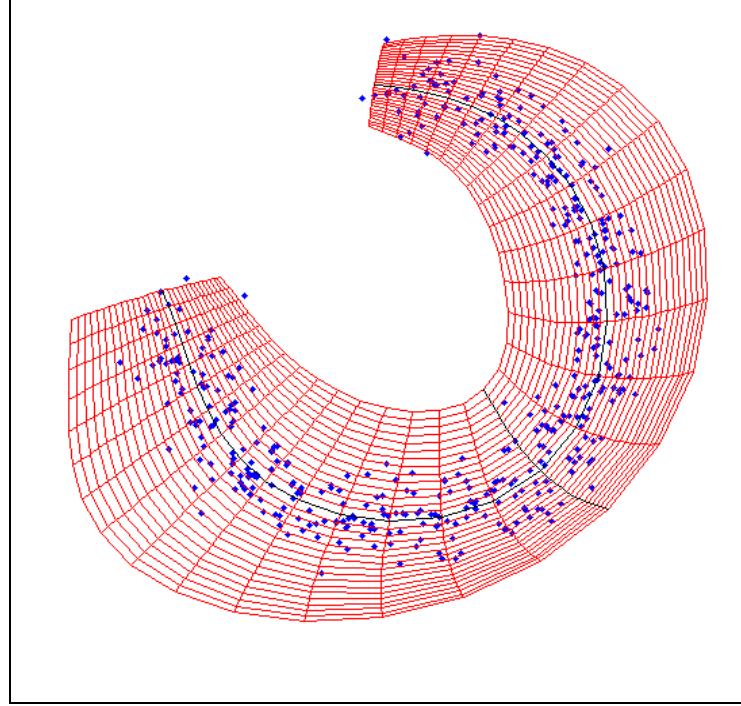
$$E[w_1^2] = \zeta_1^T R_x \zeta_1 = \lambda_1 \Psi_1^T \Psi_1 \quad (3.17)$$

3.6.9 Nonlinear PCA (NLPCA)

When we consider the data distribution is obeying normal or Gaussian distribution function, PCA transformation could be the solution. Nonetheless, in case of non-Gaussian distributed variables, PCA cannot be proper solution for dimensionality reduction. Therefore, we need nonlinear PCA or NLPCA. NLPCA is generally performed by the help of ANN addition with an auto associative architecture. This procedure is also known as auto encoder, bottle-neck, replicator network, or sandglass type network [3.13]. This type of network is a multi-layer perceptron that generally performs to evaluate an identity mapping which means that the network output is essential to be identical regarding the input. The middle portion of the aforesaid network is a layer which works like a bottleneck where dimensionality reduction of the data is enforced. Such a layer actually provides the desired component values (scores). The required component spaced of Linear PCA and NLPCA are shown in Figure 3.6(a) and Figure 3.6(b), respectively.



(a)



(b)

Figure 3.6: (a) Standard PCA applied to a simple two-dimensional data set & (b) Nonlinear PCA (auto encoder neural network) applied to a 3/4 circle with noise [3.14].

3.6.10 Independent Component Analysis (ICA)

ICA is a powerful tool that is able to separate independent sources from a linearly mixed signal formed by several sensors. Let $X_t = (x_{t1}, \dots, x_{tm})'$ be the observed m -dimensional stationary data vector. These data vector is generated by a linear combination of $r \times m$ unobserved components as [3.15],

$$X_t = As_t, \quad t=1,2,\dots,T \quad (3.18)$$

Where, A is a $m \times r$ full rank parameter matrix, $s_t = (s_{t1}, \dots, s_{tr})'$ is the vector of latent components, which are assumed mutually independent. Generally, in ICA model, neither A nor s_t are known and the problem is to estimate both from the observations (X_1, \dots, X_T) .

For the solution of the problem arisen in ICA is to find an $r \times m$ matrix B such that the components of $\hat{s}_t = BX_t$, where $t=1,2,3,\dots,T$, are as independent as possible. Therefore, for identification we need- (a) $Var(s_t) = I_r$, (b) No more than one IC is Gaussian distributed, and (c) In ICA model it is assumed that $r = m$.

Before applying the ICA algorithm, it is beneficial to perform a pre-whitening of the data. This method transforms the data into a set of new variables those are uncorrelated and have unit variance [3.16]. Mathematically, we search a linear transformation of X_t ,

$$Z_t = VX_t, \quad (3.19)$$

Where, M is a $r \times m$ matrix, such that the r -dimensional vector Z_t , with $r \leq m$, have identity covariance matrix:

$$T_z(0) = E\{Z_t Z_t'\} = I_r \quad (3.20)$$

Then, the ICs are estimated by searching a rotation of the standardized principal components,

$$\hat{s}_t = WZ_t, \quad (3.21)$$

Data whitening ensures that considered all dimensions are equally treated. Here, well-known algorithm Fast ICA is used.

3.7 Proposed Feature Extraction Method

In this thesis work, we have used a slightly modified approach of common spatial pattern named by standardized common spatial pattern (SCSP). Our proposed SCSP based feature extraction method can improve the classification accuracy higher than that of conventional CSP method. According to the design proposal of filtering weight matrix of SCSP, a standard pattern of response is considered to estimate the covariance of the total trials. From the results of the covariance with respect to the standard response the weight matrix is constructed by weighted average method instead of gross averaging (as done in CSP). It prevents the negative effect of the trials having no positive response for imagery events.

3.7.1 Common Spatial Pattern and Its Modification

Common spatial pattern or CSP is a filtering technique for feature extraction that was firstly proposed for classification of multiple channel motor imagery EEG signal in [3.17]. The basic concept behind CSP is using a linear transformation to project the multiple channel information into comparatively lower dimensional spatial subspace. This linear transformation actually maximizes the variance of two classes signal pattern.

For single trial fNIRS data (either HbO or HbR) during left and right hand imagery movements, the mathematical implementation techniques of CSP based filter can be presented through the following approach. Suppose that, π_{LH} and π_{RH} denote the preprocessed fNIRS data matrices of iLH and iRH movements, respectively. The dimensions of the previous matrices (π_{LH} & π_{RH}) are $C \times S$, where C and S represent the number of total channels and number of samples per channel, respectively.

Therefore, the normalized spatial covariance (NSC) of LH and RH can be calculated as,

$$H_L = \frac{\pi_{LH} \pi_{LH}^T}{\text{trace}(\pi_{LH} \pi_{LH}^T)} \quad (3.22)$$

$$H_R = \frac{\pi_{RH} \pi_{RH}^T}{\text{trace}(\pi_{RH} \pi_{RH}^T)} \quad (3.23)$$

Here, π^T is the transpose of π and $\text{trace}(\nabla)$ sums the diagonal elements of the corresponding matrix ∇ . The average NSC \bar{H}_L and \bar{H}_R are calculated considering all the trials of each group. Eventually, the overall spatial covariance (OSC) can be estimated as,

$$H = \bar{H}_L + \bar{H}_R \quad (3.24)$$

This is a conventional approach which is slightly questionable. In our proposed approach, we have slightly modified this concept to make the OSC. Our proposed technique questions that all the trials do not possess the same range of covariance in the context of fNIRS data. In some trials, it may be found that the covariance of two tasks is very small over all the channels. As a result, we have calculated covariance coefficient (CC) of all the trials of the fNIRS data with a standard iLH or iRH movement related fNIRS data. According to the values of CC, the OSC is calculated by weighted average approach we name it global spatial covariance (GSC). This GSC method can be able to differentiate the spatial pattern of two classes better than the OSC approach. Eventually, the GSC calculating method can be presented as,

$$H = \frac{1}{2(n-1)} \left(\sum_{i=1}^{n-1} \alpha_i \bar{H}_{Li} + \sum_{i=1}^{n-1} \beta_i \bar{H}_{Ri} \right) \quad (3.25)$$

Here, n is the number of trials are taken into account to prepare the GSC matrix, α and β are the CC weights in case of iLH and iRH, respectively. The overall procedure of

calculating the modified common spatial pattern based filtering weight matrix, W_{sp} has been shown in Figure 3.7.

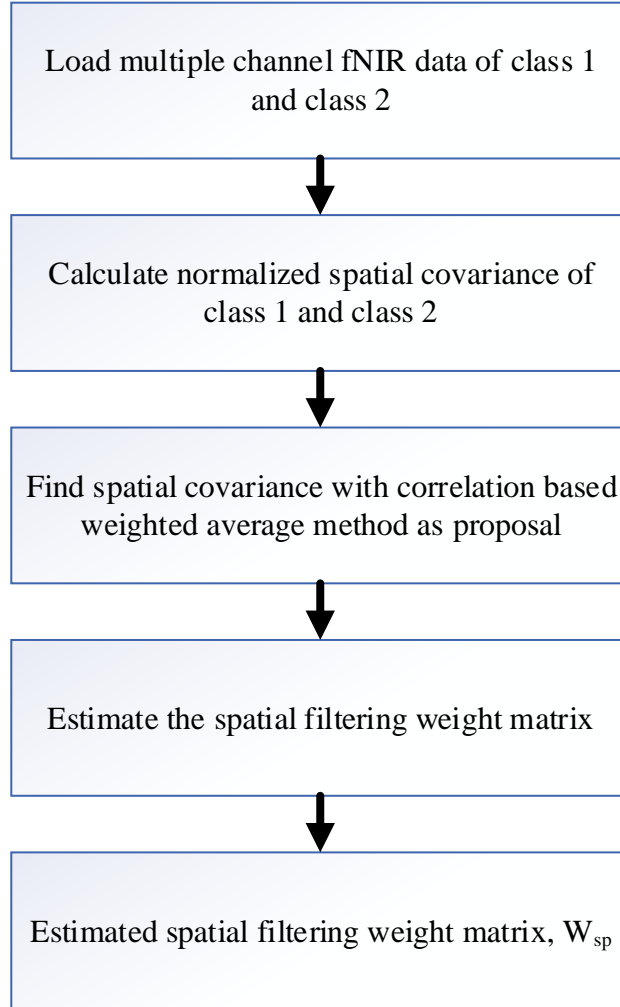


Figure 3.7: Flow diagram of spatial filtering weight matrix estimation technique for modified common spatial pattern

With the help of W_{sp} , fNIRS signals of any class can be filtered where the extracted feature will be expected to show significant variance for the training the classifier. Now, this covariance matrix H can be factorized as the following manner given in (3.26)

$$H = U_0 \Sigma U_0^T \quad (3.26)$$

Where matrix U_0 consists of eigenvectors and Σ is a diagonal matrix that contains the eigenvalues of the decomposition. From the relation found in (3.26), a whitening transformation matrix can be estimated through rules of linear algebra as,

$$W = \Sigma^{-\frac{1}{2}} U_0^T \quad (3.27)$$

Transform the average covariance matrices as

$$S_{LH} = W \bar{H}_L W^T \quad \text{and} \quad S_{RH} = W \bar{H}_R W^T \quad (3.28)$$

From the relation given in (3.28) we found that both covariance matrix S_{LH} and S_{RH} are sharing the same eigenvectors. As a result, the sum of their regarding eigenvalues will always be one. Since the relation can be written as,

$$S_{LH} = U \Sigma_{LH} U^T ; S_{RH} = U \Sigma_{RH} U^T ; \Sigma_{LH} + \Sigma_{RH} = 1 \quad (3.29)$$

Eventually, the eigenvectors found for S_{LH} corresponding to the largest eigenvalues should provide the lowest eigenvalues for S_{RH} . This relation is also inversely applicable. The transformation for fNIRS data whitening onto the eigenvectors of the largest eigenvalues in Σ_{LH} and Σ_{RH} are optimal for separating the variances of the matrices regarding the corresponding signal. Therefore, projection matrix, Ψ of this consequence can be formulated as,

$$\Psi = U^T P \quad (3.30)$$

With the values found in the projection matrices Ψ , the original fNIRS can be re-formed into some uncorrelated components as,

$$\Omega = \Psi \pi \quad (3.31)$$

Ω can be taken as fNIRS source elements comprising common and specific elements of two different tasks. The original fNIRS data, π can be reconstructed by,

$$\pi = \Psi^{-1} \Omega \quad (3.32)$$

Where, Ψ^{-1} is the inverse matrix of Ψ . The every columns of Ψ^{-1} are considered as spatial patterns, those can be envisaged as distribution vectors of fNIRS sources. The most spatial patterns are the first and last columns of Ψ^{-1} that bring out the highest variance of one task and the smallest variance of the other.

The inverse form of the projection matrix helps to make the signal variance sharper between the data of two events than that of the actual one. This effective method facilitates to extract more significant features that can be able to discriminate the two classes. Therefore, using the conventional CSP and the proposed SCSP method, the features are extracted from the signals. As features, we have calculated mean, slope, and variance according to the recommendation of [1.8]. It is previously described that how the 16-channel were reduced to 4-channel (Considering the 4 regions of interest: LL, LM, RM, and RL). These three features were extracted from each of the regions of interests. Therefore, the feature vector of each task for a trial become $3 \times 4 = 12$. It can be represented as the Figure 3.8. The features are extracted from the signal considering the window length 2-7sec because this window length of the signal is more effective for feature extraction and motor imagery event classification for the fNIR signals [3.18].

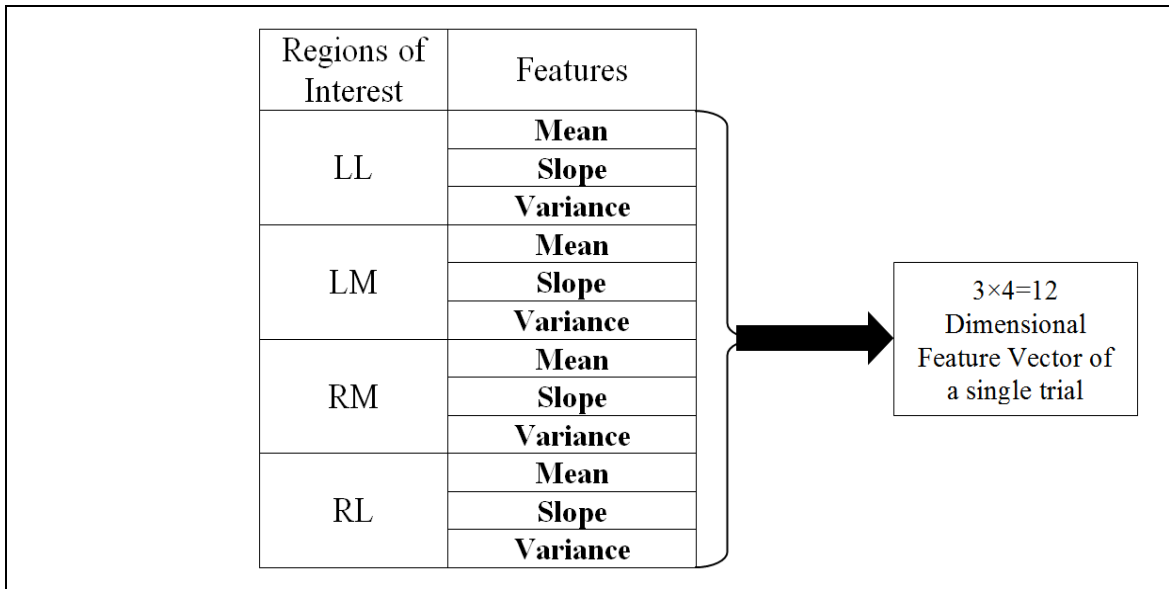


Figure 3.8: Pattern of extracted features to be loaded in a classifier for training and testing.

3.8 Classification Methodology

For classification of the extracted feature, some methods are used. Artificial Neural Network (ANN), k-Nearest Neighbor Algorithm (kNN), Support Vector Machine (SVM), and Linear Discriminant Analysis (LDA) are used for classification. LDA classifier is used to train a predictive network for the further classification of two class fNIR signal regarding imagery movements. Additionally, other classifiers like ANN, kNN, SVM, etc. can be applied, as well to check the effect of classification accuracy enhancement. The procedure can be presented by the following flow diagram given in Figure 3.9.

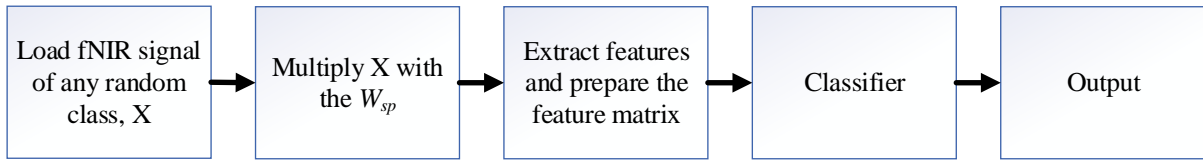


Figure 3.9: fNIR signal classification by proposed method

Since this method filters the original multiple channel signals and transformed it to a single channel signal with maximum variance over all the spatial variance of the signals, definitely it provides better accuracy than that of multiple channel signal classification method. The classification methods are evaluated by their specification like accuracy, sensitivity and specificity. Using these parameter different decisions can be taken and it can be used for further processing. Using this specification, which method is more accurate or more sensitive, that can be determined. Using these, relation among different persons and relation between right arm and left arm can be established.

3.8.1 Artificial Neural Network (ANN)

ANN is a processor which is parallel distributed and it is made of a number of simple processing units. All these units are known as neuron. ANN is a unique technique of artificial intelligence that is able to mimic the comporment of human brain [3.16]. For the feed forward networks, commonly multilayer preceptors consist of three type layers: input, output, and hidden layer. A typical model of multilayer preceptors of ANN is illustrated in Figure 3.10.

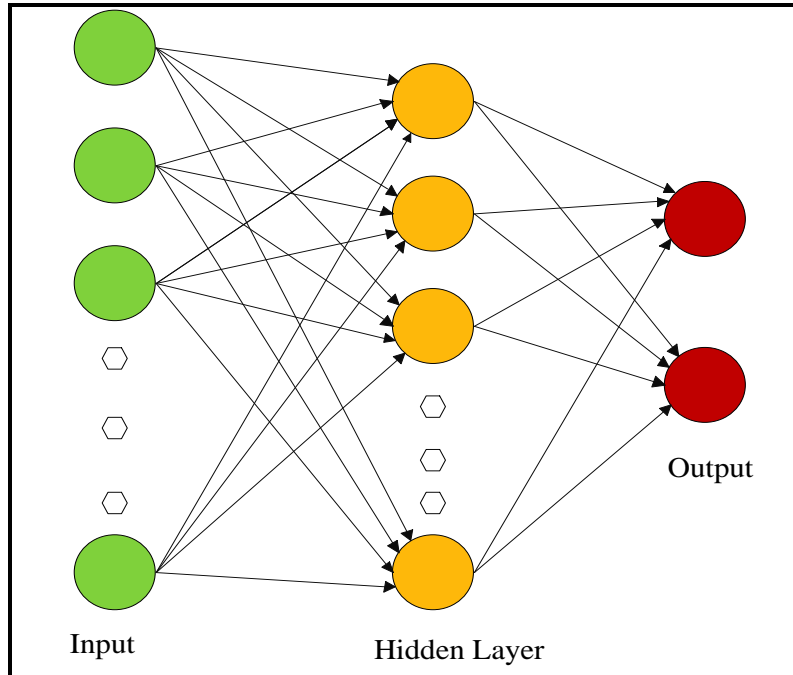


Figure 3.10: Architecture of artificial neural network

The objective of input layer is to buffer the distribution of the input signals x_n ($n=1, 2, 3, \dots$) towards the hidden layer neurons. Each hidden layer neuron adds the input signals (x_n) after weighting the input signals by the strengths W_{nj} from the input layer and calculated the output, Y where Y is as a function of their summations [1.16].

$$Y_j = f\left(\sum_{n=1}^n W_{jn}x_n\right) \tag{3.33}$$

Here j represents the neuron numbers. In addition, this function can be sigmoidal or radial basis or hyperbolic tangent function. It provides the change, ΔW_{jn} by back propagation algorithm which is actually the weight of a connection between n and j according to the relation, $\Delta W_{jn} = \eta \delta_j x_n$. Here η is rate of learning parameter and δ_j depends on whether j is an input or hidden neuron.

3.8.2 k-Nearest Neighbor Algorithm (kNN)

kNN is considered as a non-parametric method in pattern recognition which is used for classification and regression. The input of k-NN consists of the k closest training examples in the considered feature space [3.19].

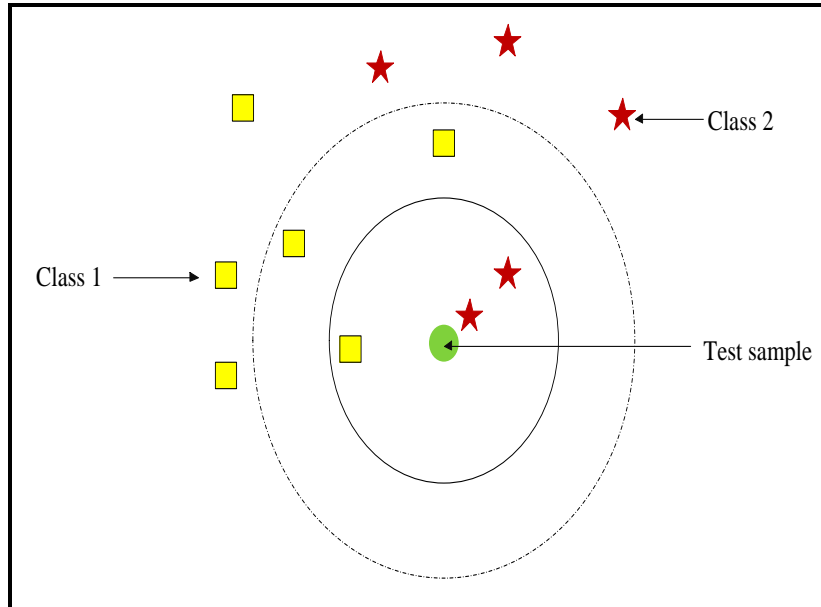


Figure 3.11: Example of kNN classification.

For classification by kNN, the output of this network is a class membership. An object is always classified by the mainstream vote of its neighbors and with the assigned object for the most common class midst of the k nearest neighbors. If k is considered as 1, then the assigned object is single nearest neighbor. In case of kNN regression, the property value for the object is considered as the output. This value is actually the mean value of their k nearest neighbors. For both classification and regression, weight to the contributions of the neighbors can be assigned so that the nearer neighbors can contribute supplementary to the mean than the more distant ones. As for an example, suppose a common weighting scheme consists in providing each neighbor a weight of $1/d$. Here d represents distance to the neighbor. Generally, the neighbors are assigned from a set of objects so that the class value can be known. We can observe the Figure 3.11 where the test sample marked as green circle should have to be classified either to the first class of yellow squares. Besides, it may be the second class those are marked as red stars. If $k = 3$, it is assigned to the second class since, there exist 2 stars and only 1 square inside the inner circle.

3.8.3 Support Vector Machine (SVM)

SVM is a discriminative classifier that can be defined by an isolating hyperplane. Besides, supervised training data of this algorithm creates an optimal hyperplane that classifies the features [1.13]. This is actually a set of supervised learning methods which are used for classification and regression. In the field of machine learning, SVM can create

hyperplanes of very high dimensions that facilitates this method for high classifying performance. If the feature space is big enough it works well. But for the lower feature spaces SVM sometimes provides lower classifying accuracy. Therefore, for high classifying accuracy, SVM should be trained with a very big size of feature value.

From the Figure 3.12 we can easily observe a typical model of SVM. Here, two different colors are assigned to represent the features of two different classes. A hyperplane is estimated by SVM algorithm that clearly separates the feature spaces and classified the two different classes. This hyperplane can be either of straight line or radial basis. For nonlinear property of the SVM hyperplane, kernel based radial method is often used to separate the classes. Basically, this type of method is necessary when the class sizes are big.

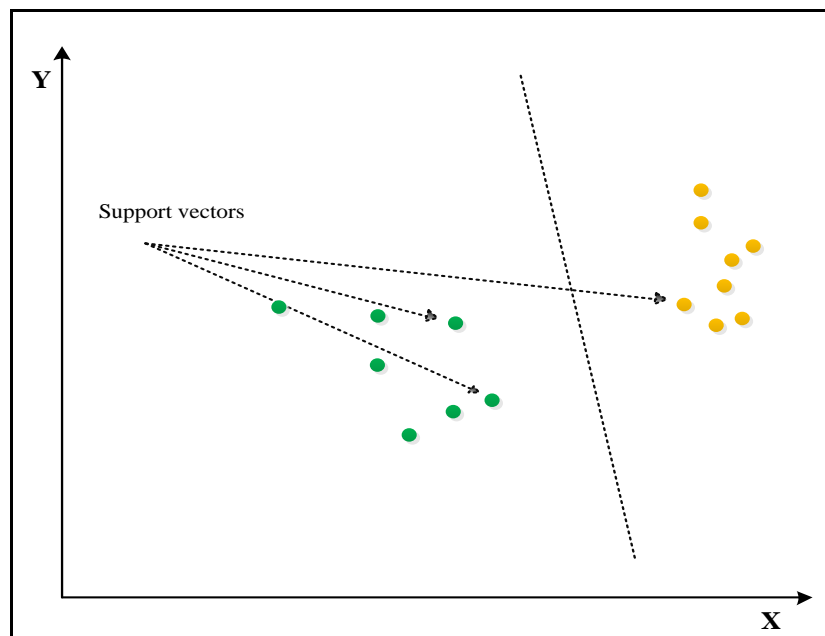


Figure 3.12: A model of hyperplane that differs the feature space.

3.8.4 Linear Discriminant Analysis

Linear discriminant analysis is a widely used binary decision classifying technique mostly used in case of non-dependency of the variance or covariance matrix on the population. Suppose that we have a set of observations \bar{x} for two known classes, Y_1 and Y_2 . The features having in the set is called the training set. Therefore, through the LDA technique it is obligation to find a good predictor for the predefined classes for a given new data feature. A demo presentation of LDA classification on the feature space can be presented by the Figure. 3.13.

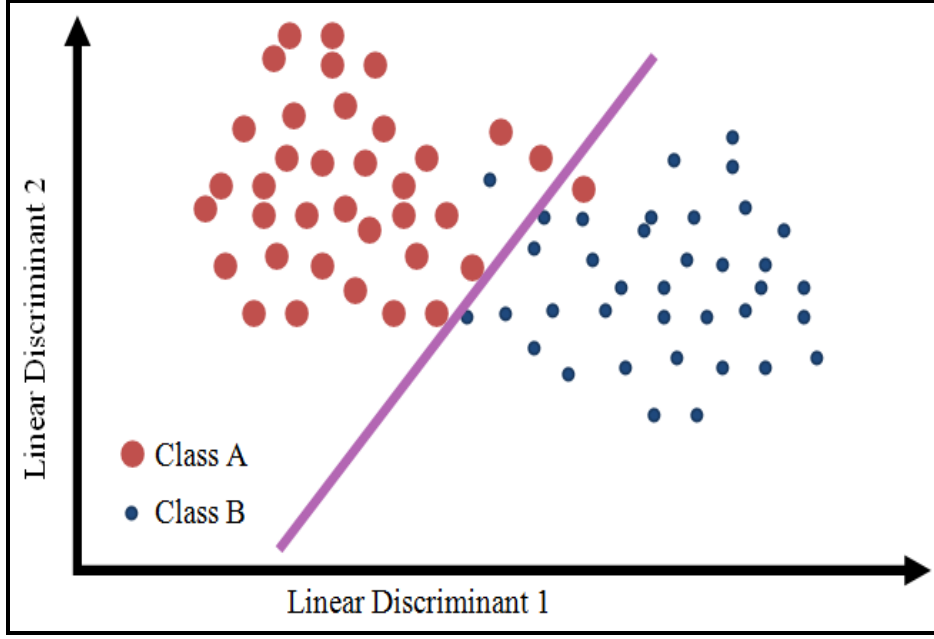


Figure 3.13: Illustration of LDA classification method

For a given population Φ_i , the probability density function of x can be considered to be multivariate normal where their mean vector is μ_i and variance-covariance matrix is θ_i . According to the formula of LDA estimation [3.20],

$$f(x|\Phi_i) = \frac{1}{(2\pi)^{n/2}|\theta|^{1/2}} \exp\left[-\frac{1}{2}(x-\mu_i)'\theta^{-1}(x-\mu_i)\right] \quad (3.34)$$

Where, n is the number of features. Through LDA, it is to classify the population for which $p_i f(x|\Phi_i)$ is maximum. Here p_i is the prior probability and can be estimated as,

$$p_i = \Pr(\Phi_i); i = 1, 2, \dots, N (N = \text{number of population}) \quad (3.35)$$

Because of being monotonic of this log transformation, this is equivalent to event classification of the population so that $\log [p_i f(x|\Phi_i)]$ is largest. The score on LDA space is calculated as [3.21],

$$\hat{\delta}_i(x) = x \cdot \frac{\hat{\mu}_i}{\sigma^2} - \frac{\hat{\mu}_i^2}{2\sigma^2} + \log(p_i) \quad (3.36)$$

where, $\hat{\delta}_k$ is LDA score, $\hat{\mu}_i$ is the average found from the training observations, and σ^2 is the weighted average of the sample variances.

In this thesis work, LDA is used for its simplicity. In addition, LDA mostly depends on the statistical pattern of the signals. If the nature of the signal is statistically separable,

LDA should provide good result. This is why the results through LDA classifier are more acceptable.

3.9 Performance Measurement Criteria

The performances of the classifiers were determined by the calculation of sensitivity, specificity, and total classification accuracy by the following relationships.

$$\text{Sensitivity (True positive rate)} = \frac{TP}{TP + FN} \quad (3.37)$$

$$\text{Specificity (True negative rate)} = \frac{TN}{TN + FP} \quad (3.38)$$

$$\text{Total classification accuracy} = \frac{TN + TP}{TN + FN + TP + FP} \quad (3.39)$$

Where,

Total number of correctly classified positive patterns = TP ,

Total number of actual positive patterns = $TP+FN$

Total number of correctly classified negative patterns = TN

Total number of actual negative patterns = $TN + FP$

Total number of correctly classified patterns = $TN + TP$

Total number of applied patterns = $TN + FN + TP + FP$.

3.10 Chapter Summary

In this chapter the mathematical details for the governing methods of the thesis work has been discussed with proper graphical representations and technical details of the applicability of the methods. A block diagram is presented to show the steps of working procedure. The short outcome of the procedure is also discussed slightly. In the next chapter, all the results have been presented with discussion.

REFERENCES

- [3.1] N. Naseer, M. J. Hong, and Keum-Shik Hong, "Online binary decision decoding using functional near infrared spectroscopy for the development of brain–computer interface," *Experimental Brain Research*, vol.232, no.2, pp. 555-564, February 2014.
- [3.2] H. Ayaz, "Functional near infrared spectroscopy based brain computer interface," PhD Thesis, Drexel University, Philadelphia, 2010.
- [3.3] Monson H. Hayes "Statistical Digital Signal Processing and Modeling", John Wiley & Sons, Inc. ISBN: 978-0-471-59431-4.
- [3.4] H. Ayaz, P. A. Shewokis, S. Bunce, K. Izzetoglu, B. Willems, and B. Onaral, "Optical brain monitoring for operator training and mental workload assessment," *NeuroImage*, vol. 59, pp. 36-47, 2012.
- [3.5] Feller and William, "Introduction to Probability Theory and its Applications," Vol I. Wiley. p. 221.
- [3.6] David J. Sheskin, "Handbook of Parametric and Nonparametric Statistical Procedures: Third Edition," CRC Press. pp. 7, 2003.
- [3.7] M. A. Rahman and M. Ahmed, "Lie Detection from Single Feature of Functional Near Infrared Spectroscopic (fNIRS) Signals" International Conference on Electrical and Electronic Engineering, December 27-29, 2017, Rajshahi University of Engineering and Technology, Rajshahi, Bangladesh.
- [3.8] Available in: <https://stattrek.com/statistics/dictionary.aspx?definition=variance>.
- [3.9] Available in Weisstein, Eric W. "L¹-Norm." From MathWorld--A Wolfram Web Resource. <http://mathworld.wolfram.com/L1-Norm.html>.
- [3.10] Available in Weisstein, Eric W. "L²-Norm." From MathWorld--A Wolfram Web Resource. <http://mathworld.wolfram.com/L2-Norm.html>.
- [3.11] Available in Weisstein, Eric W. "L[∞]-Norm." From MathWorld--A Wolfram Web Resource. <http://mathworld.wolfram.com/L-InfinityNorm.html>.
- [3.12] H. Abdi & J. L. Williams, "Principal Component Analysis-Wiley Interdisciplinary Reviews: Computational Statistics," 2 (4): 433–459, 2010.

- [3.13] Matthias Scholz, "Validation of nonlinear PCA," *Neural Processing Letters*, vol. 36, no. 1, Pages 21-30, 2012.
- [3.14] Matthias Scholz, "Nonlinear PCA : Nonlinear PCA toolbox for MATLAB," Available in : <http://www.nlpca.org/>
- [3.15] A. Hyvärinen and E. Oja, "Independent Component Analysis: Algorithms and Applications," *Neural Networks*, 13(4-5):411-430, 2000.
- [3.16] A. Hyvärinen, "Independent component analysis: recent advances," *Philosophical Transaction of Royal Society A*, vol. 371, no. 20110534, 2013.
- [3.17] H. Ramosar, J. M. Gerking, and G. Pfurtscheller, "Optimal spatial filtering of the single trial EEG during imagined hand movement," *IEEE Transactions on Rehabilitation Engineering*, vol. 8, no. 4, pp.441-446, 2000.
- [3.18] S. Haykin, "Neural Network and Learning Machines," 3rd Edition, Pearson Education Inc., New Jersey, 2009.
- [3.19] Available in : <https://machinelearningmastery.com/k-nearest-neighbors-for-machine-learning/>
- [3.20] Available in: <https://newonlinecourses.science.psu.edu/stat505/node/94/>.
- [3.21] Available in: http://uc-r.github.io/discriminant_analysis.

CHAPTER IV: Experimental Results and Discussions

Chapter Outlines

4.1 Introduction

4.2 Experimental results for Conventional Method

4.3 Experimental results of Imagery Hand Movement

4.4 Result Analysis

4.5 Comparison between the Results of the Proposed Work and
Existing Works

4.6 Chapter Summary

References

CHAPTER IV

Experimental Results and Discussions

4.1 Introduction

The technical outcomes and the analytical results of the whole study have been discussed in this chapter with suitable numerical values, tables, and graphs based on two types of database.

4.2 Experimental Results for Conventional Method

In conventional method it is already discussed that the data of left hand and right-hand imagery movement with pain was acquired by 24 channel ETG4000 fNIR system. The fNIR signals of 24 channels for a specific task of participants 1 is shown in Figure 4.1. For the right-hand and left hand, the fNIR data changes in different pattern. Sample results of fNIR data for left arm and right arm are given in Figure 4.2, where data corresponding to channels 19 to channel 24 are presented. This data presents the oxygenated hemoglobin (HbO) change in case of left arm and right arm imagery movement with pain stimulation. First of all, all raw fNIR data is filtered by lowpass FIR filter with cutoff frequency 0.1 Hz. From these filtered data, various features are extracted those are mean, median, linear PCA, nonlinear PCA, ICA components. Using these individual features of left arm and right arm data are classified by four well-known classifying techniques named by ANN, kNN, SVM and LDA. Based on the features, different classifying tools showed different accuracy for different participants. Using Artificial Neural Network, the classification of the featured data can be achieved by setting the target and hidden layer size. By the accuracy and sensitivity, the classification can be justified by comparing with others. In ANN, it has the confusion matrix from which accuracy of test, training and validation can be measured. For person 2, right arm of HbO data, the confusion matrix (for SVM) is given in Figure 4.3.

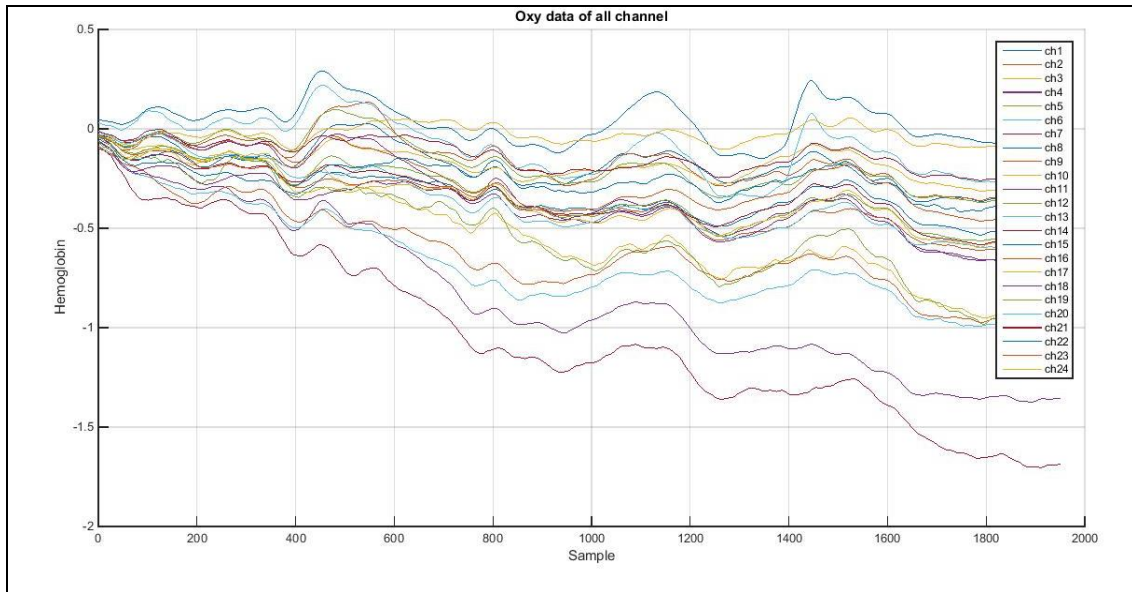


Figure 4.1: HbO data for all 24 channel for participant 1 right arm.

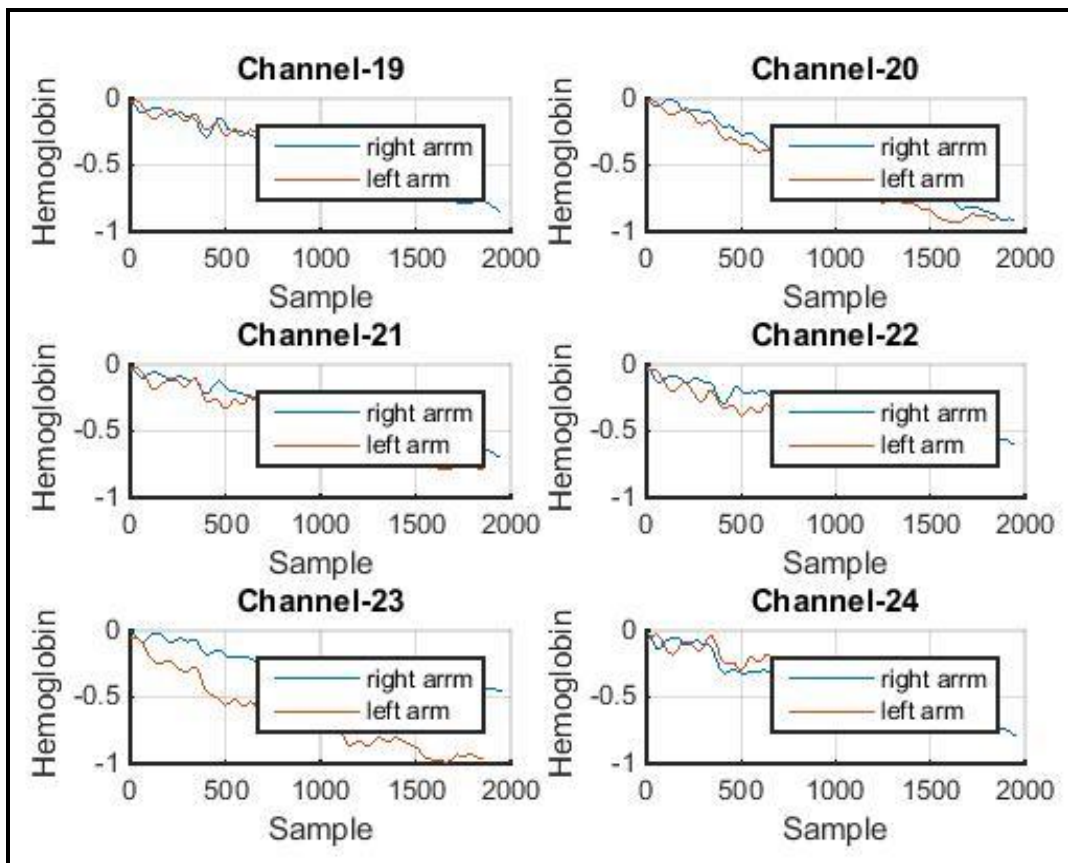


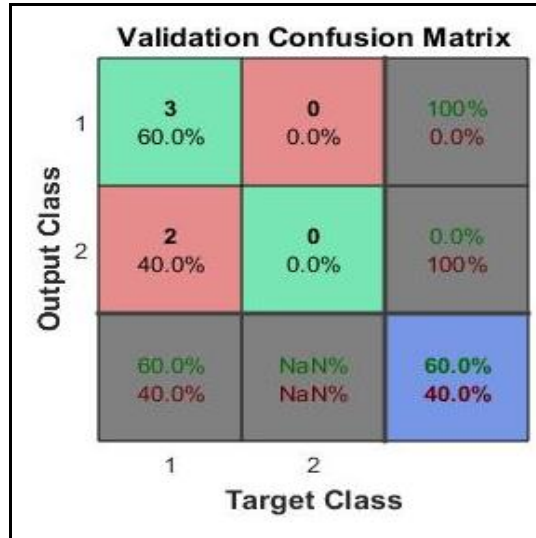
Figure 4.2: HbO data from left and right hand of same participant (ch19-ch24).

	1	2	
1	15 88.2%	0 0.0%	100% 0.0%
2	2 11.8%	0 0.0%	0.0% 100%
	88.2% 11.8%	NaN% NaN%	88.2% 11.8%
	1	2	
	Target Class		

(a)

	1	2	
1	2 100%	0 0.0%	100% 0.0%
2	0 0.0%	0 0.0%	NaN% NaN%
	100% 0.0%	NaN% NaN%	100% 0.0%
	1	2	
	Target Class		

(b)



(c)

Figure 4.3: Confusion matrix for SVM (of HbO data for participant 2 right arm).

The classification accuracy and their specificity and sensitivity for all the methods are also calculated and the results are reported by the **Table 4.1**. These results present the report of 7 different participants. From these results we get overall concept about the performance of features and classifiers for fNIRS data classifications. Here the network is fed by data of oxygenated hemoglobin (HbO) change.

From the comparisons among the **Table 4.1**, we actually found that the classifying accuracy in average SVM is best than the other. In addition, with that, ANN classifies better than SVM. By similar process, fNIRS data of seven participants are classified to identify the left hand and right-hand imagery movement with pain stimulation. From the all results, the average accuracies, sensitivities, specificities of classifications are calculated for individual classifiers based on the features.

Table 4.1: Classification Performance of Participants 1-7.

Participants 1-7 (HbO)									
<i>For right arm</i>									
Feature Extraction Method	ANN			kNN			SVM		
	Accuracy (%)	Sensitivity (%)	Specificity (%)	Accuracy (%)	Sensitivity (%)	Specificity (%)	Accuracy (%)	Sensitivity (%)	Specificity (%)
Mean	80.0	82.5	81.8	80.0	81.0	81.4	82.4	83.2	83.5
Median	74.2	79.5	78.6	77.5	78.8	79.0	79.5	80.2	81.0
L ₁ -Norm	79.5	76.5	75.8	77.2	75.4	74.0	79.0	78.5	77.9
L ₂ -Norm	80.2	81.2	78.7	78.5	77.5	79.2	81.4	80.5	81.5
L _∞ -Norm	76.0	77.3	75.5	74.5	75.2	74.7	78.8	79.5	76.7
Spectral Norm	78.5	79.0	78.0	75.8	76.0	75.6	78.8	77.5	78.8
PCA	84.0	86.3	85.7	84.9	85.6	86.7	86.6	87.6	87.9
ICA	83.5	85.5	86.5	84.5	85.8	87.1	86.5	87.0	88.4
NLPCA	84.5	87.7	88.3	85.5	86.0	88.3	87.7	88.3	89.3
<i>For left arm</i>									
Mean	80.0	81.4	80.3	80.3	80.1	80.2	80.1	82.2	82.7
Median	78.0	81.7	79.1	78.7	80.7	79.7	78.7	81.7	81.3
L ₁ -Norm	81.0	80.7	77.7	77.3	75.3	75.1	79.4	79.1	78.7
L ₂ -Norm	81.0	79.7	79.7	78.7	77.7	78.7	79.3	78.3	80.3
L _∞ -Norm	80.0	77.1	76.3	74.3	75.7	75.2	78.2	78.1	76.4
Spectral Norm	84.5	79.1	78.1	76.7	77.7	78.3	78.2	77.2	79.6
PCA	84.0	83.3	85.1	84.7	85.3	86.1	85.4	86.1	86.7
ICA	85.0	84.4	86.8	84.7	85.3	87.1	86.4	87.1	88.8
NLPCA	85.5	86.1	88.2	86.1	86.4	88.3	87.5	88.2	89.3

Finally, these results in Table 4.1 reveal that which feature is more suitable than the other for a specific classifier.

The comparison for ANN, it is found that the features of PCA and NLPCA, NLPCA for kNN and NLPCA for SVM give highest accuracy in average as shown in Figure 4.4 & 4.5. For sensitivity case, the feature PCA, ICA, NLPCA for left arm and NLPCA for right arm in the ANN classifier. PCA, ICA and NLPCA for kNN and all features show highest sensitivity for SVM classifier as shown in Figure 4.6 & 4.7. Figure 4.8 & 4.9 shows the feature PCA, ICA & NLPCA has highest specificity in ANN, kNN, SVM classifiers. On the Other hand, in case of SVM the highest accuracy is achieved by the features of NLPCA. The average accuracy results of different features are given in Figure 4.4 - 4.9 and **Table 4.1**. Therefore, the features showing lower classifying accuracy those should be considered insignificant for that classifier. In to this bargain, kNN & SVM provides the nice accuracy and best among the considered classifiers. For the features: PCA, ICA, and NLPCA, it provides almost 90% classifying accuracy. In addition, the other two features PCA and ICA are also classified by k-NN with almost 90% average accuracy which is also quite satisfactory. Besides, the sensitivity and specificity of kNN & SVM are also at the highest level.

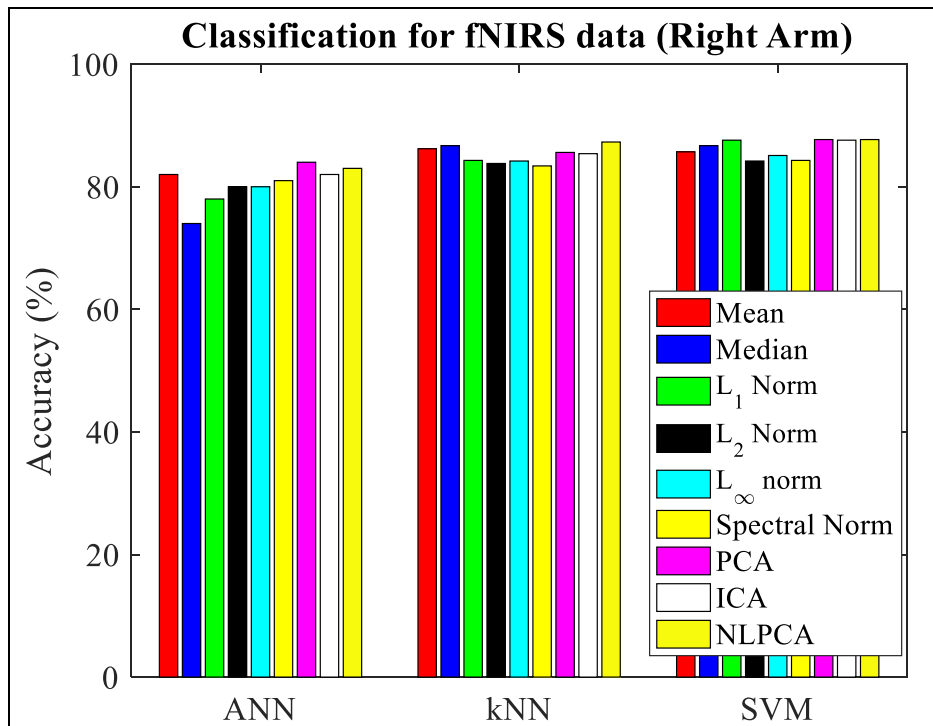


Figure 4.4: Comparison of average accuracy of ANN, kNN, SVM for different features for right arm of 7 patients.

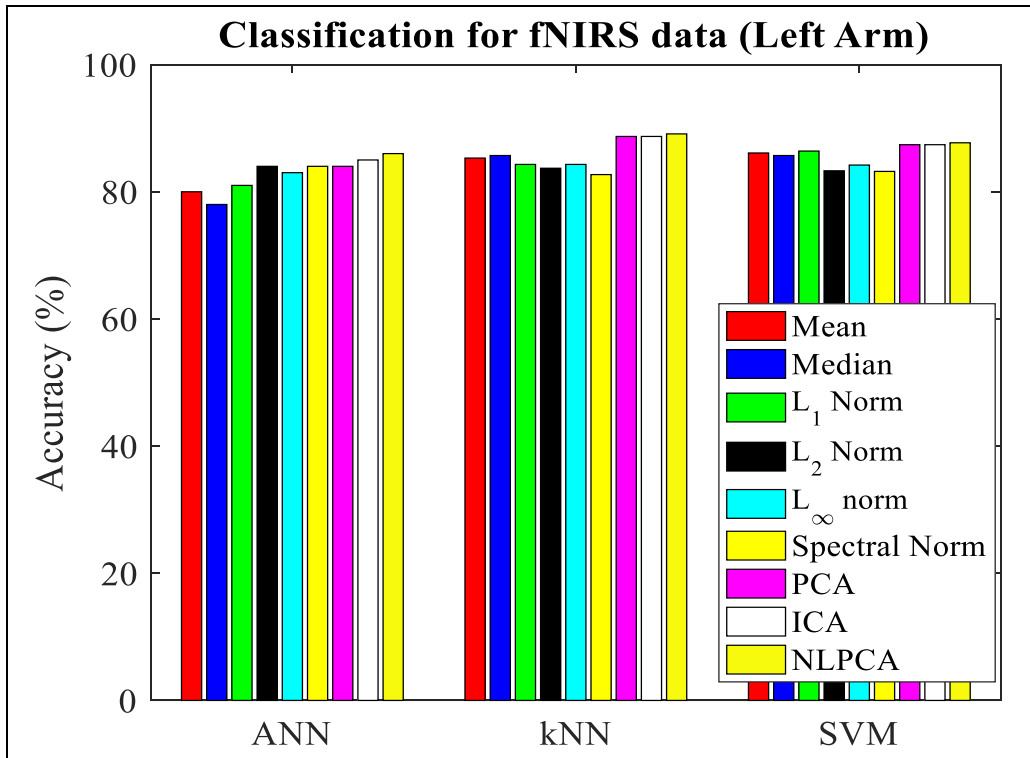


Figure 4.5: Comparison of average accuracy of ANN, kNN, SVM for different features for left arm of 7 patients.

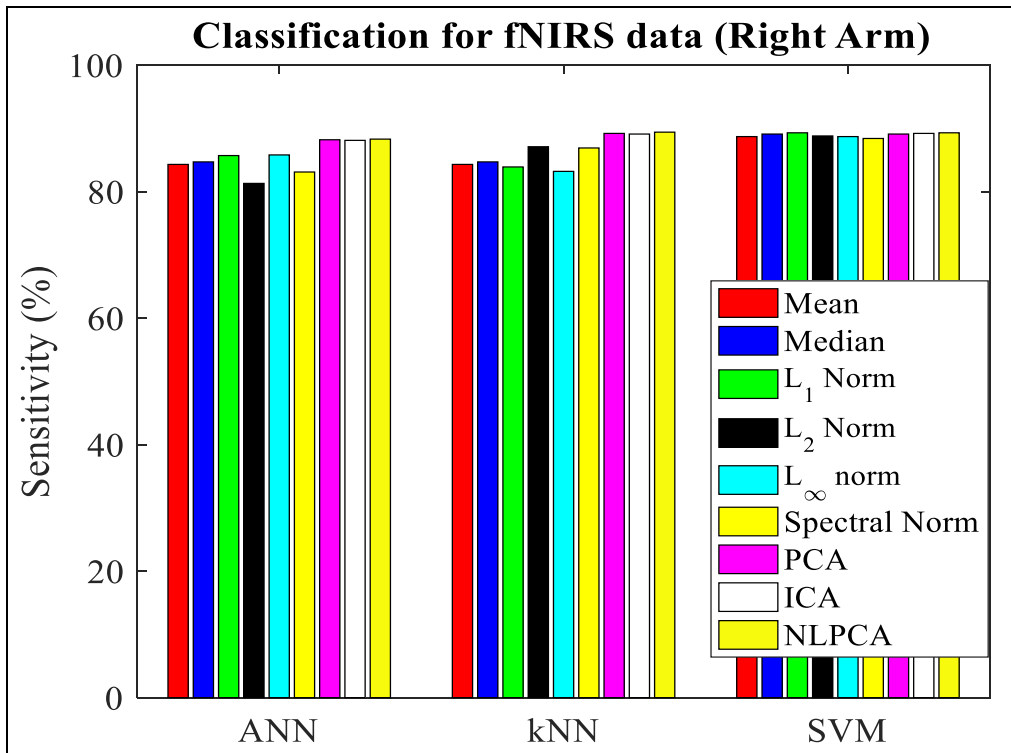


Figure 4.6: Comparison of average sensitivity of ANN, kNN, SVM for different features for right arm of 7 patients.

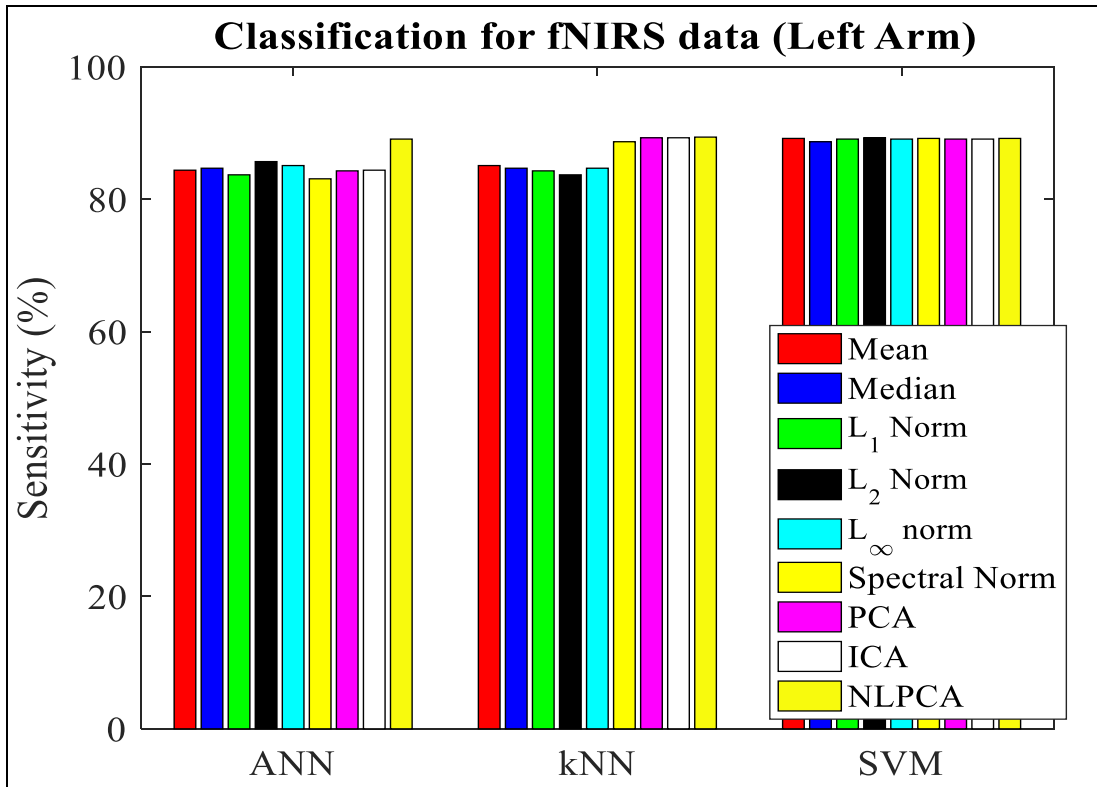


Figure 4.7: Comparison of average sensitivity of ANN, kNN, SVM for different features for left arm of 7 patients.

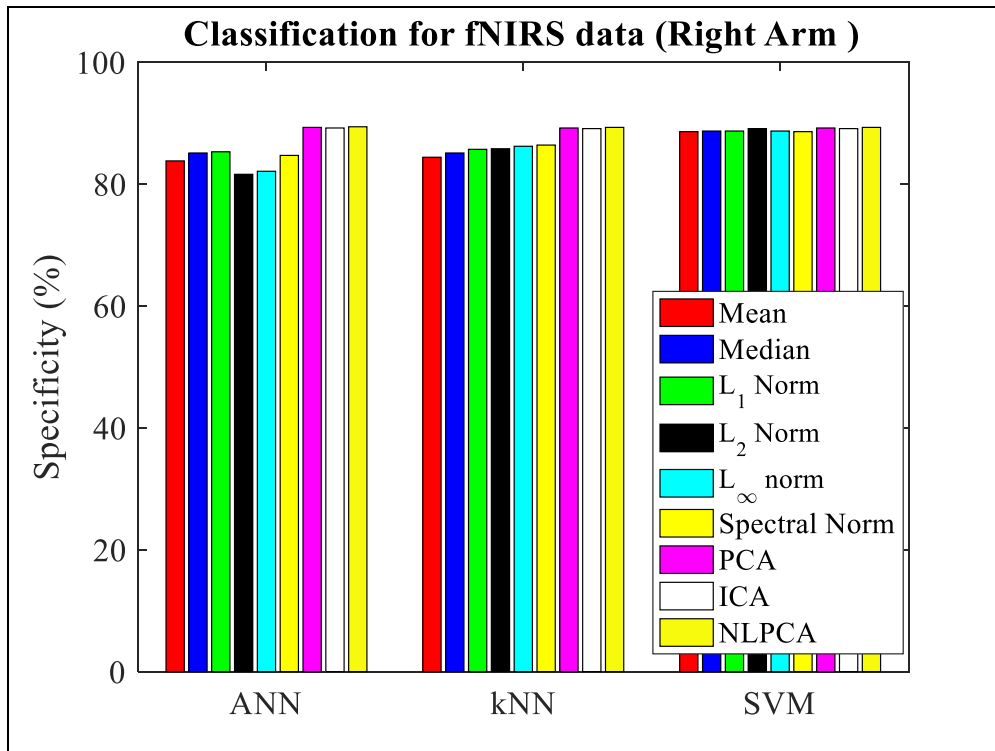


Figure 4.8: Comparison of average specificity of ANN, kNN, SVM for different features for right arm of 7 patients.

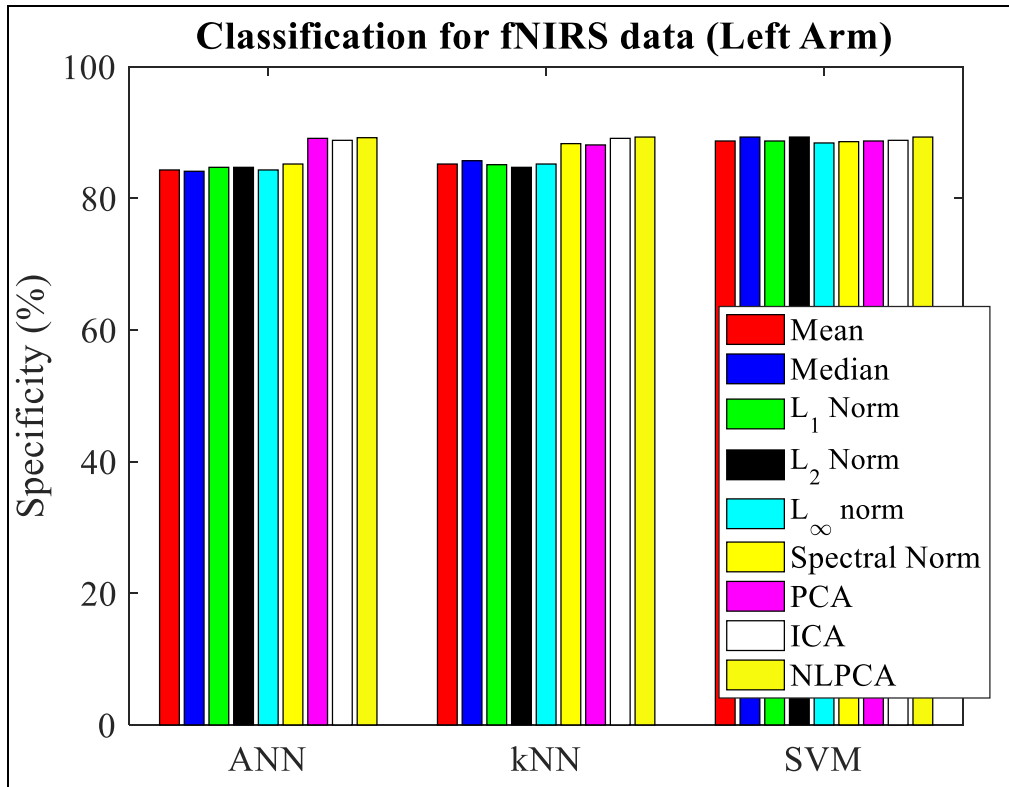


Figure 4.9: Comparison of average specificity of ANN, kNN, SVM for different features for left arm of 7 patients.

4.3 Experimental Results of Imagery Hand Movement

The raw fNIRS signals (HbO and HbR) and their corresponding filtered outputs are given in Figure 4.10. This filtering method removed the physiological noises like respiration & heart rate, and power line noises from the signals.

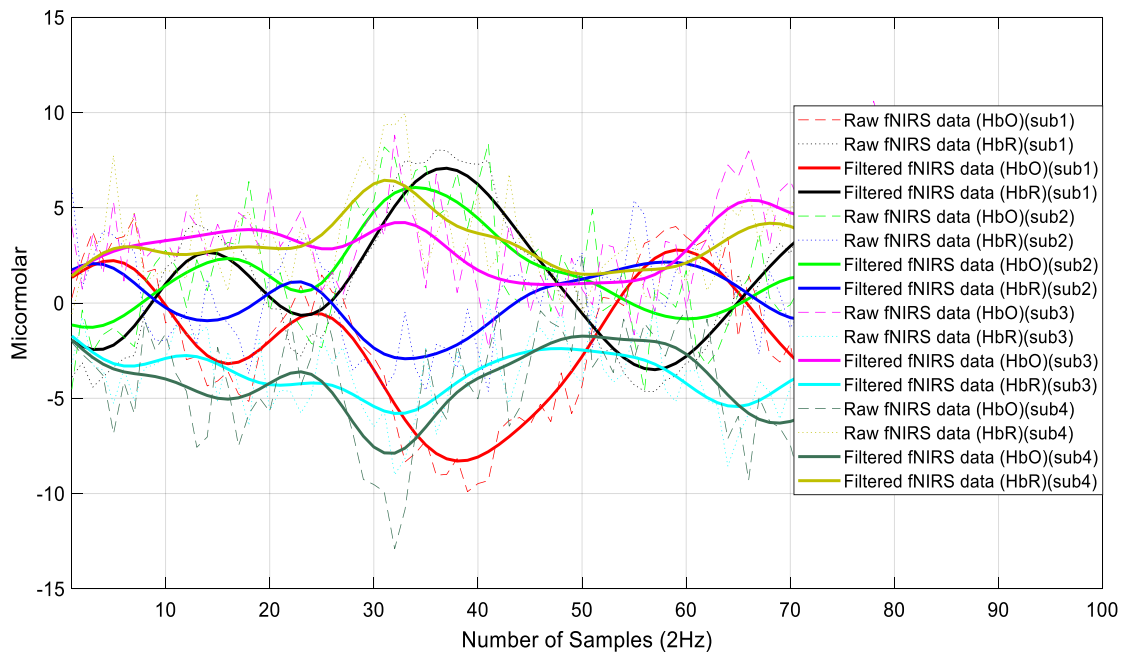


Figure 4.10: Raw and filtered fNIRS data of HbO and HbR of four participant. This data is representing the information of only one channel among sixteen.

From the Figure 4.10, it is also mentionable that the relation between HbO and HbR almost always maintain a negative correlation to each other. After filtering the data, the signal was segmented according to the description of the data acquisition paradigm. Then, the segmented all the signal partitions were corrected with their baseline obeying the rule described in the methodology section of this thesis work.

The LH and RH imagery movements create the neural activation in the right hemisphere and the left hemisphere, respectively. The neural activations regarding the concentration of HbO and HbR for iLH and iRH activities have been presented by the Figure 4.11 and Figure 4.12, respectively. In these figure, the resting state activation has also been given.

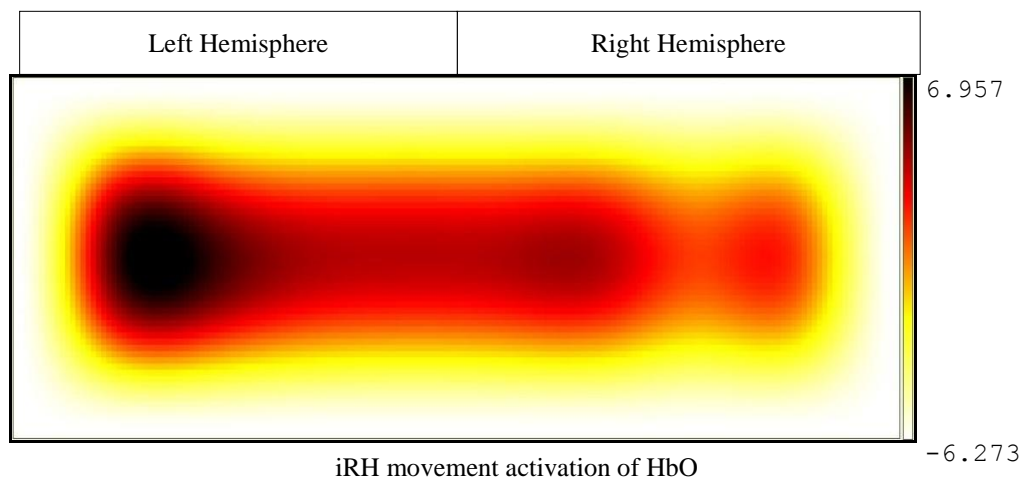
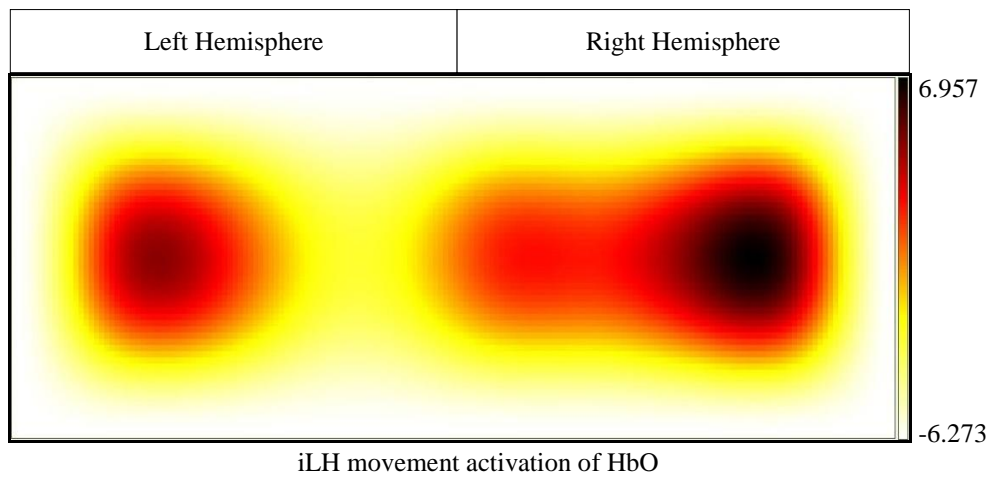
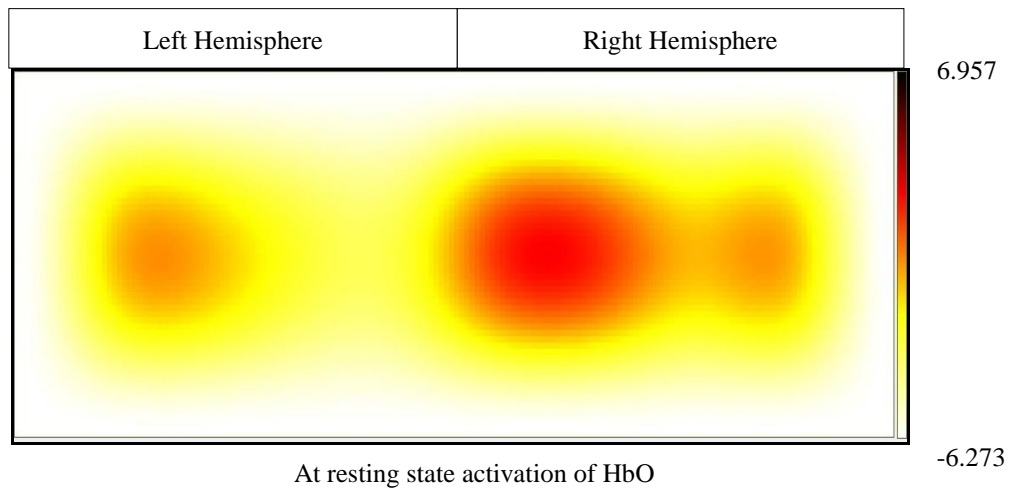


Figure 4.11: Functional images of different tasks with respect to the activation level of HbO. The black color gives the highest activation while the yellow gives the lower activation and the red represents the neutral activation at rest.

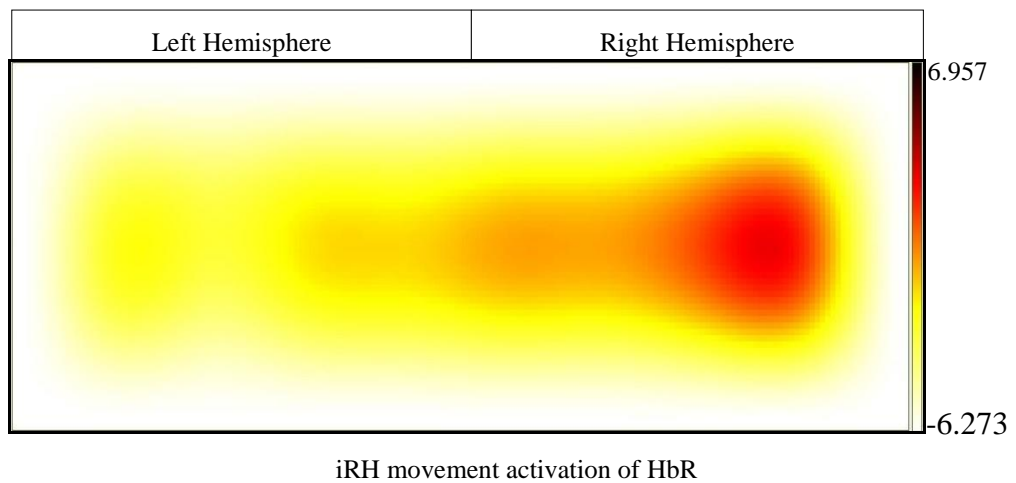
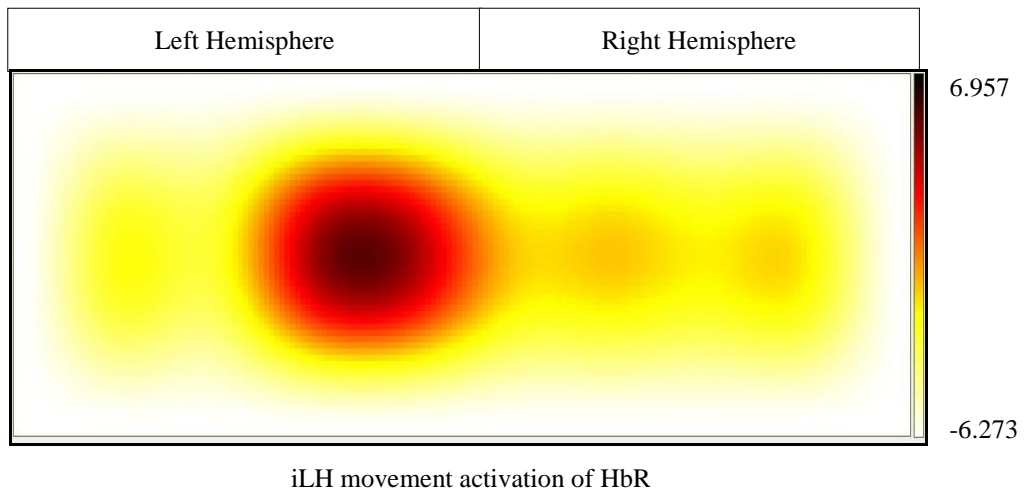
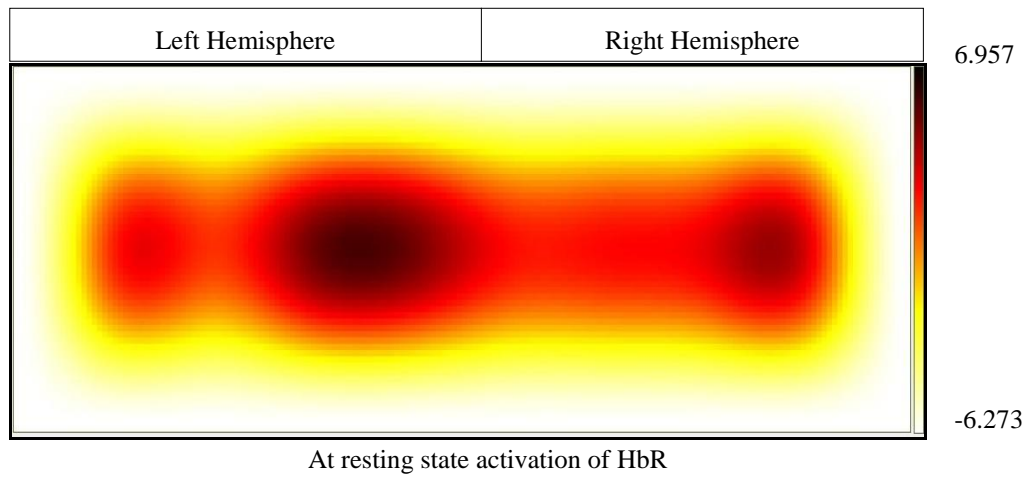


Figure 4.12: Functional images of different tasks with respect to the activation level of HbR. The images of Figure 4.11 and Figure 4.12 are constructed considering 20 point B-Spline interpolation using fNIRSoft professional software.

These functional images inform that the activations regarding the tasks have significant differences over the left hemisphere and right hemisphere on both HbO and HbR concentration. Specially, during the imagery movements of LH, the HbO concentration was increased and consequently decrement of the concentration of HbR was occurred in the right hemisphere as given in second row of Figure 4.10 and Figure 4.11. On the other hand, during the imagery movements of RH, the HbO concentration was increased and consequently decrement of the concentration of HbR was occurred in the left hemisphere as given in third row of Figure 4.10 and Figure 4.11.

As the result, to classify the event regarding iLH and iRH movement we need both the left and right hemisphere information. In this situation the concept of common spatial pattern plays very important role to transform the signals corresponding two different tasks to present them with possibly highest variance. Functional images of different tasks with respect to the activation level of HbR has been given in figure 4.12. The images of Figure 4.11 and Figure 4.12 are constructed considering 20 points B-Spline interpolation using fNIRSoft professional software.

Since the signals were of multiple channels (16 channels), the conventional CSP algorithm and the propose SCSP algorithm were employed to the signal. The CSP method improves the quality of the signal from the consideration of the multiple trials of a single task. Nonetheless, if several numbers of trials have the neural activations not similar to the actual; it would be the weight matrix calculated by the conventional CSP method cannot be proved as efficient method. To remove this limitation of CSP, SCSP has been proposed to make the improvement of the signal quality based on the variation of two different tasks with a standard pattern of the signal. The variance improvements between two classes of signals regarding the CSP and SCSP algorithm are shown in Figure 4.13.

From the Figure 4.13, we found that the improvement through the SCSP algorithm have the more consistent form. Although CSP algorithm also improved the variance between the signals of two different tasks. The proposed SCSP algorithm considered the case where the expected activation had not been happened. As the result, providing them less importance by the proposed SCSP method, the variance became consistent. Applying both the CSP and SCSP method, three features (mean, slope, and variance) of the signals were extracted. The features were then used to train the LDA network. The training was

accomplished with 50% of the features and the rest of the features were reserved for the testing and validations.

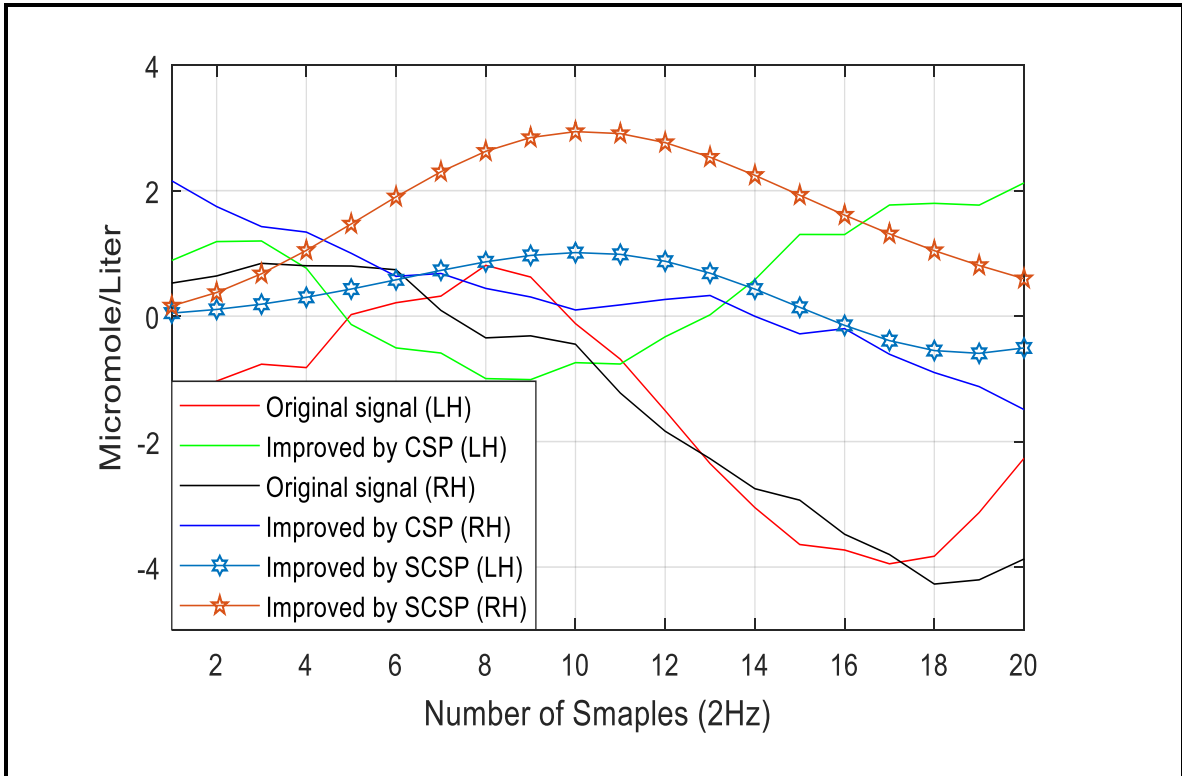


Figure 4.13: Functional images of different tasks with respect to the activation level of HbO.

The training state with LDA algorithm of participant 1 with respect to 10 set of normalized features of each task is shown in Figure 4.14. From the results found from the figure, it is easily observable that within 20 feature point, confusions lie for 3 points which indicates that the training accuracy is $(17/20) = 85\%$. This result was corresponding to the proposed SCSP algorithm. On the other hand, for the CSP algorithm regarding this performance we found is $(16/20) = 80\%$.

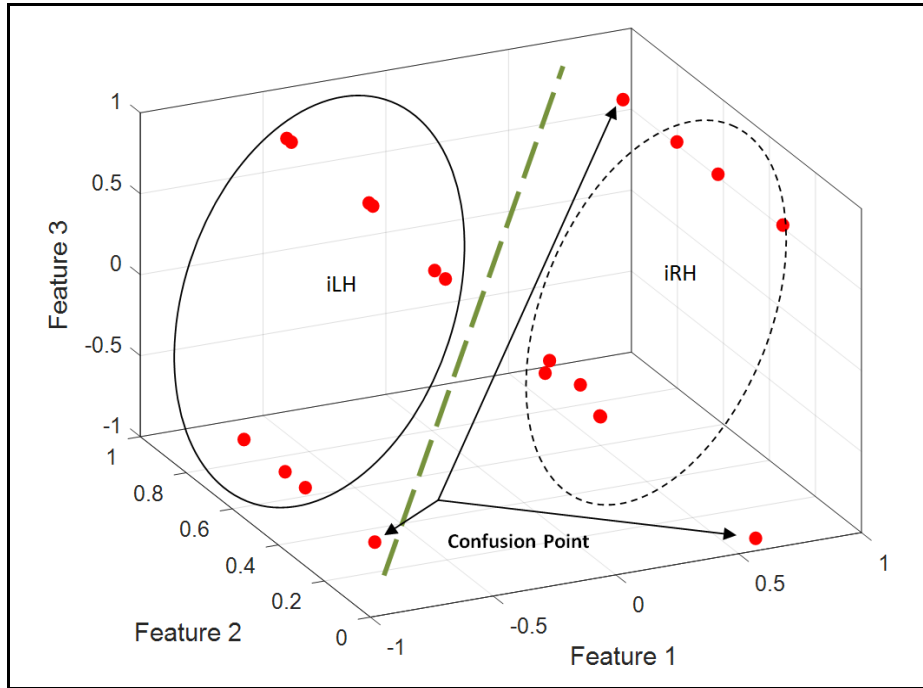


Figure 4.14: Training state of participant#1 with LDA classifier considering the 10 set of features (mean, slope, and variance) of iLH and iRH.

Since every participant performed 20 trials for each task, 10 trials (50%) of LH and 10 trials (50%) of RH features were used for training purpose and rest 50% were used for testing. The classification results of the trials of the 1st participant have been given as confusion matrix in Figure 4.15. This figure indicates the overall classification accuracy as 80%. The individual class performance can also be found from the given confusion matrix in Figure 4.15.

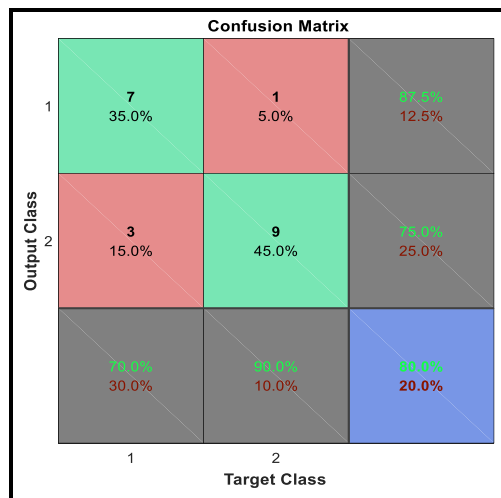


Figure 4.15: The confusion matrix of the classification results regarding the testing features of the participant 1.

Table 4.2: Accuracy of the Training and Testing of the Classification LH and RH Imagery Movement fNIRS Data

<i>Participant No</i>	<i>Performance of Training</i>		
	<i>Only fNIRS</i>	<i>With CSP</i>	<i>With SCSP</i>
1	70%	80%	85%
2	65%	80%	85%
3	60%	75%	80%
4	70%	80%	85%
Average=	66.25%	78.75%	83.75%
	<i>Performance of Testing</i>		
1	60%	70%	80%
2	60%	75%	85%
3	65%	75%	80%
4	70%	80%	85%
Average=	63.75%	75%	82.5%

From the similar procedure, the results corresponding to the testing of all the participants are given in **Table 4.2**. In addition to that, the training performance of the feature sets by LDA has also given by the **Table 4.2**. From the results, we can observe that in training and testing phase of LDA the results we found are very convincing. Additionally, from the results found through LDA classifier, it is also mentionable that the proposed SCSP algorithm has outperformed the conventional CSP algorithm. Eventually, it can be claimed that, the proposed method can improve the classification accuracy 17% in average and 7.5% more than that of the conventional CSP.

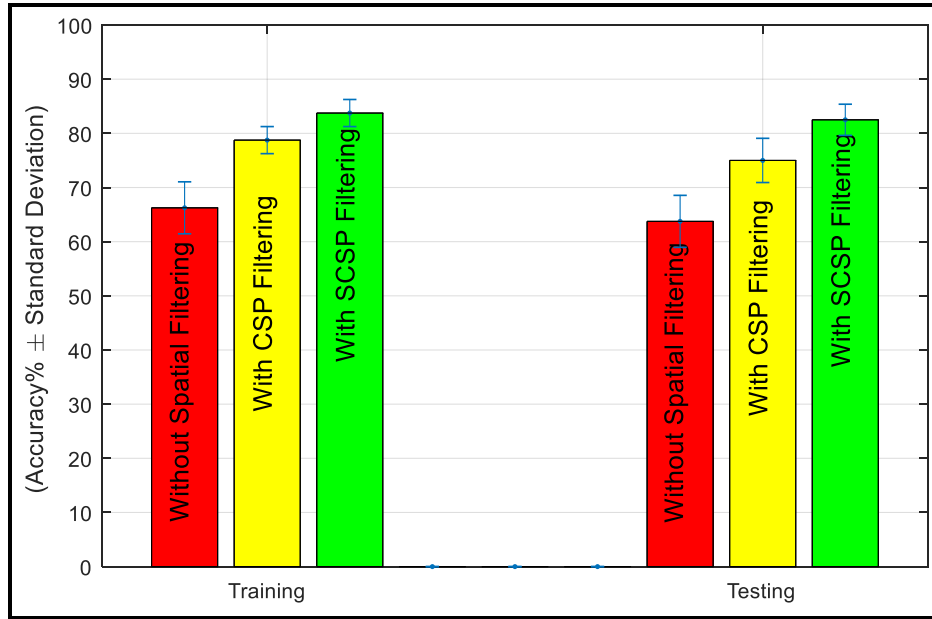


Figure 4.16: Comparison of the proposed SCSP algorithm with the others considering the accuracy% \pm standard deviation in training and testing.

Table 4.3: Sensitivity and Specificity With Respect to the Accuracy of the SCSP Algorithm.

<i>Participant No</i>	<i>Accuracy</i>	<i>Sensitivity</i>	<i>Specificity</i>
1	80%	90%	70%
2	85%	80%	90%
3	80%	80%	80%
4	85%	80%	90%
Average	82.5%	82.5%	82.5%

The difference in the improvement of accuracy by the proposed algorithm over the conventional methods has been given in Figure 4.16. The results given in **Table 4.2** are based on the concentration of HbO. We calculated the same features from the HbR of fNIRS signals and applied the same techniques of the training and testing. In case of the consideration of HbR concentration, we found slightly lower performance. It can improve

the classification accuracy 15% in average and 6% more than that of conventional CSP. It may happen due to the lower amount than that of the HbO concentration.

To understand the performance of the SCSP algorithm in case of accuracy improvement, sensitivity and specificity were also calculated. Sensitivity and specificity of the participant can also be found in Figure 4.15. The sensitivity and the specificity of all participants have been tabulated in **Table 4.3**.

4.4 Result Analysis

4.4.1 Results of Statistical Analysis

To observe the noteworthy neuro-activation from the total motor imagery fNIRS data, statistical analysis, one-way repeated ANOVA has been performed. For this analysis, three levels: 0-3, 4-7, and 8-11 sec are considered for one-way ANOVA investigation for the tasks (left-hand and right-hand). The ANOVA was conducted on the mean value of HbO and HbR concentration. From the results of ANOVA, the following significant hypothesis has been found:

For the imagery left hand movement, significant ($p < 0.05$) increase of HbO concentration ($F(2,11)=13.24$) and decrease in HbR concentration ($F(2,11)=12.659$) are found in 9, 10, 11, and 12 channels. The other channels showed no significance in mean activation ($p > 0.05$). For the imagery right hand movement, significant ($p < 0.05$) increase of HbO concentration ($F(2,11)=23.915$) and decrease in HbR concentration ($F(2,11)=16.96$) are found in 5, 6, 7, and 8 channels. The other channels showed no significance in mean activation ($p > 0.05$) in case of right hand imagery movement. Eventually, from the ANOVA analysis we find that the left hemisphere become more activated due to right hand imagery movements and this is correct inversely for the left hemisphere, as well.

To observe the impact of the features, t -test has been performed between two types of stimuli: left hand and right hand. To do this, the channels of left frontal lobe (channel 1- channel 8) and right frontal lobe (channel 9 - channel 16) are averaged. As a result, the averaged information of left hemisphere and right hemisphere of prefrontal cortex show two different regions activation. The t -test was performed between the activation (HbO) of resting activation and the stimuli (either Left hand or Right hand). The significance levels of the features due to the performed tasks are given in Table 4.4, where the inferences between the groups have been shown by their p -value, t -value, and standard error difference (SED).

Table 4.4: Significance level of the features due to the performed tasks

Events	Features/Feature Extraction Method	Hemisphere Information	
		<i>Left hemisphere of the PFC</i>	<i>Right hemisphere of the PFC</i>
Rest vs LH	Mean	$p=0.8059; t=0.6124; SED^*=0.127$	$p=0.0035; t=3.2779; SED=0.507$
	Median	$p=0.7145; t=0.3145; SED=0.072$	$p=0.0221; t=1.1450; SED=0.107$
	Slope	$p=0.9415; t=0.2784; SED=0.451$	$p=0.0091; t=2.1741; SED=0.601$
	Variance	$p=1.1025; t=0.1108; SED=0.027$	$p=0.0125; t=1.8459; SED=0.451$
	NLPCA(mean)	$p=1.1257; t=0.1414; SED=0.102$	$p=0.0241; t=1.0779; SED=0.507$
	CSP	$p=0.9195; t=0.1895; SED=0.334$	$p=0.0019; t=2.9748; SED=0.641$
	Proposed SCSP	$p=0.1241; t=0.6947; SED=0.667$	$p=0.00041; t=4.2814; SED=0.317$
Rest vs RH	Mean	$p=0.0032; t=4.7101; SED=0.242$	$p=0.7335; t=0.3473; SED=0.761$
	Median	$p=0.0451; t=1.1779; SED=0.664$	$p=0.8191; t=0.2504; SED=0.327$
	Slope	$p=0.0059; t=3.4025; SED=0.358$	$p=0.9451; t=0.1729; SED=0.240$
	Variance	$p=0.0108; t=2.1417; SED=0.745$	$p=1.1045; t=0.2178; SED=0.741$
	NLPCA(mean)	$p=0.0301; t=1.2748; SED=0.325$	$p=0.9817; t=0.6779; SED=0.845$
	CSP (mean)	$p=0.0024; t=3.2058; SED=0.741$	$p=0.2817; t=0.9779; SED=0.124$
	Proposed / SCSP (mean)	$p=0.00007; t=4.2748; SED=0.554$	$p=0.4879; t=0.3356; SED=0.345$

4.4.2 Results of Classification

From the all results of imagery hand movements classification (with pain), an overall comparative result of different extracted features regarding HbO data are given in Table 4.4. From the results, we get the performances if the different features with different classifiers in the aspect of accuracy, sensitivity, and specificity. These results reveal the performances of the individual features with the corresponding classifiers.

Table 4.5: Comparison of different parameter of classification of different feature of oxygenated hemoglobin (HbO) for the participants

Imagery hand movement with pain task of participant (1-7) (HbO)												
Features/ Feature Extraction Method	ANN			KNN			SVM			LDA		
	Accuracy (%)	Sensitivity (%)	Specificity (%)	Accuracy (%)	Sensitivity (%)	Specificity (%)	Accuracy (%)	Sensitivity (%)	Specificity (%)	Accuracy (%)	Sensitivity (%)	Specificity (%)
Data	71.4	71.5	72.3	69.4	73.4	68.2	71.2	75.8	74.2	73.8	72.2	74.3
Mean	80.0	82.5	81.8	80.0	81.0	81.4	82.4	83.2	83.5	83.0	81.4	81.0
Median	76.0	79.5	78.6	77.5	78.8	79.0	79.5	80.2	81.0	82.7	81.5	82.0
Slope	78.0	78.6	77.5	78.0	77.8	76.5	80.4	81.6	82.7	81.0	82.2	80.6
Variance	82.7	82.9	82.0	80.4	79.3	82.5	83.6	82.8	83.0	83.4	82.8	83.0
L ₁ -Norm	79.5	76.5	75.8	77.2	75.4	74.0	79.0	78.5	77.9	78.6	77.3	77.8
L ₂ -Norm	80.2	81.2	78.7	78.5	77.5	79.2	81.4	80.5	81.5	83.6	81.8	82.7
L _∞ -Norm	76.0	77.3	75.5	74.5	75.2	74.7	78.8	79.5	76.7	79.7	78.4	77.8
Spectral Norm	78.5	79.0	78.0	75.8	76.0	75.6	78.8	77.5	78.8	79.0	78.6	77.5
PCA	84.0	86.3	85.7	84.9	85.6	86.7	86.6	87.6	87.9	86.6	85.4	86.9
ICA	83.5	85.5	86.5	84.5	85.8	87.1	86.5	87.0	88.4	87.4	86.8	87.2
NLPCA	84.5	87.7	88.3	85.5	86.0	88.3	87.7	88.3	89.3	89.5	88.5	88.1
With CSP (Mean, Slope, Variance)	79.5	80.3	81.1	78.8	80.4	78.0	80.7	81.7	82.7	82.7	81.0	82.0
Proposed/ SCSP (Mean, Slope, Variance)	88.7	88.5	89.6	86.3	87.2	88.5	87.0	88.4	89.6	89.9	88.8	88.8

In addition, the separate results of the accuracy, sensitivity, and specificity of the different feature extraction methods are presented with the bar-plots given in Figure 17 - 19, respectively for the HbO data only. The overall results reveal that the proposed SCSP (taking the same features-mean, slope, and variance as the CSP after spatial filtering) method outperforms than the other conventional feature extraction methods in cases of the all classifiers.

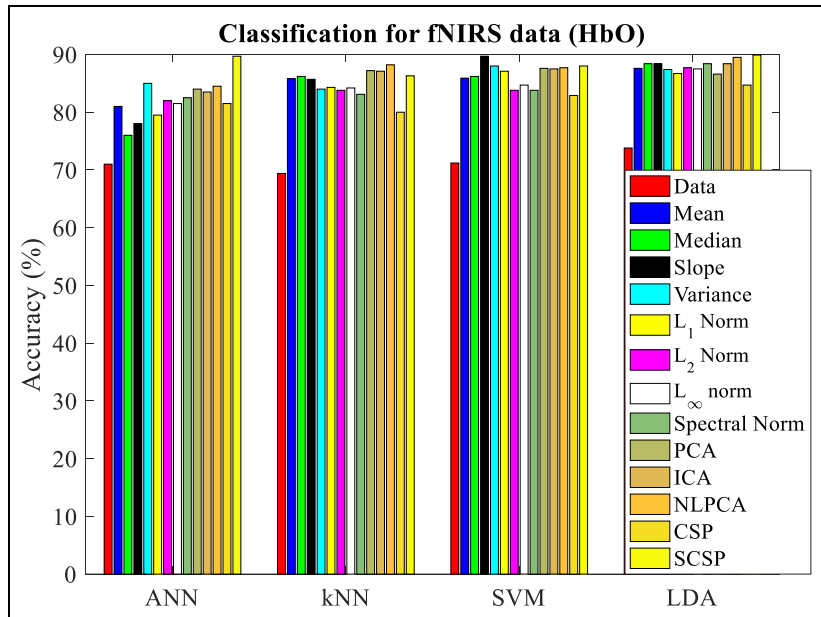


Figure 4.17: Comparison of average accuracy of different classifier for different features of HbO data (imagery hand movement with pain task) for the participants.

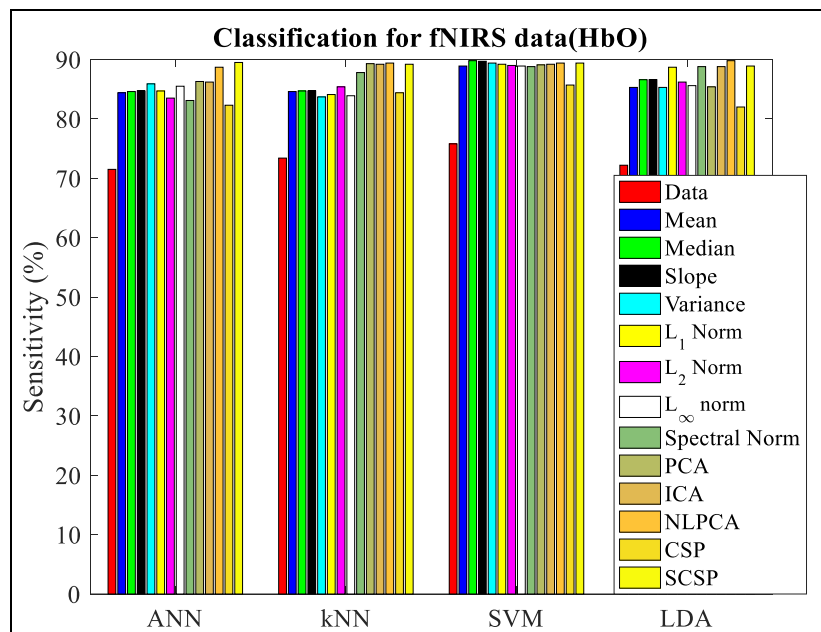


Figure 4.18: Comparison of average sensitivity of different classifier for different features of HbO data (imagery hand movement with pain task) for the participants.

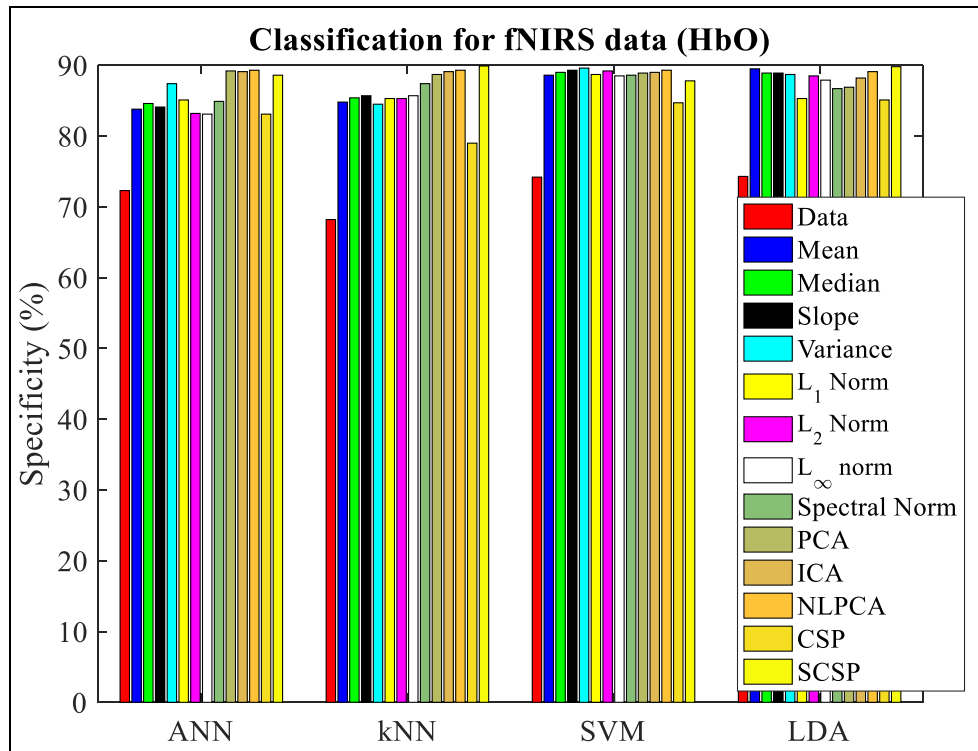


Figure 4.19: Comparison of average specificity of different classifier for different features of HbO data (imagery hand movement with pain task) for the participants.

The classification results of imagery hand movement (with pain) with their sensitivities and specificities with respect to the different extracted feature methods regarding HbR data are given in Table 4.5. From the results given in this table, we get the performances of the different features with different classifiers in the aspect of accuracy, sensitivity, and specificity. These results reveal the performances of the individual features with the corresponding classifiers. In addition, the separate results of the accuracy, sensitivity, and specificity of the different feature extraction methods are presented with the bar-plots given in Figure 20 - 22, respectively for the HbR data only. The overall results reveal that the proposed SCSP method outperforms the other conventional feature extraction methods in cases of the all classifiers.

Table 4.6: Comparison of different parameter of classification of different feature of deoxygenated hemoglobin (HbR) for the participants

Imagery hand movement with pain of participant (1-7) (HbR)												
Features/ Feature Extraction Method	ANN			KNN			SVM			LDA		
	Accuracy (%)	Sensitivity (%)	Specificity (%)	Accuracy (%)	Sensitivity (%)	Specificity (%)	Accuracy (%)	Sensitivity (%)	Specificity (%)	Accuracy (%)	Sensitivity (%)	Specificity (%)
Data	69.2	69.4	69.8	67.2	71.0	66.0	69.4	73.5	72.2	72.6	70.0	72.2
Mean	79.4	80.1	78.2	78.4	81.6	81.6	80.3	81.5	81.5	81.3	79.6	79.4
Median	74.5	77.5	76.9	76.2	77.2	77.2	76.8	78.6	79.2	80.8	79.9	81.4
Slope	75.7	76.2	75.7	76.7	76.0	74.0	78.8	79.8	80.0	79.4	80.5	79.0
Variance	81.6	81.4	80.4	78.4	77.6	80.6	81.4	81.0	81.4	81.7	81.0	81.5
L ₁ -Norm	77.8	74.7	74.5	75.4	75.5	73.0	77.4	76.9	76.2	76.9	75.6	76.1
L ₂ -Norm	78.3	79.2	77.2	76.8	76.8	77.5	79.6	78.8	79.7	81.8	79.9	80.2
L _∞ -Norm	74.6	75.4	73.8	74.0	73.0	73.3	76.3	77.7	72.9	77.8	76.5	76.2
Spectral Norm	77.7	77.3	76.7	74.2	74.4	74.0	77.0	75.8	77.2	77.4	76.8	75.8
PCA	82.3	83.3	84.2	83.3	84.2	85.2	85.0	86.2	86.0	85.4	83.9	85.2
ICA	81.7	82.8	84.8	83.0	84.5	85.5	84.8	85.5	86.4	86.0	85.0	85.5
NLPCA	82.9	86.2	86.7	83.7	84.7	86.6	86.0	86.5	87.8	87.8	86.7	86.5
With CSP (Mean, Slope, Variance)	78.7	79.5	80.1	77.7	79.3	76.2	79.8	80.7	81.5	81.3	79.9	81.1
Proposed/ SCSP (Mean, Slope, Variance)	87.8	86.5	87.6	84.4	85.6	86.8	85.5	86.8	88.3	88.5	87.3	87.0

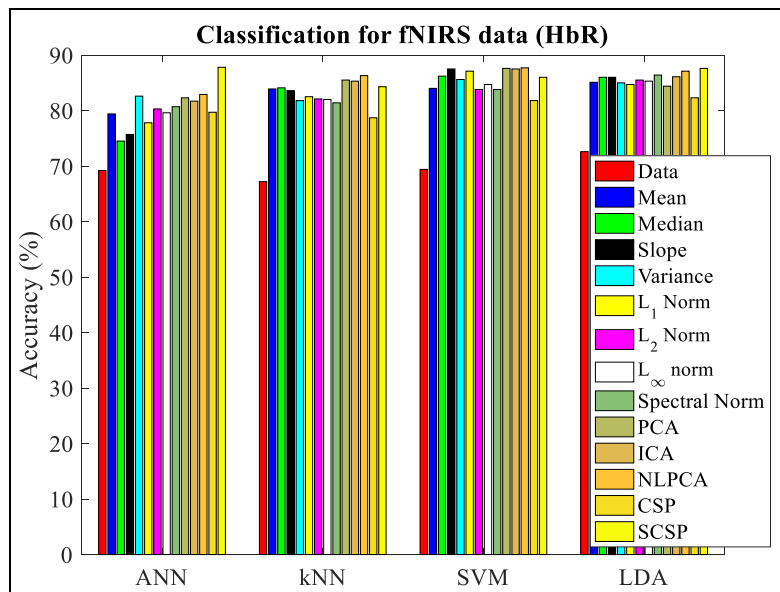


Figure 4.20: Comparison of average accuracy of different classifier for different features of HbR data (imagery hand movement with pain task) for the participants.

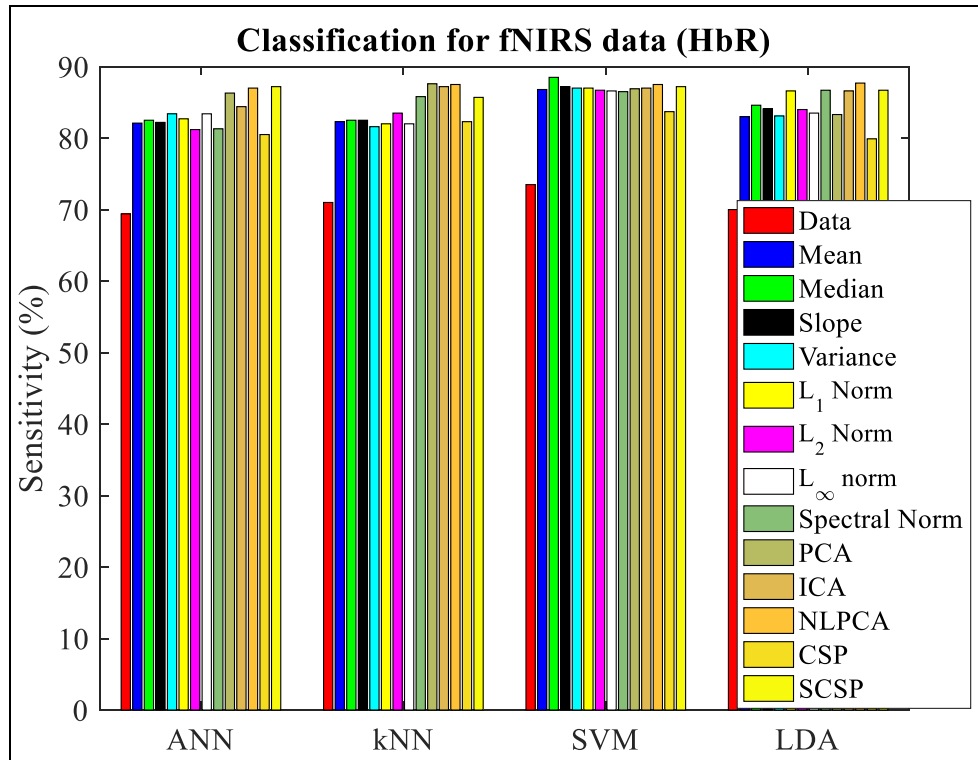


Figure 4.21: Comparison of average sensitivity of different classifier for different features of HbR data (imagery hand movement with pain task) for the participants.

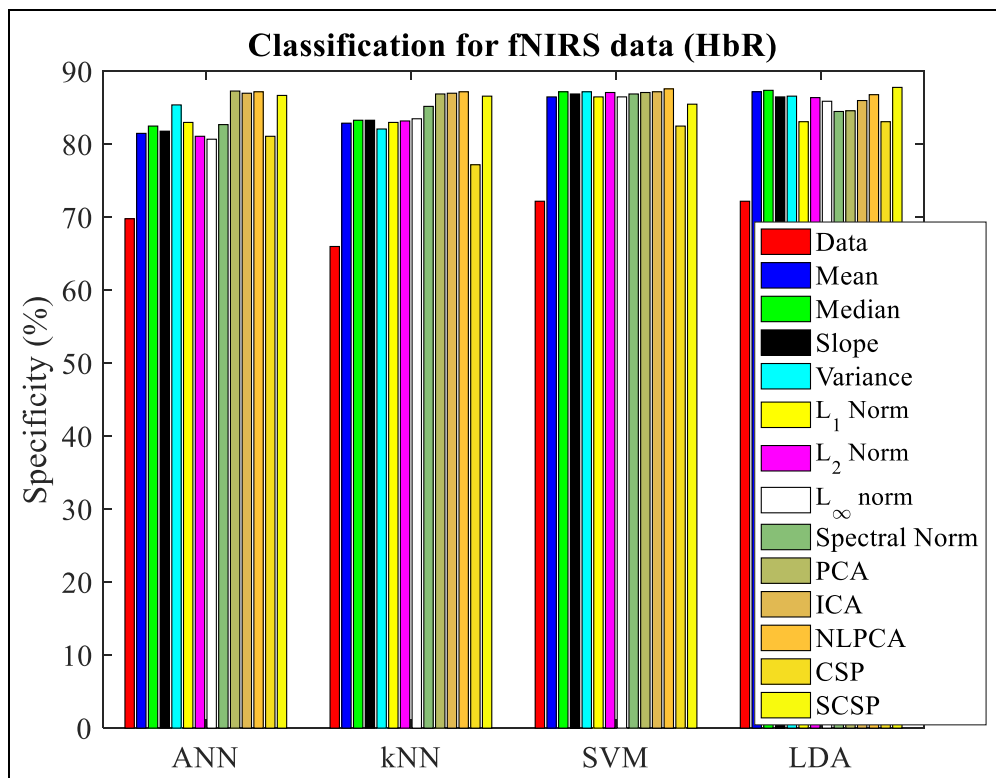


Figure 4.22: Comparison of average specificity of different classifier for different features of HbR data (imagery hand movement with pain task) for the participants.

These outcomes provide the performances of the different features with different classifiers with respect to the accuracy, sensitivity, and specificity. These results reveal the performances of the individual features with the corresponding classifiers. In addition, the separate results of the accuracy, sensitivity, and specificity of the different feature extraction methods are presented with the bar-plots given in Figure 23 - 25, respectively for the HbO data only. The overall results reveal that the proposed SCSP (under the extracted features: mean, slope, and variance after spatial filtering) method outperforms the other conventional feature extraction methods in cases of the all classifiers.

Table 4.7: Comparison of Different Parameter of Classification of Different Feature of oxygenated hemoglobin (HbO) for the Participants

Imagery hand movement without pain task of participant (1-4) (HbO)												
Features/ Feature Extraction Method	ANN			KNN			SVM			LDA		
	Accuracy (%)	Sensitivity (%)	Specificity (%)	Accuracy (%)	Sensitivity (%)	Specificity (%)	Accuracy (%)	Sensitivity (%)	Specificity (%)	Accuracy (%)	Sensitivity (%)	Specificity (%)
Data	58.8	58.0	59.8	50.0	49.2	48.3	53.8	52.9	55.7	63.8	65.6	62.2
Mean	77.0	78.7	75.5	66.0	66.7	63.0	74.0	73.1	75.0	73.0	73.5	72.6
Median	54.0	53.6	54.5	60.0	59.3	60.9	67.0	65.5	68.9	70.0	70.0	70.0
Slope	79.0	78.9	77.4	73.0	71.7	74.5	79.0	78.4	78.6	78.0	76.9	79.2
Variance	78.0	75.4	82.7	73.0	70.2	76.7	76.0	77.5	78.6	77.0	78.8	78.3
L ₁ -Norm	71.0	73.3	69.1	59.0	58.5	59.6	71.0	73.3	69.1	76.0	79.6	73.2
L ₂ -Norm	71.0	67.8	75.6	69.0	66.7	72.1	75.0	72.7	77.8	77.0	77.6	76.5
L _∞ -Norm	55.0	54.9	55.1	62.0	63.0	61.1	61.0	60.0	62.2	75.0	79.1	71.9
Spectral Norm	51.0	51.1	50.9	50.0	50.0	48.0	60.0	60.9	59.3	56.0	55.2	57.1
PCA	76.0	79.6	73.4	63.0	63.3	62.8	78.0	78.0	78.0	75.0	74.5	75.5
ICA	56.0	56.0	56.0	45.0	44.9	45.1	56.0	55.4	55.4	61.0	60.0	62.2
NLPCA	58.0	57.7	58.3	47.0	47.3	46.8	51.0	51.2	51.2	69.0	74.4	65.6
With CSP (mean, slope, variance)	68.8	72.3	67.1	63.8	65.4	63.0	68.8	66.7	71.7	75.0	78.5	72.5
Proposed/ SCSP (mean, slope, variance)	83.8	83.2	85.9	76.3	77.2	78.9	80.0	80.4	79.9	82.5	82.5	82.5

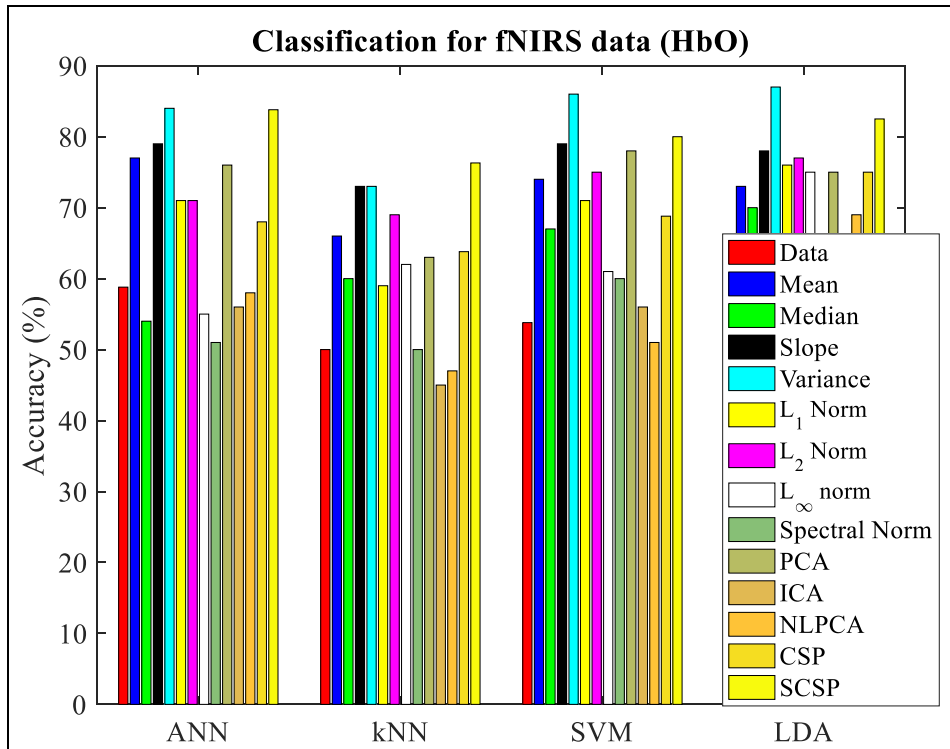


Figure 4.23: Comparison of average accuracy of different classifier for different features of HbO data (imagery hand movement without pain task) for the participants.

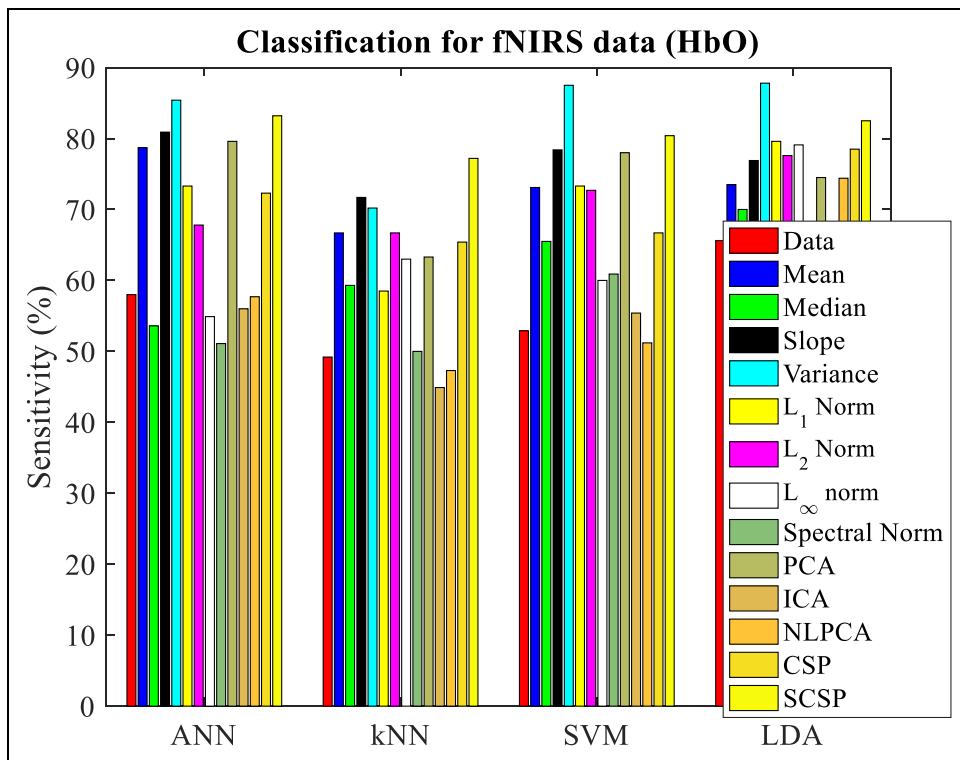


Figure 4.24: Comparison of average sensitivity of different classifier for different features of HbO data (imagery hand movement without pain task) for the participants.

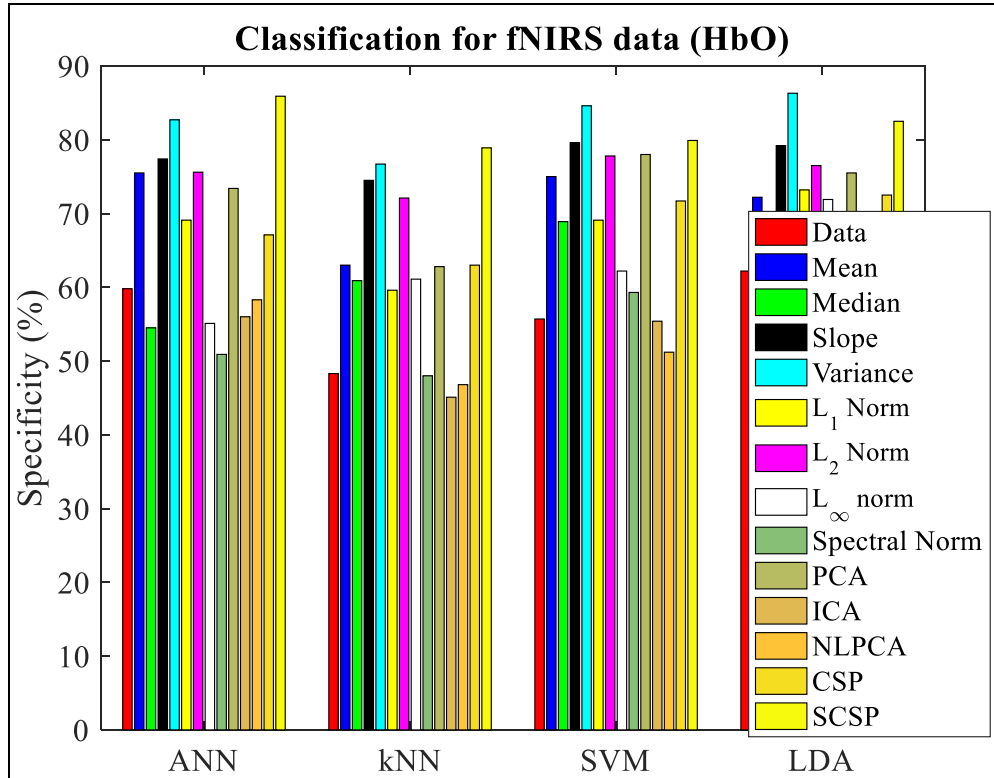


Figure 4.25: Comparison of average specificity of different classifier for different features of HbO data (imagery hand movement without pain task) for the participants.

Finally, the classification performances of imagery hand movement (without pain) of the HbR data are given in Table 4.6 based on the individual features or feature extraction method. These outcomes provide the performances of the different features with different classifiers with respect to the accuracy, sensitivity, and specificity. The outcomes provide the performances of the individual features with the different classifiers. In addition, the separate results of the accuracy, sensitivity, and specificity of the different feature extraction methods are given in Figure 26 - 28, respectively for the HbR data only. The overall results divulge that our proposed SCSP method overtakes the other conventional feature extraction methods in cases of all classifiers (ANN, SVM, kNN, and LDA). Besides, it has been also found that the classification accuracy has been found highest for the LDA classifiers.

Table 4.8: Comparison of Different Parameter of Classification of Different Feature of deoxygenated hemoglobin (HbR) for the Participants

Imagery hand movement without pain of participant (1-4) (HbR)												
Features/ Feature Extraction Method	ANN			KNN			SVM			LDA		
	Accuracy (%)	Sensitivity (%)	Specificity (%)	Accuracy (%)	Sensitivity (%)	Specificity (%)	Accuracy (%)	Sensitivity (%)	Specificity (%)	Accuracy (%)	Sensitivity (%)	Specificity (%)
Data	57.5	56.6	58.4	48.8	48.5	47.0	52.4	51.7	54.2	62.6	64.0	61.0
Mean	75.0	76.8	74.3	64.5	65.4	62.0	72.7	72.0	74.0	72.1	72.2	71.5
Median	52.6	52.2	53.1	58.5	58.0	59.5	65.5	64.1	67.6	69.0	68.9	68.7
Slope	77.5	79.4	76.0	71.7	70.4	73.0	77.7	77.2	75.3	76.6	75.5	77.9
Variance	79.9	80.1	78.2	71.7	69.2	75.4	77.0	77.8	76.3	77.6	76.6	77.6
L ₁ -Norm	70.0	71.8	67.6	57.5	57.8	58.4	69.6	72.3	68.0	74.7	78.2	72.2
L ₂ -Norm	69.3	65.9	73.7	67.0	65.3	71.0	74.0	71.5	76.4	75.8	76.4	75.0
L _∞ -Norm	54.0	53.5	53.8	60.5	61.7	59.6	59.9	59.0	61.0	73.8	77.1	70.4
Spectral Norm	49.8	50.0	49.6	49.0	48.8	47.0	59.2	59.6	57.9	54.8	54.0	55.5
PCA	75.0	78.5	72.1	61.7	62.0	61.6	76.8	77.3	76.2	73.6	73.2	74.3
ICA	54.7	54.0	54.5	43.8	43.6	44.0	54.1	54.3	53.6	59.2	58.6	60.7
NLPCA	56.5	56.3	57.0	45.7	46.1	45.5	49.6	50.0	49.8	67.8	72.6	64.3
With CSP (Mean, Slope, Variance)	67.5	70.6	65.5	62.5	64.1	62.0	67.2	65.4	70.2	73.5	77.0	71.1
Proposed/ SCSP (Mean, Slope, Variance)	82.0	81.5	84.0	74.5	75.2	77.0	78.2	78.5	78.2	80.5	80.8	80.1

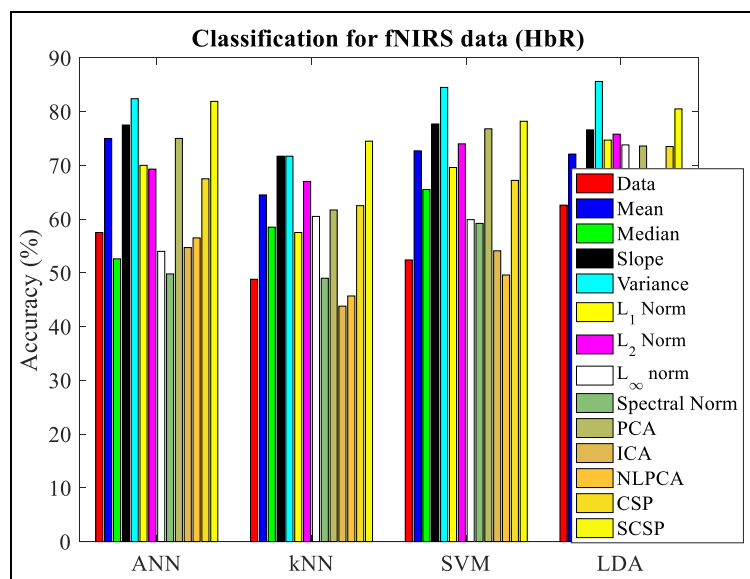


Figure 4.26: Comparison of average accuracy of different classifier for different features of HbR data (imagery hand movement without pain task) for the participants.

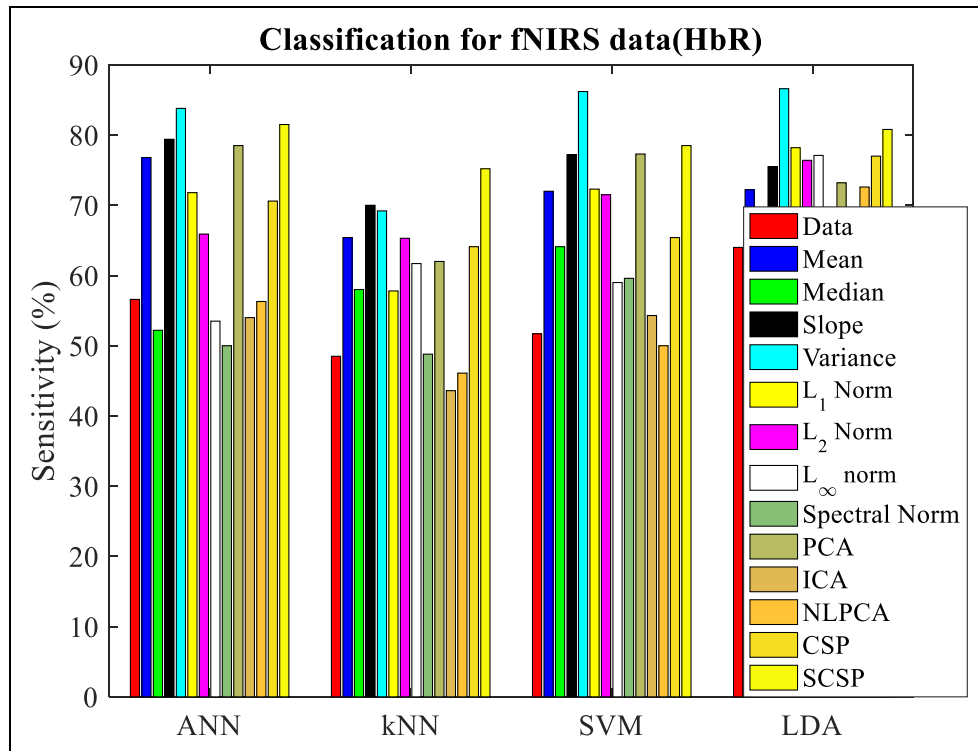


Figure 4.27: Comparison of average sensitivity of different classifier for different features of HbR data (imagery hand movement without pain task) for the participants.

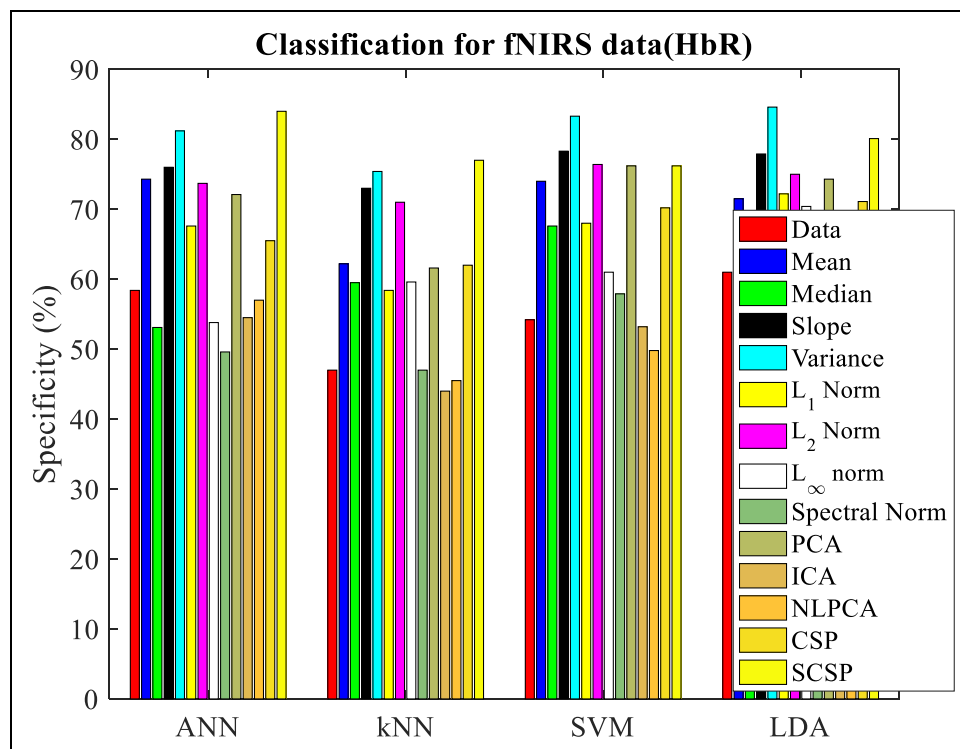


Figure 4.28: Comparison of average specificity of different classifier for different features of HbR data (imagery hand movement without pain task) for the participants.

4.5 Comparison between the Results of the Proposed Work and Existing Works

A summarized result of comparison between proposed thesis work and related other research works those have been developed in recent years are given in Table 4.8. From this comparison we get that the performance of the proposed thesis work is outstanding and very convincing to outtakes the other methods in the regarding field of researches and applications.

Table 4.9: Comparison between result of proposed work and some recent years work

Research works	Task	Features/ Classifiers	Results
N. T. Hai, et al., (2013)[4.1]	Finger movements of left hand and right hand	Features: Polynomial regression coefficients Classifier: ANN & SVM	SVM: 72.5-82.5% ANN: 72-85%
K. S. Hong, et al., (2015)[4.2]	mental arithmetic, right-hand and left-hand motor imagery	Features: Slope and Mean Classifier: LDA	75.6%
M. A. Rahman & M. Ahmad; (2016)[4.3]	Voluntary left and right hand movement	Temporal Features: Mean, Median, Kurtosis, Skewness, standard deviation Classifier: ANN	Average 79.5%
A. M. Batula. et al., (2017)[4.4]	Left, right, forward, and backward movement	Temporal Features: Mean, Median, Slope, & Max Classifier: LDA	Average 29.72%
S. H. Jin, et al, (2015)[4.5]	Finger movements of left hand and right hand	Methods: CSP (Mean, Slope, Variance) Classifier: SVM	Accuracy: 71.82%
S. Zhanga, et al, (2018)[4.6]	right-hand and left-hand motor imagery	Methods: CSP (Mean, Slope, Variance) Classifier: LDA	Accuracy: 63.3% ± 13.3
Proposed work	Imagery hand movement with and without pain	Methods: SCSP (Mean, Slope, Variance) Classifier: ANN, KNN, SVM and LDA	Accuracy: LDA: 82.5%

4.6 Chapter Summary

In this chapter all the simulations and performances of this study are discussed. The procedures of features extraction, feeding to the classifiers, the performances of the classifiers has been presented with suitable figures, tables, barplot. The classification accuracy, sensitivity, and the specificity of the proposed algorithms were tested. The classification parameters are also compared with other methods to understand the significance of the proposed methodology in the context of the fNIR signal classification performance.

REFERENCES

- [4.1] K. S. Hong, N. Naseer, and Y. H. Kim, "Classification of prefrontal and motor cortex signals for three-class fNIRS-BCI," *Neuroscience Letter*, vol. 587, pp. 87-92, February 2015.
- [4.2] N. T. Hai, N. Q. Cuong, T. Q. Dang Khoa, and V. V. Toi, "Temporal hemodynamic classification of two hands tapping using functional nearinfrared spectroscopy," *Frontiers in Human NeuroScience*, vol. 7, no. 516, pp. 1-12, September 2013.
- [4.3] M. A. Rahman and M. Ahmad, "Movement Related Events Classification from Functional Near Infrared Spectroscopic Signal," 19th International Conference on Computer and Information Technology, December 18-20, 2016, North South University, Dhaka, Bangladesh.
- [4.4] A. M. Batula, Y. E. Kim, and H. Ayaz, "Virtual and Actual Humanoid Robot Control with Four-Class Motor-Imagery-Based Optical Brain-Computer Interface," *Computational Intelligence and Neuroscience*, volume 2017, Article ID 1463512, pp. 1-13, July 2017.
- [4.5] S. H. Jin, S. H. Lee, G. Jang, Y. J. Lee, H. K. Shik and J. An, "An application of common spatial pattern algorithm for accuracy improvement in classification of cortical activation pattern according to finger movement," 54th Annual Conference of the Society of Instrument and Control Engineers of Japan (SICE), Hangzhou, 2015, pp. 1260-1264.
- [4.6] S. Zhanga, Y. Zheng, D. Wanga, L. Wanga, J. Maa, J. Zhanga, W. Xua, D. Lia, and D. Zhangd, "Application of a common spatial pattern-based algorithm for an fNIRS-based motor imagery brain-computer interface," *Neuroscience Letters*, vol. 655, pp. 35-40, 2018.

CHAPTER V: Conclusions

Chapter Outlines

5.1 Introduction

5.2 Future Perspective

CHAPTER V

Conclusions

5.1 Introduction

This work investigates the classifying ability of ANN, kNN, SVM, and LDA of fNIRS data corresponding to left-hand and right-hand movements regarding the condition of with pain and without pain. The classifying accuracy of the applied classifiers are calculated for different participants and based on different features. From overall thesis results, it is found that LDA provides the best accuracy, specificity, and sensitivity for almost all the features. On the other hand, ANN and SVM provide the beautiful results for some specific features like NLPCA, PCA, and CSP method. The classification accuracies of the conventional features are still lower to implement a practical BCI. To improve the classification accuracy of the fNIR data, this thesis work proposed and implemented an algorithm named SCSP that is modified form of conventional CSP algorithm. The SCSP method has been implemented as an offline fNIRS based motor imagery event classification for BCI employment. Our outcomes suggest the SCSP algorithm as an effective spatial filtering technique in the context of feature extraction from motor imagery fNIRS signals to attain the promising classification accuracies maintaining satisfactory true positive and false negative rate.

Finally, we can conclude our work mentioning the following remarkable outcomes:

- Two types of motor imagery movements (with pain and without pain) are classified by different classifiers where we have found the classification accuracies are best in case of LDA. On the other hand, SVM and ANN provide the good results for some specific features
- For finding the classification accuracies, most commonly used feature extraction procedure have been deployed where we found that existing feature extraction methods give overall accuracy less than 80%.
- To improve the classification accuracies of the imagery hand movement data, we have proposed and deployed a modified spatial filtering technique which we have

named as SCSP method. The results regarding the proposed method outtakes the performance of the conventional methods.

Eventually, we hope that our proposed method will be helpful to improve the performance of the practical BCI system.

5.2 Future Perspective

The main limitation of the proposed SCSP algorithm is to select the standard pattern of the activation, correctly which is crucial for the improvement of the classification performance. Trial based correlation could be a potential solution to find the standard activation pattern. The maximum correlated data should be selected for the selected one. Someone can also implement the canonical correlation or partial least square method to find the absolute correlation profile of the trials to find the standard pattern of the activation. Therefore, this approach can be a new way of research to modify the SCSP method. In addition to that, this proposal is based on the two-class problem only. This approach can be re-proposed for the multiple classes, as well. These two unaccomplished works can be potential guidelines for the future researchers in this regard.

--End--